UNIVERSITY OF GHANA

COLLEGE OF BASIC AND APPLIED SCIENCES

HYDROLOGICAL MODELLING OF THE BLACK VOLTA BASIN IN GHANA FOR FLOOD FORECASTING

FELICIA YEBOAH

(10510958)

THIS THESIS IS SUBMITTED TO THE UNIVERSITY OF GHANA, LEGON IN PARTIAL FULFILMENT OF THE REQUIREMENT FOR THE AWARD OF MASTER OF PHILOSOPHY DEGREE IN HYDROGEOLOGY

JULY 2022.

DECLARATION

I, Felicia Yeboah do hereby declare that, this thesis is the result of research under supervision with the exception of cited references from literature towards the award of Master of Philosophy degree in Hydrogeology from the Department of Earth Science, University of Ghana. This work has never been submitted for a degree anywhere else, either in its entirety or in part.

..... Date: 15/07/2022

Felicia Yeboah

(10510958)

..... Date: 27/07/2022

Prof. Sandow Mark Yidana

(Principal Supervisor)

..... Date: 15/07/2022

Ing. Dr Edward Kofi Ackom

(Co-supervisor)

ABSTRACT

The occurrence and devastating impacts of floods have been on the increase in recent times at the global scale. This is probably one of the manifestations of climate change/variability. The Black Volta basin is one of the flood-prone areas in Ghana, and hosts one of the most vulnerable communities in the country. The frequency and severity of these disasters require concerted efforts towards mitigation. There is therefore the urgent need for a decision support system for effective management of floods and related disasters in the basin. The objective of this study is to develop a hydrological model based on existing data, duly calibrated with field observations, for the prediction of flood events and potential high flows in the Black Volta Basin. The outcome and output of this research will prove useful to basin managers, policymakers and disaster management organizations in the basin. In this study, the Hydrologic Engineering Center – Hydrologic Modeling System (HEC-HMS) version 4.5 hydrologic model is used for event based modelling of the Black Volta catchment within Ghana. Firstly, the Spatio-temporal trend of monthly and annual rainfall amount and intensity was analyzed for the basin for the period of 1980 to 2018 using the Mann-Kendal trend test and Sen's slope estimator. On an annual scale, the basin recorded decreasing trend of rainfall amount, while the rainfall intensity showed an increasing trend. With this increasing trend of rainfall intensity, frequency of flooding in the area is expected to increase. In the event-based modeling, the Soil Conservation service (SCS) Curve Number loss approach was used to account for infiltration loss. Direct runoff and base flow were simulated using the SCS unit hydrograph method and the recession method, respectively, and the Muskingum-Cunge model used as channel routing. Calibration of the model was carried out using events in September 1996 and 2007, whiles August–September 1999 and September 2010 event were used for validation. The results yielded an overall NSE value of 0.919 for the calibration and 0.851 for the validation,

indicating a good fit between the simulated and observed discharge. The calibrated model was then applied to forecast the runoffs for 2, 5, 10, 15, 20, 25, 50, 75 and 100 years return periods of rainfall using the 2016 IDF curves developed for the area. The simulated peak flows for 2 to 100 years return periods ranges from 1,568.8 m^3/s to 2375.4 m^3/s at Chache, 3251.7 m^3/s to 5655.0 m^3/s at Bui, and 8677.7 m^3/s to 14941.4 m^3/s at Bamboi station. Comparing these values to historical peak flow values within the basin, it is inferred that the range of predicted peak flows for the return periods have the potential of causing flood. This result forms the basis for characterization of floods in terms of return periods, and subsequent application in flood risk assessment within the basin.

DEDICATION

I dedicate this work to the Almighty God, my family, all my dear friends and the staff at the department of Earth Science, University of Ghana.

ACKNOWLEDGEMENT

I thank God Almighty for His Grace, mercy, provision and protection towards me throughout the study period.

I would like to express my deepest gratitude to GMES and Africa for giving me the opportunity to pursue further studies under the Multiscale Flood Monitoring and Assessment Services for West Africa (MifMass) project RBJ5.

My deepest appreciation goes to my Supervisor Professor Sandow Mark Yidana and co-supervisor Ing Dr Edward Kofi Ackom for their selfless commitment, exceptional guidance, encouragement, support and patience throughout the course of this study.

I am grateful to my family for their love, encouragement and support.

Finally, to the entire staff and lecturers of the Department of Earth Science, University of Ghana, Legon for their academic impartation and support.

TABLE OF CONTENTS

LIST OF FIGURES

LIST OF TABLES

LIST OF ABBREVIATIONS

CMS	Cubic meter per second
CN	Curve Number
IDF	Intensity Frequency Duration
HEC-HMS	Hydrologic Engineering Center- Hydrological Modelling System
HSG	Hydrological Soil group
LULC	Land Use Land Cover
NRCS	Natural Resource Conservation Service
SCS	Soil Conservation service

CHAPTER ONE

INTRODUCTION

1.1 BACKGROUND AND JUSTIFICATION

Climate change has been demonstrated to have a substantial influence on shifting weather patterns in several parts of the world. Global warming is the major contributor to climate change, according to the Intergovernmental Panel on Climate Change's third assessment report (IPCC, 2001). Global warming has led the melting of glaciers, resulting in the washing away of shorelines, flooding, and the eventual drowning of islands (Twumasiwaah, 2016). The frequency and severity of hazardous weather events appear to have increased over the past decade, attending mainly to the effects of climate change, exacerbated by anthropogenic activities (Afriyie et al., 2018). The toll on humanity in the forms of loss of lives and livelihoods, loss or damage to property, amongst others has been immeasurably grave, especially in the low income, third world countries where the general standard of living is low.

It is globally recognized that floods are the most common natural disasters, leading to the largest loss of human life, broad devastation, and impact on social and economic development in both rural and urban areas (CRED, 2019). Flood disasters account for roughly a third of all deaths, injuries, and property damage caused by natural disasters (Wu et al., 2012). Floods and flood-related disasters claim the lives of about 20,000 people each year, leaving people homeless and affecting at least 20 million people throughout the world (Smith et al., 2011).

In Africa, floods are a major regional problem transcending many national borders, and impacting the poor and marginalized groups disproportionately. The situation is usually compounded by the lack of the financial and technological resources to deal with the effects of flooding

(Twumasiwaah, 2016). The situation has prompted several regional studies on various aspects of the hydrology and the implications of climate projections on the standard of lives of the very vulnerable communities in the region. In the West African sub-region, erratic rainfall patterns, manifesting in the forms of contracted rainy seasons and high intensity rain events have led to perennial riverine floods, destroying farms, settlements, and lives (Itiveha & Bigg, 2008).

In August and September 2007, extreme flooding hit large parts of Sub-Saharan Africa between Senegal and Kenya, affecting more than 1.5 million people and resulting in several hundred deaths, the outbreak of infectious diseases such as cholera, and the devastation of agricultural areas (Paeth et al., 2011). According to Itiveha & Bigg (2008), the negative consequences were reportedly exacerbated by the fact that the rainy season in Western Africa began later than usual, resulting in heavy rainfall falling on dry soils, increasing surface runoff and floods along rivers, particularly the Niger and Volta.

In Ghana, floods are the most serious natural hazards in terms of the number of people impacted, fatalities, economic damage, and frequency of recurrence, leading to catastrophes and has a significant impact on people and their livelihoods (Afriyie et al., 2018). Flooding caused about US$ 780,500,000 in economic damage between 1900 and 2014 (Ansah et al., 2020).Also within the last decade, flooding events have been recorded in various regions of the country caused by various factors such as; unplanned urbanization and interference with floodplains, opening of dam gates etc (Twumasiwaah, 2016). According to the National Disaster Management Organization, severe rains and thunderstorms triggered flooding in Ghana's two largest cities between June 18th and 28th, 2018, resulting in 14 deaths, displacement of 34,076, and $168,289 in property damage (Ansah et al., 2020).

The Black Volta Basin has been affected by flooding events attributed to heavy downpours and streams overflowing their channels over the years. Floods occur in the region every year between August and September causing damage to life and property (Judith, 2015). According to Global Water Partnership (GWP) report (2012), thousands of hectares of farmland and properties in the Black Volta Basin have been destroyed by several severe floods between 1991 and 2018. According to Komi et al (2016), within the last two decades, flood fatalities in Black Volta basin, has increased. In September 2007, the Black Volta basin, along with the other sub-basins of the Volta river system in Ghana, was hit by severe rainfall, causing streams and dams to overflow leading to one of the worst floods the region has ever experienced (Ansah et al., 2020). The government of Ghana declared the region a disaster zone in September 2007 due to the severity of the flood (Okyere et al., 2013). More than 35 persons died in three northern regions, and over 12,220 hectares of farmlands were destroyed, as well as 29 Ghana Highway Authority highways totaling 427.4 kilometers, 54 service roads totaling 542 kilometers, and 68 bridges and culverts (Ahadzie & Proverbs, 2011). Also in 2009 , the region experienced torrential rains which led to flooding that caused damage to properties, livestock and destruction of habitat (Ansah et al., 2020). In 2010 also, floods devastated 55 villages, displacing around 700,000 people; 3234 buildings collapsed; 23,588 acres of agriculture were lost; and 1109 domestic animals, including cattle, goats, sheep, and poultry, were destroyed (Afriyie et al., 2018). Between August and September 2018, long duration heavy downpours caused severe flooding in the region, causing about seven (7) deaths and displacement of about 100,000 people, wreaking havoc on farms, roads, and infrastructure, including bridges, and cutting off many towns (NADMO).

Increasing temperatures owing to climate change, as projected by the Intergovernmental Panel on Climate Change (IPCC) AR4 report of 2012, are common along the Black Volta basin, according

to Twumasi et al (2015). This will result in high-intensity short-duration heavy rainfalls which will cause flash floods in communities along the Black Volta (Komi et al., 2016). Hence, it is expected that flooding activities will increase over the years along this region, as supported by Jung et al (2012). In addition, some climate change projections have proposed increasing rainfall intensity in the basin (Jung et al., 2012). This raises a cause for concern. Consequently, adequate understanding of the hydro-meteorological processes, land use and adequate scientific justification to support the meteorological and hydrological causes of flooding within the Black Volta basin is crucial to the development of efficient forecasting tools for early warning, effective monitoring, adaptation and mitigating the adverse effects of flooding in the area. However, these scientific basis and mete-hydrological support to understand the causes of floods for the basin are non-existent.

Hydrologic model–based flood forecasting systems have been regarded as the most effective technique for monitoring, forecasting, as well as mitigation and management of flood hazard. Hydrological modelling has been used effectively in various regions around the world for flood forecasting (Wagener et al., 2004; Setegn et al., 2008; Viviroli et al., 2009; Shen & Chen, 2010; Pechlivanidis et al., 2011; Wu et al., 2012; among others). According to Brocca et al (2011), a good forecast of expected flood levels is required for adequate flood mitigation measures, and the design of permanent measures necessitates the estimation of flood levels for various exceedance probability. Hence, this study will provide a deeper understanding into the hydrological processes operating in the basin, estimate the hydrological response of the basin to rainfall, and also provide scientific basis for adequate decision-making in management, control and mitigation of floods and flood related hazards in the Black Volta basin.

In this study, an Event-based hydrological modelling approach using HEC-HMS software was adopted to simulate hydro-meteorological processes and flood events within the basin, as a means of gaining a better understanding of the hydrological response of the basin for flood monitoring purposes.

This research will be of benefit to local communities within the basin in terms of human safety and environmental protection, through providing an early warning system to mitigate the impact of flooding in the basin thereby safeguarding the lives of people living in the area. Results of this study can also be used by overlaying of flood-prone areas with social and economic hotspots to direct development interventions and determining the best combination of flood risk management from various flood mitigation scenarios. In addition, forecasting of flood events and delineation of flood extent would be beneficial to farmers in identifying areas suitable for planting particular crops. Furthermore, the overall hydrological conclusions can be incorporated into future land use planning and development of various areas within the basin.

1.2 RESEARCH OBJECTIVE

This study sought to perform hydrological modelling to provide the scientific basis for informed decisions on the management of floods and flood-related disasters in the Black Volta Basin.

The specific objectives of the study are the following:

1. Analyse spatio-temporal rainfall trends within the Black Volta Basin.
2. Develop a hydrological model of the Black Volta basin using HEC-HMS to assess the hydrological response of the basin.
3. Apply the hydrological model for flood forecasting.

1.3 THE STUDY AREA

1.3.1 Location and Physical setting

The Volta River basin, which is located in West Africa lies between latitudes 5º 30′ N and 14º.30′ N and longitudes 2º 00′ E and 5º.30′ W. The trans-boundary basin stretches through Mali, Burkina Faso, Côte d'Ivoire, Ghana, Togo, and the Benin Republic, covering an area of roughly 398,370 km^2. About 42% of the basin lies within Ghana, and makes up the downstream part of the basin; about 43% lies within Burkina Faso and the minor parts lies within Togo, La Cote d'ivoire, Benin Republic and Mali (Andah et al., 2014). The Black Volta, White Volta, Oti, and Lower Volta basins, which are minor basins of main tributaries of the Volta River, make up the Volta River basin (Andreini *et al.*, 2000).

The Black Volta basin is located between latitudes 7° 00′ 00″ N and 14° 30′ 00″ N, and longitudes 5°30′100″ W and 1°30′100″ W, with a total area of about 149,000 km^2. The Black Volta Basin accounts for about 38% of the Volta basin system and stretches across four West African countries namely; Burkina Faso, Cote d'ivoire, Ghana and Mali (Adjei *et al.*, 2015). The basin comprises sub-catchment areas which includes; Bamboi, Lerinord, Nwokuy, Dapola and Noumbiel. The basin encompasses nine (26) administrative districts in Ghana (based on the 216 district delineations), fourteen (14) provinces in Burkina Faso, two (2) Departments in Cote d'Ivoire, and three (3) Regions in Mali (Atulley, 2013; Amproche *et al.*, 2020)

The study's focus is on the Ghanaian section of the Black Volta basin, which covers approximately 18,384 km^2 which accounts for about 14% of the Black Volta basin area (Atulley, 2013), and includes portions of the Upper west, Savannah, Bono East, Ahafo, and Brong Ahafo Regions of Ghana. Figure 1.1 shows the location of the Black Volta basin in Ghana.

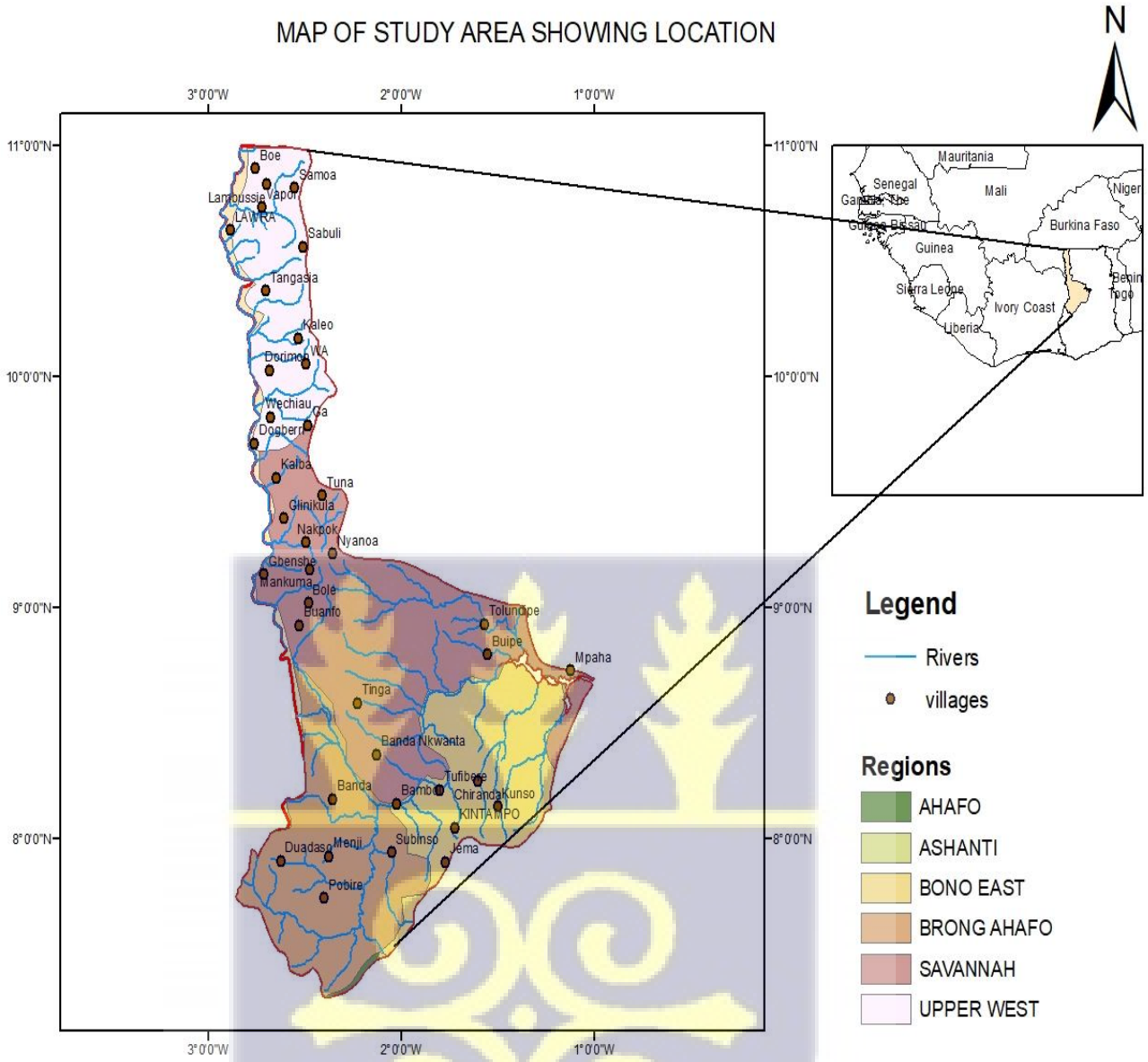

Figure 1. 1: Location of Ghana portion of the Black Volta basin

1.3.2 Climatic Conditions

The Black Volta basin area is characterized by a semi-arid to sub-humid climate (Abdollahi *et al.*, 2017). The basin is made up of Sahel and Sudan savannah in the upper parts, Guinea savannah and transitional zone in the middle sections, and wet semi-deciduous forest in the lower parts. (Atulley, 2013). The climate of the basin is tropical, with an average temperature of 24º C and a double maximum rainfall pattern. The temperature gets as high as 44 °C during the day and drop to 15 °C at night (Atulley, 2013).

The basin's rainfall is highly variable both temporally and spatially. It increases from 400 mm/year in the north to 1500 mm/year in the south, with an average of 1000 mm/year in the northern parts and 1400 mm/year in the south. In most sections of the basin, over 70% of the yearly total rainfall falls in the months of July, August, and September, with little or no rain falling in the months of November to March (Kabo-bah et al., 2014; Shaibu et al., 2012). March and September are the driest and wettest months, respectively (Ofosu, 2016).

1.3.3 Land use and Vegetation

The major land use activity in the Volta basin is agriculture. Bush fallow system is extensively practised. Cassava, yam, maize, beans, sorghum, rice, millet, and groundnuts are among the most major food crops, while vegetables that are grown include cabbage, tomatoes, lettuce and okra (Atulley, 2013). The main tree types in the area include the baobab, shear nut, dawadawa, and neem trees. These trees have long taproots and are able to survive the harsh dry season conditions. Free-range animal grazing is a common practice, with some herders moving to adjacent towns in search of grass and water for their animals. The majority of herders move from Burkina Faso and Mali to the lower portions of the basin in Ghana, and this migration has dire consequences on the host communities, which sometimes leads to conflict between herders and these communities.

Lands in the basin's northern corner are severely deteriorated and can hardly sustain agricultural production. (Adjei *et al*., 2015). A land use map in Figure 1.2 below shows the various land use classes in the Ghana portion of the Black Volta basin.

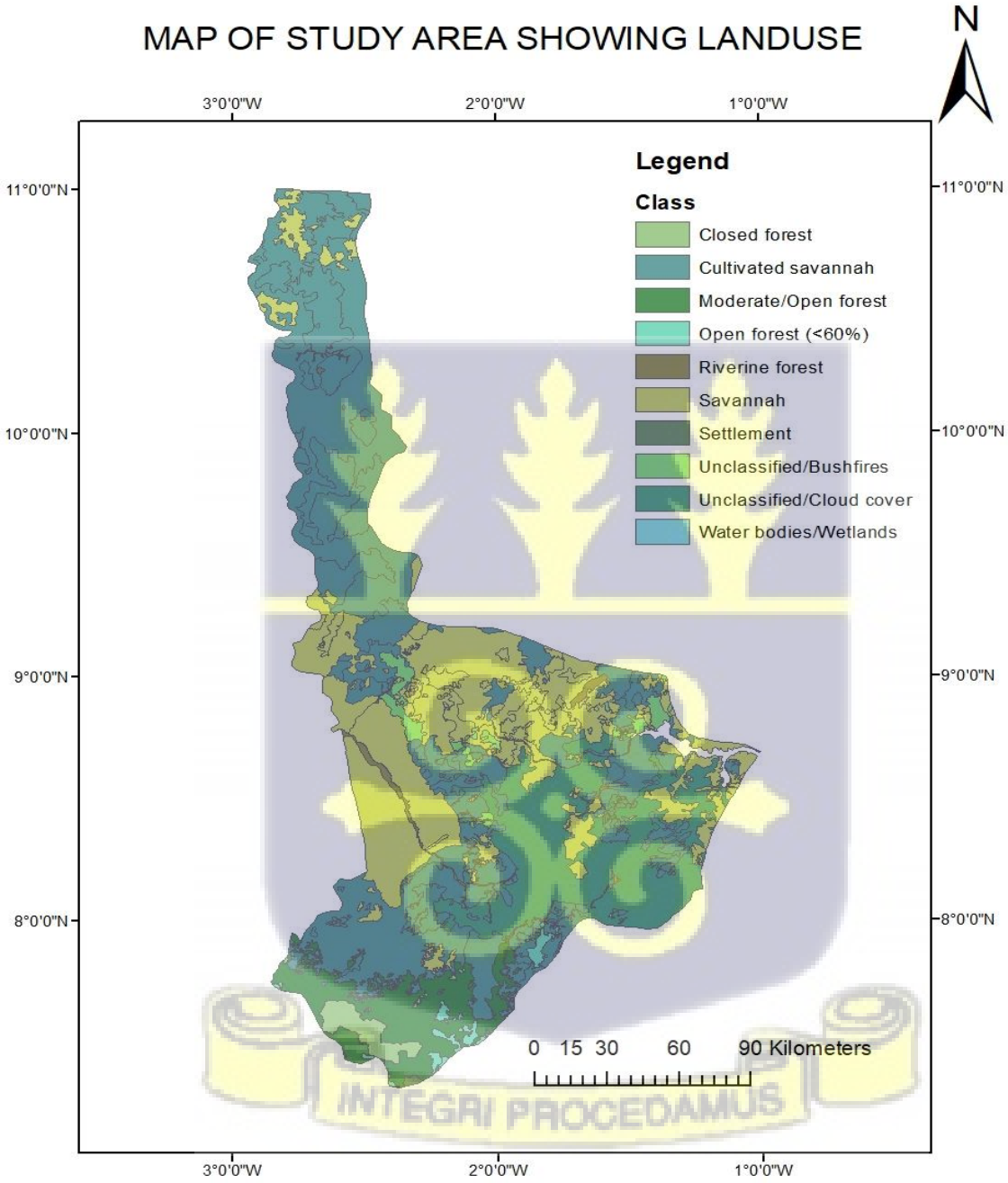

Figure 1. 2: Land use map for the Ghana portion of the Black Volta basin

1.3.4 Relief and Drainage

The Black Volta basin is a relatively flat basin with an average slope of 1.2 percent and elevations ranging from 59 meters above sea level in the south to 762 meters in the north, with an average of 287 meters (Abdollahi *et al.*, 2017). According to Abungba et al. (2020), greater proportion of the Black Volta basin falls within the savannah zone which is undulating with gentle slopes that stimulate overland flow. The average runoff in the Black Volta is estimated at 7 km^3 per annum.

The Bougouriba, Sourou, Gbongbo, Grand Bale, VounHou, Bambassou, Bondami, Wenare, and Mouhoun (main Black Volta) rivers drain the Black Volta basin in West Africa (Atulley, 2013). In Ghana however, its main tributaries are Tain and Poni (Abungba et al., 2020).

The surface flow pattern is controlled primarily by the nature of the topography in the area. The pattern of flow is generally north-south, with a dense network of ephemeral streams which are tributaries of the Black Volta river system. In the south of the terrain, they develop into a dendritic network with a general southward flow pattern. According to Annor (2012), most of these rivers diminish during the dry season, with little or no flow, with only pockets of stagnant water remaining.

1.3.5 Geology, Hydrogeology and Soil

The granitoids of the Cape Coast and Dixcove granites, the Birimian and Voltaian Supergroup, and to a lesser extent the Tarkwaian system make up the geology of the Black Volta basin (Shaibu *et al.*, 2012) as shown in Figure 1.3.

The Brimian system which dominates the northern part of the study area comprises the Birimian metavolcanics and metasediments which is made of metamorphosed lavas, pyroclastic rocks, tuffs,

greywackes, phyllites/schists of different shades, conglomerates and associated Eburnean Plutonic rocks including biotite granite, biotite-hornblende granite and quartz monzonites (Atulley, 2013).

The southeastern part of the study area is underlain by rocks of the Voltaian Supergroup of Neoproterozoic age comprising slightly metamorphosed sedimentary rocks, which includes mudstones, siltstones, sandstones, and conglomerates of a variety of shades. The rocks were affected by the Pan-African tectono-thermal events and are therefore partially metamorphosed.

The Cape Coast granite is made of well-foliated medium grained potash rich muscovite-biotite granites, pegmatites, porphyroblastic-biotite gneisses, aplites and granites (Abungba *et al.*, 2020). The Dixcove (belt) granitoids comprise quartz diorite, tonalite, trondhjemite, granodiorite, admellite, and to a minor extent granite (Ganyaglo *et al.*, 2012). According to (Dramani, 2013), the Tarkwaian formation is of the middle continental origin derived from Birimian and its associated granitic complexes. The formation consists of quartzites, phyllites, schists, grits and conglomerates. Generally, it rests unconformable on the Birimian systems.

The Black Volta Basin is underlain by crystalline basement complex rocks and well-consolidated sedimentary formations that are almost comparable to the crystalline basement complex rocks in terms of their features (Shaibu *et al.*, 2012). These rocks lack primary porosities and are basically impermeable. However, some of these rocks develop secondary porosities due to joints, fractures, faults or weathering. These secondary structures commonly provide room for groundwater storage. The occurrence of groundwater in the Black Volta basin therefore largely depends on secondary porosity. Borehole yield in the basin have been reported to range between 0.1 m^3/h to 36.0m^3/h with a mean yield of 2.2m^3/h (Williams, 2016).

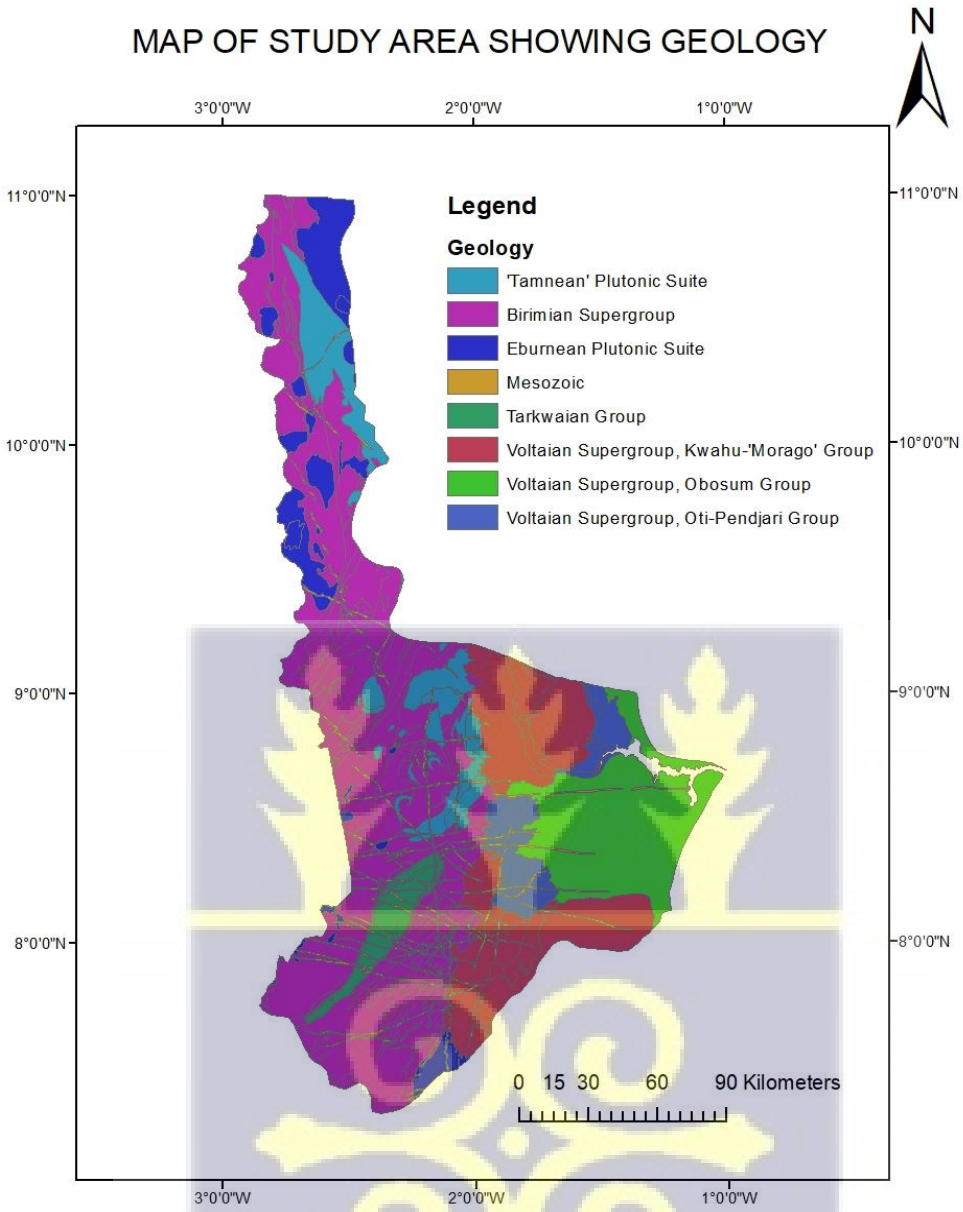

Figure 1. 3: Geological map of the Ghana portion of the Back Volta basin

The basin area is characterized by lixisols, shallow or brashy savannah ochrosols and lithosols which usually develop on steep slopes or have extensive exposures of hard rock and iron-pan (Adjei-Gyapong & Asiamah, 2002; Abdollahi *et al.*, 2017). Savannah luviosols, gleysols, acrisols, arenosols, fluvisols, leptosols, planosols, plinthosols, vertisols ochrosols–rubrisol intergrades, and gleysol–luviosol intergrades are also found in the area (Williams, 2016) as shown in Figure 1.4.

According to Atulley (2013), because of pedogenetic processes (especially clay migration) leading to an organic subsoil horizon, soil types in the Black Volta Basin have a greater clay concentration in the subsoil than in the top soil, and the soils have a primarily light textured surface horizon. They are shallow and poor in soil fertility, as well as weak and coarse-textured, with low organic matter content.

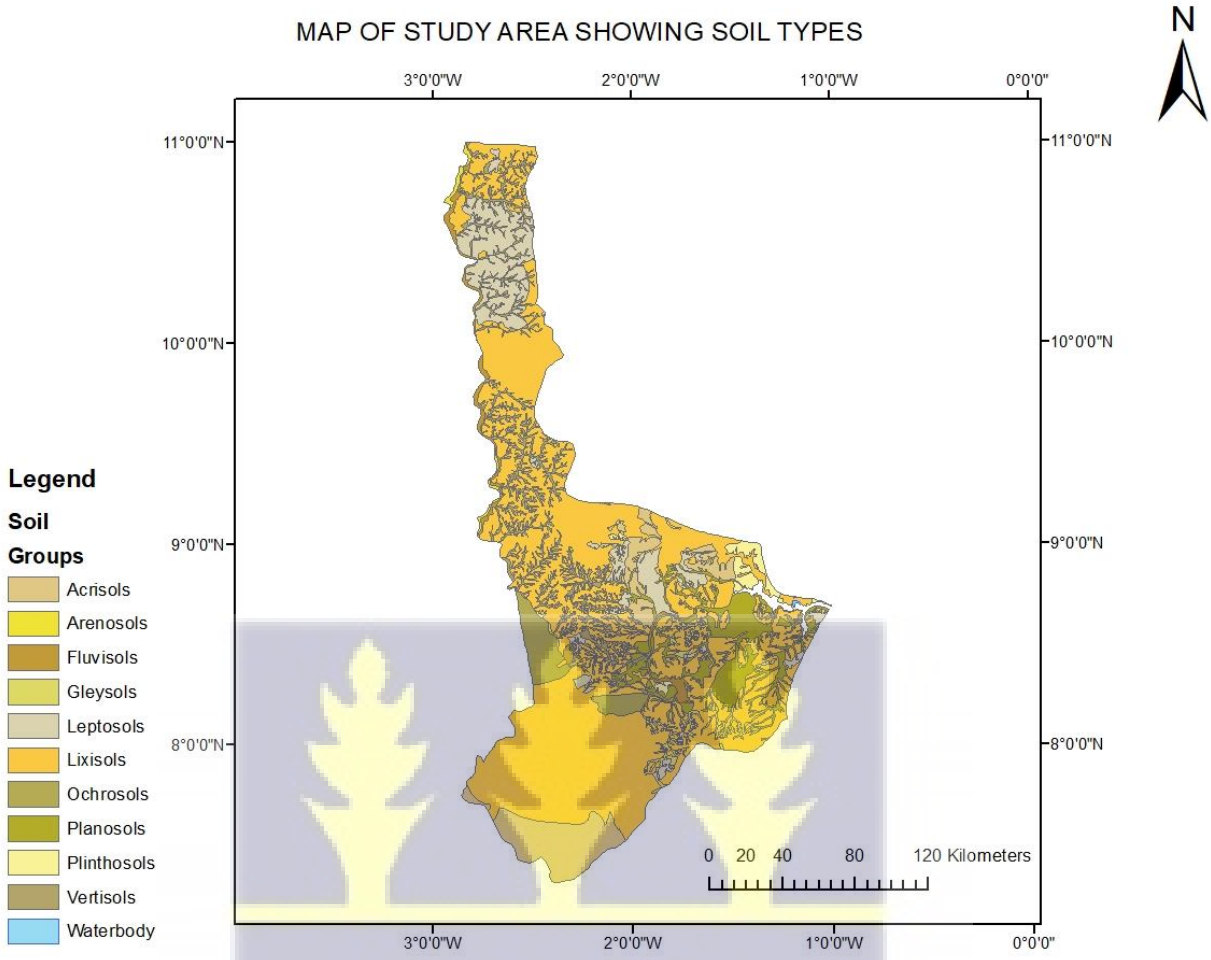

Figure 1. 4: Dominant soil groups in the Ghana portion of the Black Volta Basin

1.3.6 Population and Socioeconomic Activities

According to Atulley (2013), the basin's population was approximately 4.5 million as at the year 2000 comprising residents in Burkina Faso, Ghana, Cote d'Ivoire and Mali; and this is estimated to grow to about 8.0 million by the year 2025. The total population of the basin in Ghana as computed from the 2010 population and housing census data is 1,951,711, comprising 951,582 (48.8%) male and 1,000,129 (51.2%) female. The total population of the Upper West Region as at 2010 stood at 702,110 recording about 18% increase as compared to 576,583 in 2000 (GSS, 2012).

As at 2012, the population density in the basin was ranged from 8 to 133 people/ km^2 with Sissala district having the lowest of 8 people/km^2 and Lawra district the highest of 133 people/km^2, while the average population density was 43 people/ km^2 (Atulley, 2013). In the view of (Barry *et al.*, 2005), people aged between 18 and 40 years from the Black Volta Basin within Ghana mostly migrate to Kumasi and Accra for non-existing jobs while the age groups engaged in active subsistence farming lies between 45 and 60.

1.3.7 Flooding History

Flooding is a serious problem in the Black Volta Basin, which leads to displacement of people, loss of human lives and those of livestock, severe damage to infrastructure, destruction of crops, culminating in large economic losses for communities close to the river (Mul *et al.*, 2015). According to Aziz *et al.* (2019), a massive rainfall in 2007 caused severe flooding in the region which affected about 54,800 people in the river basin in Burkina Faso, Ghana and Togo. Another flooding, which occurred in 2009, also caused a lot of damage to properties, loss of livestock and destruction of the natural habitat.

Flash floods are prevalent along the Black Volta basin, and is caused by increased temperatures and short duration of heavy rainfalls (Twumasi et al., 2015). The Intergovernmental Panel on Climate Change (IPCC) AR4 report of 2012 (Twumasi et al., 2015), predicted that temperatures will keep increasing along the Black Volta Basin which would lead to increased occurrences of flash floods in communities along the basin.

CHAPTER TWO

LITERATURE REVIEW

2.1 OCCURRENCE AND DISTRIBUTION OF FLOODS

Floods are common natural disasters in the world (Mioc et al., 2008). They are costly and responsible for about one-third of natural catastrophes worldwide (Wu et al., 2012). According to Shen & Chen (2010), a flood can be defined as a mass of water, which produces runoff on land that is not normally covered by water. Due to many factors such as but not limited to extreme weather conditions, inadequate disaster response and urbanization, floods have caused enormous damages, affecting human lives and causing austere economic damages all over the world (Jonkman, 2005). Floods have claimed atleast 20,000 lives globally, and has affected at least 20 million people negatively worldwide. Some of the adverse effects of floods include depreciations of social services, economic disturbances, health-related issues, population displacement, injuries and disruption in the food supply chain (Najibi & Devineni, 2018).

The Centre for Research on Epidemiology of Disasters (CRED) report pointed out that the most disastrous flood to have occurred in the world in terms of loss of lives happened in Haiti in 2004 (CRED, 2015). The report indicated that continuous heavy rains caused enlargement of rivers and subsequent overflowing of riverbanks, this generated floods killing over 2,400 people.

Every year, African countries experience heavy downpours due to climate change, resulting in flooding. Fatalities caused by flood has increased radically in Africa over the past half-century (Komi et al., 2016). In 2007, this region experienced intense rainfall, which caused the worst flood the region had encountered in many years. More than a million people were displaced in Uganda, Ethiopia, Sudan, Burkina Faso, Togo, Ghana, Mali and Niger, and about 500 lives were lost

(Baldassarre et al., 2010). Also in September 2009, torrential rains and floods affected about 600,000 individuals in 16 West African nations (Komi et al., 2017).

Flooding in many Ghanaian cities and towns have become the cause of disasters on striking scale. The country has experienced flooding events over the years in different parts, with varying causes such as seasonal rainfall paired with inadequate drainage, garbage dumping into rivers, low elevation of towns, dam overflow and many more (Braimah et al., 2014).

According to Ahadzie & Proverbs (2011), flooding has become an annual problem in Ghana, and the effect of flood events is worsening due to the relatively weak structures in disaster management. The study pointed out that available evidence of flooding history in Ghana, dates as far back as 1936. However, the 1995 and 1999 flooding gained prominence as the country's worst flood disaster in the 1900s.

Between the years 2000 and 2010, about 11 different flooding events occurred in various parts of the country (Mensah & Ahadzie, 2020). The 2007 and 2010 events are considered to have been the most devastating floods to occur between 2000 and 2010 (Ahadzie & Proverbs, 2011). In the 2007 flooding event, the Upper West, Northern and Upper East Regions of Ghana were impacted resulting in over 300,000 people being affected (VBA-WMO-GWP Initiative Volta IFM, 2016). In September 2010, heavy rainfall caused prolonged flooding and the spilling of the Bagre dam, which resulted in loss of 17 human lives, collapse of 3,234 houses from 55 communities, and destruction of farmlands belonging to about 23,588 farmers. About 25,112 people were displaced in the Northern parts of Ghana and 1109 livestock animals were also carried away (VBA-WMO-GWP Initiative Volta IFM, 2016).

Within the recent decade, the country also experienced series of floods in various regions. For example, in May-June 2013, the Kumasi Metropolis reported many deaths due to flooding. The affected areas were Ahinsan Estate, New Site, Aboabo, Anwomaso, Oforikrom and Asuoyeboah (Twumasiwaah, 2016). In 2015, floods and fires wreaked havoc on the Greater Accra region, caused by both natural and human forces. The explosions at a state-owned gasoline station were caused by a cigarette thrown into flood water which had fuel sitting on the top, killing 152 people and destroying property worth millions of dollars (Almoradie et al., 2020). In 2017, Ghana was hit by severe floods that displaced over a million people. Also in 2018, floods triggered by prolonged high-intensity rains combined with water releases from the Bagre Dam in Burkina Faso and destroyed 196 square kilometers of farmland and affected about 100,000 people (Almoradie et al., 2020).

2.2 CLASSIFICATION OF FLOODS

According to Ahern et al (2005), floods can be classified based on the cause of the flood, (e.g intense rainfall, tidal excesses, failure of structures) and the nature of the flood (e.g., consistency, speed of onset, depth and velocity of water, spatial and temporal extent). Turkington et al (2016) stated that, the meteorological conditions of a flood event, such as the amount and distribution of precipitation, as well as antecedent conditions, such as snow depth and soil moisture, could be used to differentiate flood types. However Hall et al (2014) argues that, future forecasts of meteorological triggers, such as heavy precipitation and snowmelt, may differ and change the characteristics of flood types.

Ali (2018), categorized floods based on the place of occurrence, and what causes them into; river floods, coastal floods, urban floods and flash floods.

River flood occurs when the capacity of a river basin is exceeded. As it typically happens seasonally, usually during rainy seasons, river flood is regarded as an anticipated occurrence (Ali, 2018). Continuous rainfall over an apparently long period of time over the same region will cause river levels to rise (Twumasiwaah, 2016). The excess water overflows the banks of the river and runs through nearby low-lying lands (Ali, 2018). River flooding occurs all over the world, claiming many lives and causing extensive damage to property and infrastructure each year (Stein et al., 2020).

The flood that occurs in the coastal regions is known as the coastal flood and it occurs due to the drive of the ocean waters inland (Ali, 2018). According to Demirkesen et al (2007), the Intergovernmental Panel on Climate Change (IPCC) report of 2001 stated that global mean sea-level rise (MSLR) is threatening coastal communities because during the last century, the global mean sea level has risen at a rate of 1 to 2 mm per year. Natural occurrences such as tropical storm, hurricane or extreme low pressure offshore can drive exceptionally high volumes of ocean water to land, resulting in coastal flooding (Ali, 2018). Although sea-level rise is slow, it is significant and accelerating, and even minor amounts of sea-level rise can increase coastal food frequency disproportionately (Taherkhani et al., 2020).

Tectonics, glacial–isostatic adjustment, and subsidence in geologically recent sedimentary deposits such as deltas are all important geologic processes that contribute to relative sea-level rise (Nicholls et al., 2014). Similarly, coastal flooding can also be caused by tidal sea waves occurring due to earthquakes or volcanic activity in the sea (Ali, 2018).

Urban flooding is mostly caused by heavy precipitation and changes in runoff behavior (Ali, 2018). Pavements, roofs, and other impervious surfaces have sealed natural soils, due to urbanization limiting natural infiltration and evapotranspiration and converting rainfall into runoff (Qin, 2020).

According to Jeyaseelan (2003) generated runoff due to rainfall in urban areas, can be as high as six times that of a natural field.

Flash floods are one of the most damaging natural hazards, wreaking havoc on both the natural and built environments (Diakakis et al., 2020). When a large volume of rain water falls within a short period locally and unexpectedly, flash floods occur (Ali, 2018). Flash floods also occur due to sudden extreme rainfall or sudden release of water from a dam (Jeyaseelan, 2003).

Flash flooding is a source of concern in hydrologic and natural hazards science because it ranks first among natural disasters in terms of both the number of people affected globally and the proportion of individual fatalities (Marchi et al., 2010).

As a result of the effects of global climate change on storm-weather systems, and river discharge conditions, the flash flood hazard is expected to increase in frequency and severity in many parts of the world (Marchi et al., 2010). However according to Gruntfest & Handmer (2001), the location, type, and value of human activities are the major contributors to the increasing significance and vulnerability to flash flooding.

2.3 OVERVIEW OF HYDROLOGICAL MODELLING

Runoff, river discharge as well as other hydrological processes within a catchment are affected by factors such as climate, slope, vegetation, soil type, and infrastructure among others. The goal of hydrological modeling is to establish a connection between these factors (Iddrisu et al., 2017).

Hydrological modelling is the use of logical mathematical concepts to describe a complicated hydrologic natural system in a in a simple form (Bergstrom, 1991). In the field of hydrological sciences, hydrologic modelling is critical because, according to Iddrisu et al (2017), most hydrological processes are highly complex, and without modelling, we do not expect to understand

them in depth. Hence, hydrological modelling is useful for understanding hydrological processes and their interactions, quantifying non-measurable hydrological processes and hydrologic forecasting (Jutla, 2006).

Hydrological models of various types have been developed, ranging from black box models that require little basin data to physically based models that require a large amount of basin data (Sampath et al., 2015). Many of these models share a common foundation in their attempt to incorporate the watershed's heterogeneity and the spatial distribution of topography, vegetation, land use, soil characteristics, rainfall, and evaporation (Setegn et al., 2008). The quality of a hydrological model simulation is therefore determined by the underlying model's ability to describe and accurately represent the heterogeneity of hydrological systems at various spatial and temporal scales (Viviroli et al., 2009). Hence, the model selection is based on the goal of the hydrological prediction in the basin (Sampath et al., 2015).

One of the major purposes for hydrological model development has been to learn more about the hydrologic mechanisms that operate in a watershed and how changes in one or more parameters may affect the overall hydrologic process within the catchment (Iddrisu et al., 2017). In addition, hydrological models have been used to produce synthetic sequences of hydrological data for design of structures, water resource planning, development and management and for flood forecasting (Pechlivanidis et al., 2011). According to Pechlivanidis et al (2011), other factors that affect model selection include data availability, spatial representation, computational cost, and model robustness.

Effective hydrological modelling requires a clear understanding of the catchment hydrological cycle (Sakeyo, 2008). The hydrological cycle (Figure 2.1) describes the constant movement of earth's water on, above and below the surface of the earth. Precipitation, which can take the form

of snow, rain, hail, dew, or sleet, is one of the most essential processes for the development of a hydrological model at a catchment scale (Sakeyo, 2008). For the purposes of this research, the form of precipitation that will be considered is rainfall, as it is the main source of precipitation in Ghana.

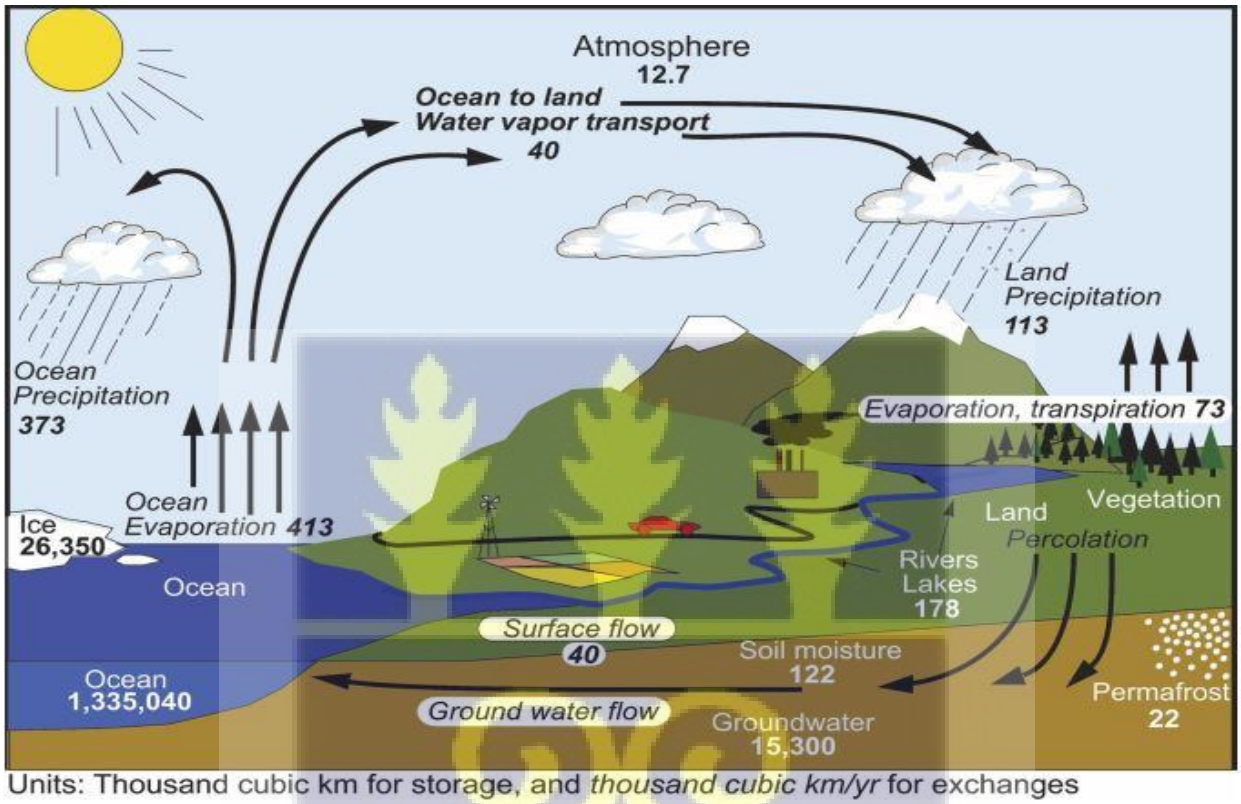

Figure 2. 1: The hydrological cycle. Estimates of the main water reservoirs, given in plain font in 103 km3, and the flow of moisture through the system, given in slant font (103 km3 yr-1) (Trenberth et al., 2007).

2.3.2 Spatio-Temporal Analysis of Rainfall

In Ghana, rainfall is the most significant process for the production of a hydrological model at a basin scale (Sakeyo, 2008). Changes in rainfall can have a big impact on surface water flows (Abungba et al., 2020). Hence, there is a need to evaluate the spatial and temporal trend or distribution of rainfall in a catchment.

According to Quaye-Ballard et al (2020), Ghana has been experiencing fluctuating rainfalls during the last few decades, as a result, rainfall availability has decreased in general. Ghana is one of the climatic variable regions in the West Africa sub-region, with intra-annual, inter-annual, and decadal variations in rainfall. Akpoti et al (2016) stated that, although the causes of rainfall variability are more global in nature, understanding and recognizing historical patterns or trends is essential in order to make better judgments, because changes in rainfall may have a beneficial or negative impact on evaporation over the basin, thereby having a direct impact on stream or river flow.

There are two types of tests in hydro-climatology for finding patterns in time series data like rainfall: parametric and non-parametric tests. For a parametric test, the data used must be normally distributed and independent, whereas for a non-parametric test the data must just be independent (Akpoti et al., 2016). One of the most widely use non-parametric tests used to determine temporal trends in meteorological time series data is the Mann-Kendall trend (Ahmad et al., 2015; Akpoti et al., 2016; Ojo & Ilunga, 2018; Pirnia et al., 2019; Quaye-Ballard et al., 2020; Abungba et al., 2020). The test compares a null hypothesis H_o, which asserts that the series has no trend, against an alternative hypothesis H_1, which assumes otherwise (Aziz & Obuobie, 2017). A statistical test called the Sen's slope estimator is used to estimate the magnitude of the trends (Abungba et al., 2020).

Akpoti et al (2016) used the Mann-Kendall trend test and Sen's slope estimator to examine the temporal variability of rainfall over the Black Volta basin for the period 1976 to 2011. The study revealed an increasing rainfall trend for rainfall stations within Ghana except for Bui station. A similar study was conducted by Aziz & Obuobie (2017), who analyzed trends in observed rainfall data within the Black Volta basin for the period 1981 to 2010. The study revealed a statistically significant (at 5% significance level) increase in the annual rainfall over the period. Abungba et al (2020) also applied Mann-Kendall trend test and Sen's slope estimator to access the rainfall trend within the Black Volta basin for the period of 1961 to 2016. The recorded downward annual rainfall trend for the upstream parts of the Black Volta basin and an upward annual rainfall trend for the downstream parts of the basin.

2.3.3 Land Use and Land Cover

Flood risk and consequences are influenced by land use and land cover (LULC) in a variety of ways (Peel & Blöschl, 2011). Land cover influences different parts of the water balance, such as evapotranspiration, infiltration and interception (Szwagrzyk et al., 2018). Because various crops have varied plant cover, leaf area indices, root depths, and albedo, evapotranspiration rates vary significantly among land use types (De Roo et al., 2001). During a storm, different land cover types have varied interception rates. Land use also has an effect on the infiltration rate of soil water because plant roots and pores generated from soil fauna influence saturated hydraulic conductivity (De Roo et al., 2001). Hence, land use and land cover have a direct impact on the production of runoff from a certain rainfall event (Szwagrzyk et al., 2018). Finally, the land cover in river channels affects hydraulic flow conditions. For instance, woody debris jams on bridges would lead to reduced hydraulic flows (Szwagrzyk et al., 2018).

Afforestation and deforestation, agricultural intensification, wetlands drainage, road development, and urbanization are all substantial changes in land use that affect hydrology (Tali & Kanth, 2013). The intensification of agricultural practices results in the formation of platy dense soil horizons favoring lateral flow, hereby leading to reduced or delayed vertical infiltration in the soils (Rogger et al., 2016) and as a result, an increase in the amount and pace of runoff (Szwagrzyk et al., 2018).

According to Obahoundje et al (2018), the various land cover types found within the Black Volta basin are; forests, woodland, herbaceous savanna, savanna, shrubs, agricultural land, settlements, bare ground and water bodies. However, Amproche et al (2020) classified six types of land cover classes for the Black Volta basin in Ghana. These land cover classes are namely; Closed Savannah, Open Savannah, Agricultural land, Water bodies, Settlements and Bare land. His classification was based on the Ghana LULC classification scheme for visual classification of remote sensing data. Table 2.1 shows the description of the various LULC classes of the Black Volta basin in Ghana as classified by Amproche et al (2020).

Table 2. 1: Land use / land cover Classification of the Black Volta basin (Amproche et al., 2020)

LULC Categories	**Description**
Closed Savannah	These include forest-like regions and reserved areas, as well as gazette forest reserves/protected areas and natural growths, with tree population density exceeding 150 trees per hectare.
Open Savannah	Sacred groves, woodlots, and heavy bushes. Its tree population density ranges from 75 to 150 per hectare.
Cropland	These include areas with agriculture crops.
Water bodies	Rivers, lakes, and dams.
Settlements	Towns, farmhouses and huts.
Bare land	Land that is devoid of trees and vegetation, including mining surfaces.

2.3.4 Classification of hydrological models

There are various classifications of hydrological models found in literature. The specific and similar features of many models make the classification of hydrological models an important issue in order to correctly classify the strengths and limitations of each model (Jajarmizadeh et al., 2012). Various criteria have been used to classify these models. The most popular criteria for which hydrological models have been classified are; processes (simulation) based, scale-based representation and method of solution (Bergstrom, 1991; Dawson & Wilby, 2001; Jajarmizadeh et al., 2012; Gebre, 2015; Duhan & Kumar, 2017).

2.3.4.1 Process based classification

Process based models can be lumped, semi-distributed or distributed (Gebre, 2015). However, based on a description of the process, a model can be deterministic, stochastic or mixed (Dawson & Wilby, 2001) as shown in figure 2.2.

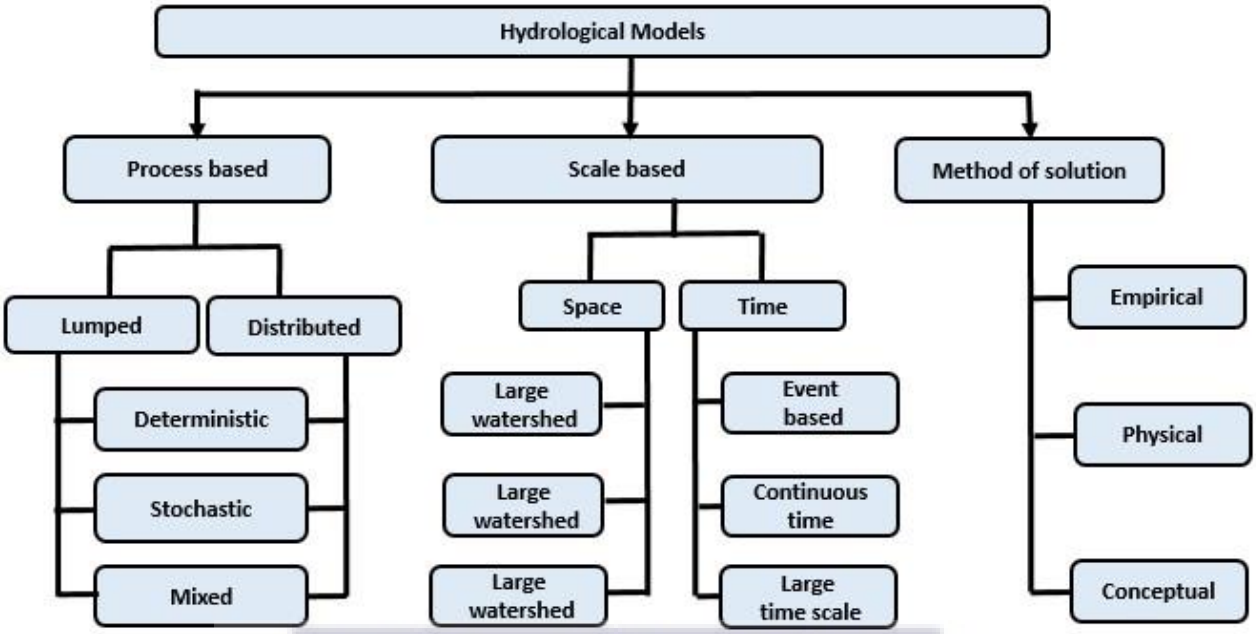

Figure 2. 2: Classification of hydrological models based on process description (Viessman et al., 1989).

a) Distributed, Semi-distributed and Lumped models

The hydrological processes that occur in nature are distributed in the sense that the processes' time and space derivatives are important and form the basis for model classification (Mujumdar & Kumar, 2012). Models that consider space derivatives from point to point are classified as distributed models while those that do not consider space derivatives are called lumped models (Viessman et al., 1989).

The distributed modeling technique aims to combine data on the regional distribution of parameter changes with computational tools to investigate how this distribution affects simulated precipitation-runoff dynamics (Akpoti et al., 2016). Generally, distributed models need large quantities of data for parameterization. A distributed model may also create simulations at interior

sites without explicit calibration, as well as provide streamflow forecasts at interior basin locations when no streamflow observations are available (Kenabatho, 2010).

The catchment is treated as a single unit in lumped (or homogeneous) models as these types of models provide no information about the spatial distribution of inputs and outputs and only simulate the catchment's gross, spatially averaged response (Dawson & Wilby, 2001). Cunderlik (2003) also stated that lumped hydrological models generally use an area-weighted average computational approach and are not necessarily applicable to processes of event scale. A transfer function/hydrograph is the basis of lumped hydrological modeling and the model is used to describe the complex relationship between rainfall and stream flow (Akpoti et al., 2016).

Some models account for spatial variations in some processes while ignoring them in other, by dividing the basin into smaller sub-basins. These are classified as semi-distributed models (Mujumdar & Kumar, 2012). According to Cunderlik (2003), there are two major types of semi-distributed models these are; Kinematic Wave theory models and Probability Distributed models. Kinematic Wave theory models (e.g. HEC-HMS) are models that are simplified versions of the surface and/or subsurface flow equations of physically based hydrologic models. While the Probability Distributed models (e.g. TOPMODEL), are models in which spatial resolution is accounted for, by using probability distributions of input parameters across the basin.

The primary benefit of semi-distributed models is that their structure is more physically dependent than the lumped model structure and that input data is much less demanding than fully distributed models (Akpoti et al., 2016).

b) Deterministic and Stochastic models

Deterministic models produce only one outcome (Alfieri et al., 2020). It does not consider randomness, the same output is always generated by a given input (Kenabatho, 2010). Whereas stochastic models have outputs that are at least partially random and creates a prediction (Viessman et al., 1989). Stochastic models allow for variability in input data, boundary conditions or model parameters, and hence allows for some randomness, difference and uncertainty in the potential results (Kenabatho, 2010). Hence, it is possible to say that deterministic models make forecasts while stochastic models make predictions (Jajarmizadeh et al., 2012). According to Beven (2012), there are some commonalities in the way these models are used. He also stated that, although some have a stochastic error function, many rainfall-runoff models are used in a deterministic manner, while some stochastic models make deterministic predictions. Whether a model structure should follow a stochastic or deterministic formulation depends on the conceptualization of the investigated process (Kenabatho, 2010).

2.3.4.2 Time-scale based classification

Hydrologic models have been classified based on time intervals as continuous models or event-based models.

a) Continuous models

On any time scale, model classification is achieved by considering them as continuous because the processes occur and are modeled continuously (Viessman et al., 1989). Continuous-process models take clear account of all runoff elements, including direct and indirect runoff. They focus on long-term hydrological abstractions that are responsible for the rate of recovery of moisture during non-precipitation times. They are ideal for daily, monthly or seasonal streamflow

simulation, typically for long-term runoff volume forecasting and for water yield estimates (Cunderlik, 2003).

b) Discrete (Event-based) models

Many digital simulation models depend on the need to slice space and time into finite increments and thus qualify as discrete models (Viessman et al., 1989). Discrete models are developed to simulate individual rainfall-runoff events. Their focus is on infiltration and surface runoff, the purpose of which is to assess direct runoff. These models usually have no provision for the recovery of moisture between rainfall events and are therefore not appropriate for dry weather flow simulation (drought analyses) (Cunderlik, 2003).

2.3.4.3 Method of solution based classification

Based on their method of solution, hydrological models have been classified into empirical, physically based and conceptual models.

i) Empirical models

Empirical models rely on observational data-driven methodologies and ignore the hydrological system's features and processes. To reveal the connection between concurrent input and output data streams, they use statistical approaches such as regression and correlation, as well as machine learning techniques. Despite their high predictive capacity, these models are heavily reliant on the training data sets employed and provide few process-related conclusions (Trautmann, 2016).

ii) Physical-based models

Physical-based models on the other hand, are based on basic physical laws. They use quantifiable state variables with physical interpretations for their parameters. Physical-based models, require a

huge number of parameters to reflect the physical properties of the catchment and hence are affected by scale related issues (Trautmann, 2016). Physical models can be further divided into scale models and analog models (Chow et al., 1988). The scale models represent the real system on a reduced scale, while the analog models applies analog technology and similarity concepts (Warren Viessman et al., 1989).

iii) Conceptual models

Conceptual models are intermediate between empirical and physical-based models (Trautmann, 2016). Conceptual models identify the hydrological processes of the entire portion perceived to be of significance as simplistic conceptualizations. This typically leads to a conceptualized system of interconnected storages that are recharged and depleted by the hydrological cycle's acceptable component processes (Sakeyo, 2008) that typically employ mathematically parameterized equations to explain the flow of water between the storages (Kenabatho, 2010). Proper parameters are very essential for this model type and the degree of accuracy is heavily dependent on the proper parameters (Jajarmizadeh et al., 2012). However, when more component processes are used in the model, there is a high probability of over-parameterization. (Sakeyo, 2008).

There are many different conceptual models some of which include: the Stanford Watershed Model (Crawford and Linsley, 1966), the Boughton (1984) model, Modydrolog (Chiew and McMahon, 1994), the Tank model (Sugawara et al., 1983), and Hydrologiska Byråns Vattenbalansavdelning (HBV) (Bergström, 1995) (Sakeyo, 2008).

2.3.5 Model Selection

Several criteria are considered in choosing a hydrologic model. These criteria depend on the type of project, because every project has its own precise requirement and purpose. However, many

hydrologists advocate for models with adaptable structures that can be tailored to 'local' observed conditions (Brocca et al., 2011). According to Cunderlik (2003), some criteria are also dependent on the user, for example, some users have personal preference for particular graphic user interface (GUI), input-output management and structure, computer operation system (OS), etc. However, there are generally four major project dependent criteria that are mostly considered in choosing the appropriate hydrological model. These are:

1. The model should be capable of predicting the variables required by the project, thus the required model outputs important to the project (Cunderlik, 2003).
2. The model should be able to simulate the different hydrological processes that need to be modelled to accurately estimate the desired outputs (Viviroli et al., 2009).
3. All the data inputs needed by the model should be available and accessible within the time and cost constrains of the project, thus data availability (Brocca et al., 2011).
4. The costs of required inputs should be of benefit to the project goals, thus the expenditure should be worthwhile (Cunderlik, 2003).

These criteria were considered thoroughly and the HEC-HMS model was chosen for hydrological modelling of the Ghana catchment of the Black Volta basin in this study.

2.4 HEC-HMS MODEL DESCRIPTION

The Hydrologic Engineering Center—Hydrologic Modeling System (HEC-HMS) model is a deterministic, semi-distributed model, capable of simulating rainfall-runoff and routing hydrologic processes, and it includes both conceptual and empirical methodologies. The United States Army Corps of Engineers (USACE) developed the HEC-HMS model. The program is a modeling system that can represent various basin types (Ibrahim-Bathis & Ahmed, 2016). The HEC-HMS model is widely used to simulate and predict streamflow in humid, tropical, subtropical, and dry watersheds.

The program's hydrographs can be used for flood predictions, water availability analysis, urban drainage design, and reservoir construction, among other things (Ramly & Tahir, 2016). The HEC-HMS can be used for either event-based or continuous modelling of a basin.

i) Event-based model

These models are intended for individual event simulations with a focus on infiltration, evaporation, and surface run-off. The basin reaction to a specific precipitation event is defined by event-based hydrological modeling, which depicts finer scale hydrologic processes (Duhan & Kumar, 2017). An event hydrologic simulation determines total runoff volume, runoff depth, peak discharge and time of peak discharge of a storm event (De Silva et al., 2014).

ii) **Continuous model**

Continuous simulation, which is used for long-term simulation, synthesizes the hydrologic process and number of precipitation events, as well as their cumulative effects, by using effective soil properties to examine soil moisture conditions over a long time period (Duhan & Kumar, 2017). It requires atmospheric data, soil type data, and soil properties data to account for evapotranspiration losses and subsurface hydrological processes (De Silva et al., 2014). Both dry and wet conditions of the watershed within that long lasting time period are incorporated in the continuous simulation process to develop hydrological model can be used to simulate daily, monthly, and seasonal streamflow (Fleming & Neary, 2004).

2.4.1 COMPONENTS OF HEC-HMS MODEL

There are four (4) main components in the HEC-HMS model development. These are the basin model, the meteorological model, the time series model (input data) and the control specifications.

2.4.1.1 Basin model

In modelling applications, the creation of basin hydrological processes is crucial. A significant amount of precipitation returns to the atmosphere through evapotranspiration. Vegetation, land surface, and aquatic bodies all produce evapotranspiration. Some of the precipitation that falls on vegetation, on the other hand, passes through the leaves or runs down stems and branches and reaches the soil before evaporating. Furthermore, some precipitation from land surfaces and water bodies may infiltrate the earth. Separating this complex hydrological cycle into manageable basin paramters yields a basin model of the study area. The HEC-HMS model separates these hydrologic parameters into; canopy storage, soil loss, transform, baseflow and reach routing. These basin parameters are estimated using various methods within the basin model. The basin model also contains other elements, which include reservoirs, sources, and sinks.

2.4.1.2 Canopy Storage methods

Leaves and branches of trees or bushes, as well as grass strains, intercept and capture a portion of the raindrops called canopy storage. Hence, the canopy is a feature of the sub-basin that represents the existence of plants in the area (Ouédraogo et al., 2018). Due to evaporation, the intercepted lot will eventually be lost from the system, leaving just the excess precipitation to proceed to the next phase in the model. The HEC-HMS model has various methods for estimating canopy storage such as; Simple canopy method, Gridded Simple canopy method and Dynamic canopy.

2.4.1.3 Soil loss methods

During a rainfall event, rainwater is lost through processes such as evaporation, interception, infiltration, and depression storage (Tassew et al., 2019). As a result, the losses are classified as both initial and constant soil loss (De Silva et al., 2014).

The HEC-HMS model has a number of methods to calculate soil loss, such as; Deficit and Constant, Initial and Constant, Green and Ampt, Soil Conservation Service (SCS) curve number, Exponential, Smith Parlange and Soil Moisture Accounting soil loss methods (US Army Corps of Engineers, 2010). Among these methods, the deficit and constant approach, as well as the soil moisture accounting method, are designed for continuous simulations, whereas the others are best used for event-based simulations (De Silva et al., 2014).

2.4.1.4 Transform methods

The transform models simulates the direct runoff of excess precipitation on the watershed and convert the excess precipitation into point runoff (Tassew et al., 2019). HEC–HMS incorporates numerous unit hydrograph methods for converting excess rainfall into runoff, including; Clark unit hydrograph method, Kinematic wave method, ModClark method, SCS unit hydrograph method, User-Specified-S graph method, User-Specified unit hydrograph and the Snyder unit hydrograph method (De Silva et al., 2014).

2.4.1.5 Reach Routing methods

The routing model is used to simulate flow from the upstream parts of a basin to the downstream or basin's outlet (Nandalal & Ratmayake, 2010). Flood runoff is attenuated as it passes along the channel reach due to channel storage effects, this reduction is taken into account by the routing models in HEC-HMS. (Tassew et al., 2019). The reach routing methods available in HEC-HMS

are; Lag routing method, Muskingum routing method, Muskingum Cunge routing method, Kinematic-Wave routing method, Modified Puls routing method, Straddle Stagger routing method, Normal depth routing method and Lag & K routing method (US Army Corps of Engineers, 2021).

2.4.1.6 Base flow methods

Water from rainfall events percolates the soil layers into the subsurface and groundwater zones, where it eventually contributes as a base flow to streams within a basin (Obeng, 2005). Five different methods of base flow estimation are available in HEC-HMS as; Bounded recession method, Constant monthly base flow method, Linear reservoir base flow method, Nonlinear boussinesq base flow method, and Recession base flow method (De Silva et al., 2014).

2.4.1.7 Meteorological model

The meteorological model contains the rainfall, snowmelt, shortwave, and evapotranspiration data (Bhuiyan et al., 2017). Various methods within this model are used to compute spatio-temporal distribution of meteorological data over a catchment.

2.4.1.8 Time series model

Time Series model is used to input various time series data types such as precipitation, evapotranspiration, stream discharge, humidity, temperature, wind speed, etc. The application uses multiple gage kinds to isolate distinct types of data and save them in a project (US Army Corps of Engineers, 2021).

2.4.1.9 Control specifications

Control specifications is used for controlling simulations. It consists of a starting date and time, an ending date and time, and a time interval. Different control specifications can be used based on the modeling approach (Ersahin, 2020).

2.4.2 Model Calibration

Most of the parameters used in the conceptual models do not have direct physical interpretation, hence they have to be assessed through calibration using observed data in order to improve the model fit (Lee et al., 2004). Calibration is the process of adjusting parameter values in order to obtain an optimized model performance agreeing to predefined criteria (Kenabatho, 2010). This involves optimization of parameter values by comparing the results of repeated simulations with whatever observations of the catchment response were available at the time (Beven, 2012). The parameter values are modified between model runs, either manually by the modeler or by computerized optimization algorithm until some best-fit parameter set has been found (Beven, 2001).

2.4.2.1 Objective functions

Objective functions are criteria for determining a model's quality of fit (Garcia et al., 2017). In general, the goal of an objective function is to produce parameters in the response surface in order to acquire the greatest or smallest objective function value possible, based on the accepted optimal ranges (Baddoo et al., 2020). The usefulness of an objective function is determined by the goal of the simulation, as well as the time step used in hydrological modeling (Garcia et al., 2017). The various objective functions that are contained within the HEC-HMS model for model quality evaluation are:

1. First lag autocorrelation
2. Maximum of absolute residuals
3. Maximum of squared residuals
4. Mean of absolute residuals
5. Mean of squared residuals
6. Peak-weighed root mean squared error (RMSE)
7. Percent error in peak discharge
8. Percent error in peak volume
9. Nash-Sutcliffe efficiency measure
10. Root mean square error (RMSE)
11. Sum of absolute residuals
12. Sum of squared residuals
13. Time-weighted RMSE
14. Variance of absolute residuals
15. Variance of squared residuals

However, in this study, objective function used to access model accuracy are the Nash-Sutcliffe efficiency measure (NSE), Root Mean Square Error (RMSE), Percent bias (δ_b), Percent Difference in Runoff Volume (V_R) and the Percent Difference in Peak Discharge (Q_P) (Ferreira et al., 2020; Baddoo et al., 2020; Huo & Liu, 2020).

I) The Nash–Sutcliffe model efficiency (NSE)

The Nash–Sutcliffe model efficiency (NSE) is used to measure of how well the simulated and observed hydrographs matched. This is because the NSE is one of the best objective functions for reflecting the overall fit of a hydrograph (Nash and Sutcliffe, 1970), and is one of the most

extensively used metrics for evaluating the performance of hydrological models (Emerson et al., 2005; Lincoln, 2009; Basarudin et al., 2014; Trautmann, 2016; Thapa et al., 2020). The Nash-Sutcliffe model efficiency equation is illustrated below (Nash & Sutcliffe, 1970):

$$\text{NSE} = 1 - \frac{\sum\left(Q_n^{sim} - Q_n^{obs}\right)^2}{\sum\left(Q_n^{obs} - \bar{Q}_n^{obs}\right)^2} \quad \text{.....equation (2.1)}$$

Where, Q_n^{sim} and Q_n^{obs} are the simulated and observed discharges at time step n, respectively. $\bar{Q}_n^{obs}$ is the average observed flow. A value of 1.0 for the NSE coefficient implies that the model output matches the observed measurements. NSE values can range from -∞ to 1 (Bai et al., 2019). A value of 0.70 – 0.80 is considered good; however, the goal is to attain values in the 0.85 – 0.95 range. This objective function offers an overall assessment of the model's ability to capture all aspects of the discharge hydrograph, including peak, volume, timing, and shape (Trautmann, 2016).

II) The Root Mean Square Error (RMSE)

The Root Mean Square Error (RMSE) is the root of the Mean Square Error and similarly expresses the error between simulated and observed data, in the units of the constituent of interest. It ranges from zero (0) to infinity. A value of zero (0) implies that the modelled volume is perfectly suited (Trautmann, 2016). The RMSE is given by (Fleming & Neary, 2004):

$$\text{RMSE} = \sqrt{\frac{(Q_o - Q_s)^2}{n}} \quad \text{.....equation (2.3)}$$

Were Q_o, Q_s, and n are hourly-observed streamflow, hourly-simulated streamflow and number of data points respectively.

III) The percentage bias (PBIAS)

The percentage bias (PBIAS) is a measurement of the modeled data's average tendency to be bigger or smaller than the observation. The ideal value, like RMSE, is zero. PBIAS, on the other hand, is given in percentages rather than the units of the constituent of interest, allowing comparisons between places and seasons with significantly varying values (Trautmann, 2016). It ranges from -100% to 100%, with positive values indicating model underestimation whereas negative values imply model overestimation bias. The percentage bias is expresses as (De Silva et al., 2014):

$$\delta_b = \left| \frac{\sum_{i=1}^{n} (S_i - O_i)^2}{\sum_{i=1}^{n} O_i} \right| \times 100\% \quad \text{.....equation (2.4)}$$

Where O_i, S_i, n and n are observed discharge, simulated discharge and number of data points respectively.

IV) Percent difference in Runoff Volume (V_R)

This percent difference in runoff volume indicates the model's ability to accurately predict total runoff volume. It is computed as;

$$V_R = \frac{V_R^{sim} - V_R^{obs}}{V_R^{obs}} \times 100(\%) \quad \text{.....equation (2.5)}$$

Where V_R^{sim} and V_R^{obs} are the simulated and observed total runoff volume, respectively.

V) Percent difference in Peak Discharge (Q_p)

Percent difference in Peak Discharge (Q_p) is given by the equation below (Ismael et al., 2017):

$$Q_p = \frac{Q_p^{sim} - Q_p^{obs}}{Q_p^{obs}} \times 100(\%) \quad \text{.....equation (2.6)}$$

Where Q_p^{sim} and Q_p^{obs} are simulated and observed peak discharges, respectively. This metric reflects how well a model can reproduce similar peak discharges during a single flood event. Table 2.2 shows a general performance rating for the three recommended statistics.

Table 2.2: General performance rating for recommended statistics (Hussain et al., 2021; Ouédraogo et al., 2018)

SI. No.	Performance Rating	NSE	V_p / (%)	Q_p (%)	PBIAS (%)
1	Very Good	0.75 – 1	< ± 10	< ± 15	< ± 5
2	Good	0.65 – 0.75	± 10 - ± 15	± 15 - ± 30	± 5 - ± 10
3	Satisfactory	0.50 – 0.65	± 15 - ± 25	± 30 - ± 40	± 10 - ± 15
4	Unsatisfactory	< 0.50	> ±25	> ±40	> ± 15

2.4.3 Model Validation

Model Validation is a step that is commonly used to assess the suitability of a chosen model to suitably represent the catchment under investigation. It is a method of demonstrating that a given site-specific model is capable of making suitable predictions for periods outside the calibration period (Kenabatho, 2010). Model validation is normally accomplished by a split-sampling test, in which a data set is separated into two periods of calibration and validation cycles. (Wagener, Wheater, et al., 2004). Klemes (1986) presented a rigorous hierarchical model assessment system with four stages in which the model's ability to predict output is assessed as summarized in Wagener et al (2004):

(i) A split-sample test, in which a data set is split into two halves, with one set used for calibration and the other used to assess the model's performance (validation).

(ii) A proxy basin test, which assesses the model's capacity to predict flow in a hydrologically similar basin. The model is calibrated for one basin in this test, and then verified by running it with data from another basin.

(iii) A differential split sample test in which the two data periods chosen have distinct hydrological properties (e.g. dry and wet periods), i.e. the model is calibrated for dry periods and verified using data from the wet periods.

(iv) A proxy-basin differential split sampling test, i.e. combining tests (ii) and (iii).

2.4.4 Applications of Hydrological models for flood forecasting in the Black Volta Basin

Previous studies have employed various hydrologic model-based systems such as HBV-IWS model, SWAT model and WetSpass-M model among others, to simulate and forecast streamflow, in the BVRB. In this regard, a study conducted by Akpoti et al (2016), used SWAT model to assess rainfall variability impacts along with changes in land use and land cover on streamflow in the BVRB. The results of the study suggested that, SWAT modeling performed well, with relatively high Nash-Sutcliffe Efficiency (NSE) value of 0.83 and 0.9, and coefficient of determination (R^2) values of 0.82 and 0.85 for the calibration for the validation periods respectively. The study concluded that the hydrological model was an invaluable tool in assessing the impacts of rainfall and land use changes on streamflow in the BVRB.

In contrast, a study conducted by Ampofo et al (2021) on investigating how well the SWAT model can be used to predict surface runoff flows in the BVRB, obtained low initial NSE value of -0.02. However, during calibration, the study recorded a satisfactory NSE value of 0.67, with a Correlation Coefficient (R2) of 0.73. The study concluded that, the model performed reasonably well in comparison to observed discharges, however, uncertainties in the model's conceptual framework, as well as a high frequency of missing data gaps, resulted in poor model performance.

Abdollahi et al (2017) used the WetSpass model, which can simulate spatially distributed recharge, surface runoff, and evapotranspiration for seasonally averaged conditions to simulate runoff in the BVRB. The study's findings revealed that the model performed well, and that small changes in rainfall could result in large changes in surface runoff within the BVRB. The model, according to the study, is applicable to medium- and large-sized catchments and can be used as an assessment tool to evaluate the response of hydrological processes to changes in associated hydrological variables.

Furthermore, Kwakye & Bárdossy (2020) investigated the performance of HBV–IWS version (Hydrologiska Byrans Vattenbalansavdelning) in the BVRB in the West African sub-region using a lumped version of the conceptual model. The results of the study revealed that the model performed well, with an average NS of 0.75 for calibration and 0.6 for validation for sub catchments Lawra and Chache, respectively, and it also responds well to precipitation signals. A robust hydrological model for the BVRB, according to the study, would be essential and critical for the proper management of water resources and hydropower in the West African sub-region, as well as for good policy decisions and investments in water-related projects.

Although several studies have been conducted using various models to simulate runoff in the study area, little effort has been made in employing the HEC-HMS model in the Black Volta basin.

2.4.5 HEC-HMS model Applications

Previous studies on HEC-HMS has shown that it can simulate and forecast streamflow using a variety of datasets and basin types. The findings of the model simulation were found to be location specific in the majority of these investigations, with different combinations of a model set incorporating loss methods, runoff transform methods, and base flow separation approaches responding differently.

In a study conducted by Silva et al (2014), HEC–HMS model was used to carry out an event and continuous modelling of the Kelani River basin in Sri Lanka. The model parameters were calibrated using a high rainfall event in November 2005, and the event model was validated using exceptionally high rainfall occurrences in April–May 2008, May–June 2008, and May 2010. The calibrated, direct runoff and base flow parameters were then used in the continuous hydrologic model. For event-based modeling, the Green and Ampt loss method was used to account for infiltration loss, while soil moisture accounting loss method was used for the continuous modeling. The Clark unit hydrograph method and the recession base flow method were used to simulate direct runoff and base flow, respectively. The study concluded that HEC–HMS is capable of accurately reproducing stream flows in the basin, with Nash–Sutcliffe efficiencies of 0.91 for event–based simulations and 0.88 for continuous simulations.

Ramly & Tahir (2016) in a similar study, simulated flood occurrence at the upper Klang–Ampang River Basin, which is a flood-prone area, near the capital city of Malaysia using HEC-HMS model. According to them, the study produced an illustrative and comprehensive representation of the sub-basin with reasonable accuracy indicated by the Nash–Sutcliffe coefficient of 0.86 and Percentage error in peak discharge of 3.2 %.

Another similar study conducted by Skhakhfa & Ouerdachi (2016) used HEC-HMS to model short duration floods for wadi Ressoul in El Berda watershed, northeast of Algeria. Different sets of data were used in the calibration and validation processes (CN, SCS Lag and Muskingum). Evaluation on the performance of the developed flood model derived yielded a correlation coefficient R^2 of 0.87 and the Nash–Sutcliffe efficiency of 0.99.

Ouédraogo et al (2018) in their study used the soil moisture accounting (SMA) loss method in the HEC-HMS model for the continuous modeling of stream flow in the Mkurumudzi catchment in Kenya. Data from 1988 to 1991 was used for calibration and 1992 to 1995 for validation at a daily time step. Calibration results showed a good model performance with a coefficient of determination R2 = 0.80, Nash-Sutcliffe Efficiency NSE = 0.80.Similarly, the model performance for the validation period was good, with R2 = 0.67 and NSE = 0.65. They concluded that the HEC-HMS model gave a satisfactory prediction of stream flow in the Mkurumudzi Catchment.

Tassew et al (2019) simulated surface runoff of various rainfall events using the HEC-HMS for the Gilgel Abay Catchment, Upper Blue Nile Basin, Ethiopia. The Soil Conservation Service Curve Number (SCS-CN), Soil Conservation Service Unit Hydrograph (SCS-UH), and Muskingum methods were employed to account for the soil loss, transform, and reach routing, respectively. Sensitivity analysis results showed that the curve number is the sensitive parameter. In addition, the model validation results gave a reasonable difference in peak flow of 1.49% and relative difference in peak volume of 2.38%. The model's performance (NSE = 0.884) and correlation (R^2 = 0.925) and comparison of actual and simulated hydrographs, demonstrated that the model it is suitable for hydrological simulations in the Gilgel Abay Catchment.

2.5 APPLICATION OF INTENSITY-DURATION-FREQUENCY (IDF) CURVES IN FLOOD FORECASTING

Rainfall data from a single site on the watershed, taken at a single rainfall gauge, is usually reported as depth in millimeters or intensity in millimeters per hour. This type of rainfall data is more valuable if it can be statistically linked to two additional rainfall variables: duration and frequency (Mahdi & Mohamedmeki, 2020).

Chow (1953) highlights the relationship between rainfall intensity, duration, and frequency. According to him, the intensity is the ratio in millimeters of precipitation to duration in an hour, measured in millimeters per hour. According to Mahdi & Mohamedmeki (2020), it is worth noting that the duration does not always imply the entire duration of the rainfall event, but every rainfall event can be segmented and analyzed for a specific range of durations as needed.

Frequency is the inverse of the return period. A return period is a popular representation of rainfall frequency. If an annual maximum rainfall event has a T-year return period, it means once every T years on average, the rainfall amount is equalized in value (Mahdi & Mohamedmeki, 2020).

The rainfall intensity duration frequency curves (IDF) show how rainfall intensity I, duration D, and return period T are related for a given location (Ewea et al., 2018). According to Mahdi & Mohamedmeki (2020), the rainfall IDF curves are a graphical representation of the likelihood of a specific rainfall intensity, duration, and return period with similar features occurring.

Civil engineers and hydrologists use the IDF curves to produce design storms (DS) or theoretical storms that are required in the construction of hydraulic projects of a given watershed. These design storms are used to compute the peak runoff in order to construct safe and cost-effective flood mitigation and flood control structures (Ewea et al., 2018). Hence, the application of rainfall

intensity-duration frequency (IDF) curves, as significant factors in hydrological modeling, is crucial for flood estimation (Ghazavi et al., 2017).

Ghavasieh & Norouzi (2009) used IDF curves to create design storms for flood forecasting in the Madarsou basin in Iran. HEC-HMS model was used to simulate runoff for the design storms using various return periods. Their results showed that the 10-year return period IDF curve deduced very close forecasted to observed flood peaks for the region. It was concluded in the study, that IDF curves could be used in the forecasting component of Flood Warning System.

IDF curves developed by Dankwa in 1974, using rainfall data that was available at the time were used in Ghana to create drainage infrastructure in various cities. These IDF curves were created on the assumption that the rainfall data was stationary. Meaning that, climate trends and variability, have no effect on the curves (Abubakari et al., 2017).

However, climate variability has had significant effects on rainfall in Ghana, both increases and declines, have been observed in several parts of the country (Asante & Amuakwa-Mensah, 2015). Hence, there was the need to revise and update the IDF curves for Ghana. In 2016, the Ghana Meteorological Agency (GMet) in collaboration with the Council for Scientific and Industrial Research-Water Research Institute (CSIR-WRI) developed a new IDF curve for various stations within the country, which is now used by Engineers and Hydrologist for flood mitigation and development of flood control structures.

CHAPTER THREE

RESEARCH METHODOLOGY

In order to achieve the set objectives of this study, this research was carried out in three stages: desk study, data collection, and data processing and analysis. Desk study involved gathering and review of relevant material by authors with extensive experience in the study field. Data collection involved the acquisition of field, temporal, spatial and other ancillary data and careful research for a thorough and consistent analysis. The data processing and analysis involved the use of various software for processing and analysis of acquired data.

3.1 DESK STUDY

Electronic searches, journals, applicable textbooks and papers were used to conduct a literature review on relevant topics. Previous studies on the Black Volta basin, as well as similar works from other parts of Ghana and other nations, were also reviewed. Documented papers on the various procedures and steps necessary to achieve the set aims and objectives of the study were reviewed. Shape files on maps of the hydrology of the study area were also obtained and examined.

3.2 DATA COLLECTION

Rainfall data, time series discharge data, Digital Elevation Model (DEM), soil types, and landuse/land-cover data of the research area are the essential data necessary for hydrologic models. These data sets were obtained and gathered from different sources as shown in table 3.1. They were analyzed and modified so that they could be used as input to the models properly. Daily precipitation data for 1961 to 2018 periods for the catchment was obtained from Ghana Meteorological Agency. The stations considered were Bamboi, Bole, Buipe, Lawra, Damongo, Bui, Wenchi, Sunyani, Kintampo, Babile and Wa because these stations were the only stations

within the catchment with available rainfall data. The rainfall data was found to contain missing data for some periods in some stations, and hence this study considered rainfall data for stations for the period 1980-2018.

Daily discharge data for the 1964 to 2018 periods was obtained from the Hydrological Services Department Ghana. The discharge stations considered were Bamboi, Bui, Bole (chache) and Lawra. However, discharge data from 1980-2018 was used in this study in order to correspond to the daily rainfall data.

Daily evapotranspiration data for Wa and Bole for the periods of 1980 to 2018 was used in this study. The data was provided by the Ghana Meteorological Agency. Evapotranspiration data for only these two towns were available.

Table 3. 1: Data types collected and sources

S/No	SOURCE	DATA TYPES
1.	Ghana Meteorological Agency	Daily Rainfall Data (1980-2018), Evapotranspiration (1964-2019) and IDF curves
2.	Hydrological Services Department (Ghana)	Daily Stream Discharge Data (1960-2019)
3.	USGS Earth Explorer (http://www.usgs.gov/)	Digital Elevation Model (DEM)
4.	International Council for Research in Agroforestry (ICRAF) (http://landscapeportal.org/)	Soil Map
5.	GMES and Africa project's database	Geology maps
6.	USGS Global Visualization Viewer (USGS GLOVIS) (http://glovis.usgs.gov/).	Landsat (ETM+) satellite images (2020)

3.3 PROCESSING AND ANALYSIS

3.3.1 Spatio-Temporal Rainfall Trends within the Black Volta Basin

Assessment of rainfall variability within the Black Volta basin in Ghana is a crucial part of this study. Available daily rainfall data from Wa, Bui, Bole, Damongo, Wenchi, Sunyani and Kintampo rain gauge stations from 1980-2018 within the Black Volta basin in Ghana was used to achieve this objective. Figure 3.1 provides a summary of the methods used to obtain results for this objective in a systematic manner.

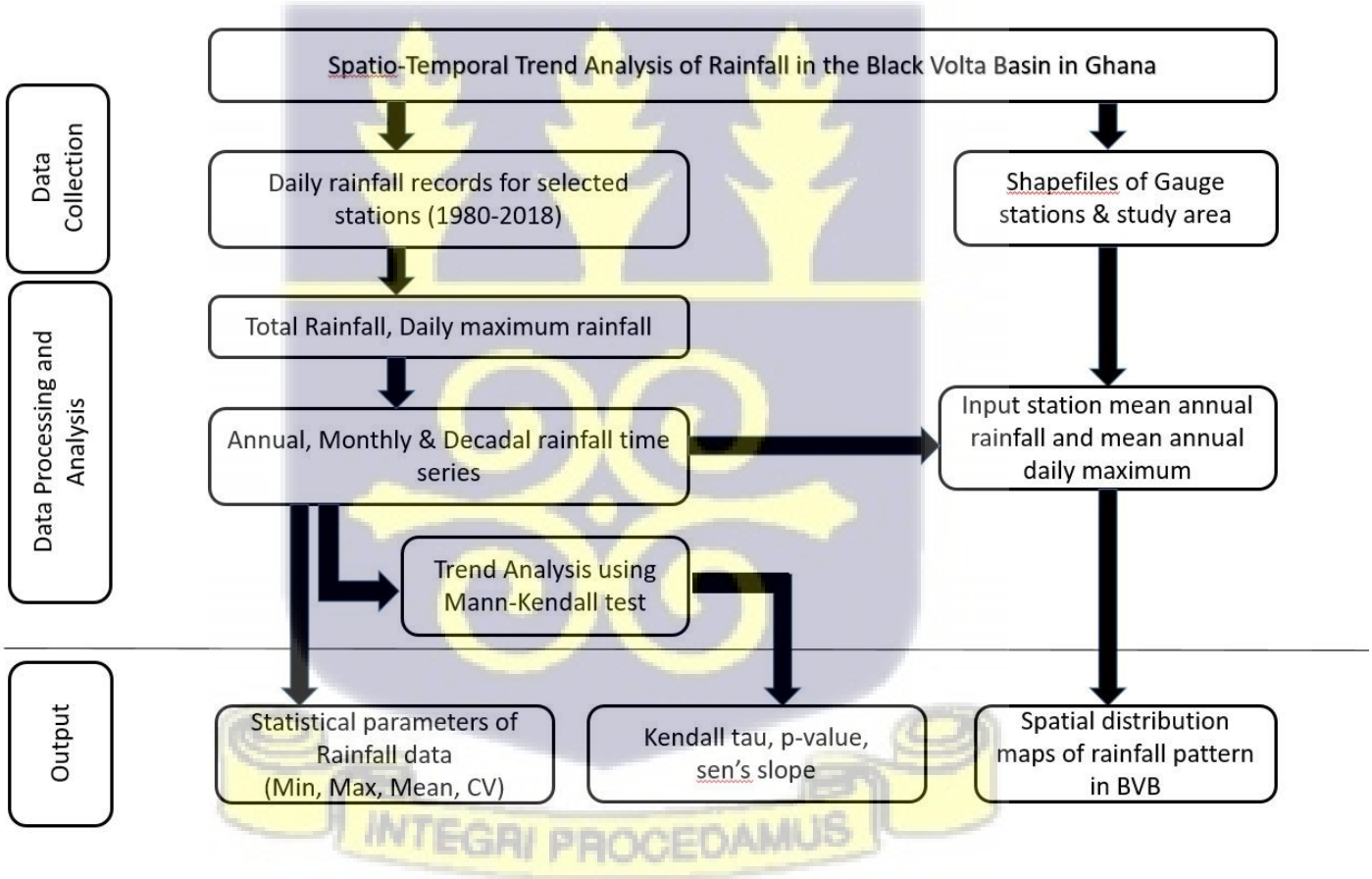

Figure 3. 1: Flow chart of Spatio-temporal analysis of rainfall

3.3.1.1 Temporal rainfall Trend Analysis Using Mann-Kendall Trend Test and Sen's Slope Estimator

Mann-Kendall trend test and the Sen's slope estimator were used to detect statistical parameters and possible temporal trends of rainfall in the basin, and the statistical significance of these trends.

The rank-based Mann–Kendall test (Mann 1945; Kendall 1975) is a non-parametric statistical method recommended by the World Meteorological Organization (Ojo & Ilunga, 2018; Pirnia et al., 2019; Ahmad et al., 2015) to determine temporal trends in meteorological data. The benefits of using this test is that it is not necessary for data to be normally distributed and also, the presence of outliers in the data or inhomogeneous time series has no impact on the test results.

The null hypothesis (Ho) asserts that there is no trend in time series data over a particular period, and it is compared to the alternative hypothesis (H_1), which assumes that there is a rising or falling trend in time series data over that period (Quaye-Ballard et al., 2020). The theoretical calculation of the Mann-Kendall statistic S is given by (Abungba et al., 2020):

$$S = \sum_{i=1}^{n-1} \sum_{j=i+1}^{n} Sgn(x_j - x_i) \quad \text{.....equation (3.1)}$$

Where n is the number of data points, x_i and x_j are the data values in time series i and j ($j > i$).

$Sgn(x_j - x_i)$ is the sign function defined as (Abungba et al., 2020):

$$Sgn(X_j - X_i) = \begin{cases} -1, & if\ x_j - x_i < 0 \\ 0, & if\ x_j - x_i = 0 \\ +1, & if\ x_j - x_i > 0 \end{cases} \quad \text{.....equation (3.2)}$$

The variance of the statistic S, V(S) as (Ackom et al., 2020):

$$V(S) = \frac{n(n-1)(2n+5) - \sum_{i=1}^{g} e_i(e_i-1)(2e_i+5)}{18} \quad \text{.....equation (3.3)}$$

Where n is the number of data points, e_i is the number of existent ties up to sample i.

The test statistic (t) is standardized, and the significance is also estimated by equation 3.4 as follows (Quaye-Ballard et al., 2020):

$$Z = \begin{cases} \frac{t-1}{\sqrt{v}} \rightarrow t > 0 \\ 0 \rightarrow t = 0 \\ \frac{t+1}{\sqrt{v}} \rightarrow t < 0 \end{cases} \quad \text{.....equation (3.4)}$$

Ho is accepted if $|Z| \leq Z_1 - \alpha/2$, otherwise H_1 is accepted at a significant level.

The Sen's slope estimator (Q) is used to evaluate the degree of trend in a time series. A declining trend is indicated by a negative Q, and vice versa. Q is computed as follows for a given time series (x) of length N, where x_i and x_j are observation values at the ith and jth timescales, respectively (Quaye-Ballard et al., 2020):

$$\boldsymbol{Q_i = x_i - x_j / i - j} \quad \text{.....equation (3.5)}$$

Where i = 1, 2, 3…….*N*

The Q value is calculated N times and rearranged in ascending order. If N is odd, Eq. 3.6 is used to find the median of Q, but if N is even, the median of Q is computed using Eq. 3.7

$$\mathbf{Q_{med} = Q[N + 1]/2} \quad \text{.....equation (3.6)}$$

$$\mathbf{Q_{med} = Q[Q_{N/2} + Q_{N+2/2}]/2} \quad \text{.....equation (3.7)}$$

3.3.1.2 Spatial rainfall trend

Shape files of gauge stations and study area, as well as the mean annual rainfall amounts and the mean annual daily maximum rainfall (intensity) was used to examine the spatial distribution of rainfall. The Inverse distance weighing interpolation technique (IDW) within the ArcGis 10.2 software was used to obtain the results for the analysis of spatial variation of rainfall within the study area.

3.3.2 Hydrological Modelling of the Black Volta Basin

3.3.2.1 Land Use and Curve Number Map of the Black Volta Basin

Satellite image and ancillary data of the study area for 2020 were acquired for the land use classification. The 30m resolution Landsat-Enhanced thematic mapper (ETM+) satellite images were obtained from the USGS Global Visualization Viewer (USGS GLOVIS) platform (http://glovis.usgs.gov/), and standard radiometric and geometric corrections were performed. Fourteen (14) scenes were needed to cover the entire Black Volta basin. The scenes correspond to the following Path/Row: 194/054, 195/055, 195/054, 195/053, 195/052, 195/051, 196/054, 196/053, 196/052, 196/051, 196/050, 197/053, 197/052, 197/051. Figure 3.2 provides a summary of the methods used to obtain results for this objective in a comprehensive and systematic manner.

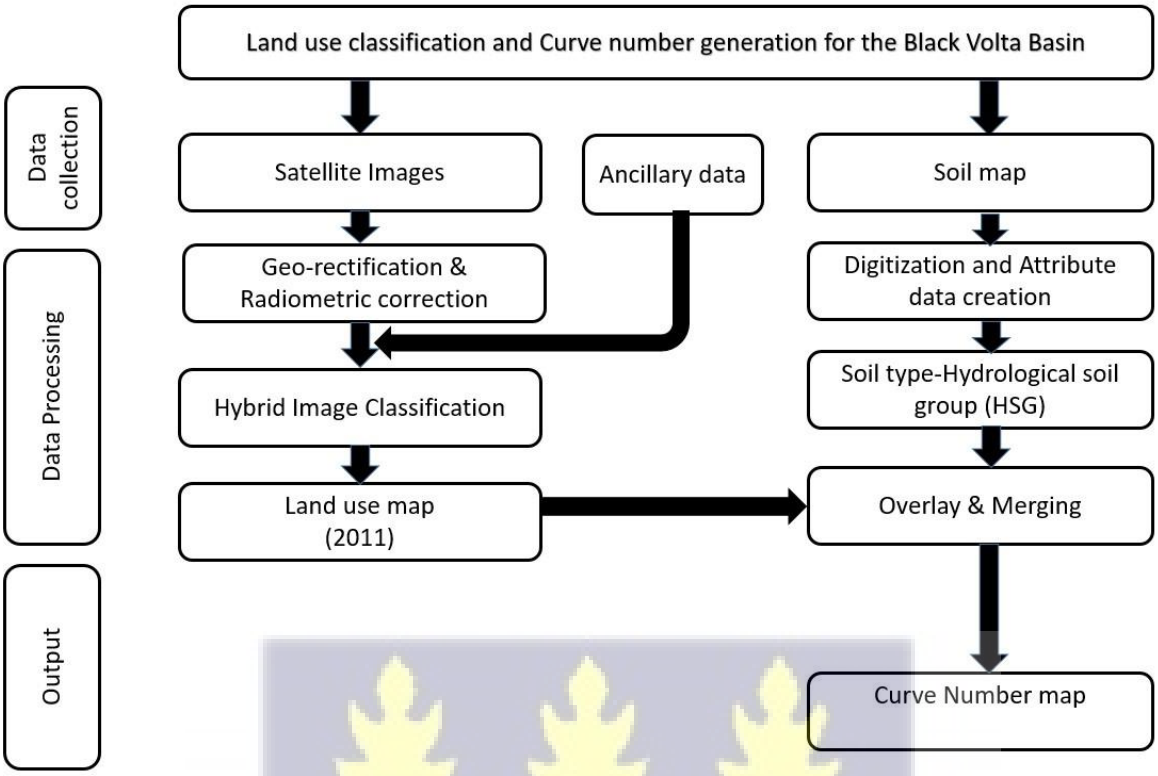

Figure 3. 2: Flow chart for land use classification and curve number map preparation

3.3.2.1.1 Image classification and Land use Map creation

Each band file is provided unlayered in GeoTIFF output format, hence the downloaded band files were layer stacked in ERDAS Imagine software for analysis (Kim, 2016). The images were georeferenced to the research area's coordinate system, which is WGS 1984 projection; UTM Zone 30°N. The Earth's atmosphere is made up of a variety of gases, liquids, and solid particles, the majority of which are optically active and cause absorption, diffusion, and scattering. The emergent radiation from the Earth surface–atmosphere system in the sensor observation direction is the signal detected at the satellite. The radiance measured at sensor is known as Top of Atmosphere (TOA) radiance (Kantakumar & Neelamsetti, 2015). Atmospheric correction was

performed on the images to convert the top of atmosphere radiance of objects to the near surface reflectance.

To determine the multi-temporal land use classification of the study area for the year 2011, a hybrid methodology was employed which combines the maximum likelihood supervised classification technique, decision tree approach, and unsupervised classification method.

Firstly, the atmospherically corrected individual satellite pictures were classified using a maximum likelihood supervised classification approach to map the land use classes at a specific point (dry and wet periods) across time. The outputs were refined and integrated into a multi-temporal categorized image using a knowledge-based decision tree approach. When recognizing theme classes based on spectral properties of remote sensing data is difficult or insufficient, the decision tree approach comes in handy. Then an unsupervised classification approach, which is the identification of natural groups within multispectral data was further applied to identify various vegetation cover types. No prior knowledge of the study area is required for the unsupervised classification technique. This strategy is completely data-driven and objective. Unsupervised categorization, even for a well-mapped area, may uncover spectral patterns that were previously undetectable (Kantakumar & Neelamsetti, 2015).

The classification was carried out in relation to previously known land use types in the basin. Land use and land cover classes were chosen or identified in five (5) categories: Water bodies, bare land, settlements, forests and vegetation. Table 3.2 Shows the description of these land use classes. Google Earth was used to verify the classification because it allows for a better visual representation of land cover categories on the ground. The classified image was used to create the land cover map of the study area.

Table 3. 2: Land use classification scheme and description

LULC	DESCRIPTION
Settlement	Areas covered with both towns; urban and rural settlement
Vegetation	Regions covered with primarily small household mosaic agricultural farms, cultivated land and cultivable land, as well as grasses or bushes, and areas covered with adequate trees and shrubs that are widely spaced
Bare land	Areas devoid of vegetation and tree cover
Forest	Area with high density of trees and shrubs with little or no disturbance
Water	Area which holds water (lakes), rivers and marshy land

3.3.2.1.2 Accuracy Assessment

Accuracy assessment involves the comparison of the categorized data to the reference data for the same sites (Kantakumar & Neelamsetti, 2015). Land classification can be subjected to errors caused by geometric errors, misclassifications and undefined classes. A random selection of pixels from the categorized maps was is to create an error matrix or confusion matrix to statistically quantify these inaccuracies (Obahoundje et al., 2018). The error matrix is the standard way of presenting results of the accuracy assessment (Kantakumar & Neelamsetti, 2015). Error matrices include: total accuracy, producer's accuracy, omission error, user's accuracy and commission error (Obahoundje et al., 2018). Kappa coefficient is also another measure of agreement or accuracy that can be used to see if a land-cover map created using remotely sensed data is significantly better than one created by randomly assigning labels to locations (Kantakumar & Neelamsetti,

2015). For this study, the Kappa coefficient, the user's accuracy and the producer's accuracy were used for accuracy assessment.

A) The producer's accuracy

This is the percentage representation of the total number of accurate pixels in a category divided by the total number of pixels in that category as established by reference data. In other words, the measure of omission error and the probability of a reference pixel being properly classified (Obahoundje et al., 2018).

B) The User's accuracy

The user's accuracy is the ratio of the total number of accurate pixels in a category, to the total number of pixels classified in that category, using classified data. It is the likelihood that a pixel labeled on a map or image corresponds to that category on the ground.

C) Kappa Coefficient

The Kappa coefficient is a measure of an error matrix's overall statistical agreement that considers non-diagonal factors. Kappa analysis is a popular method for analyzing a single error matrix because it shows the likelihood of successful classification after removing the possibility of incorrect classification by chance (Kim, 2016). The Kappa coefficient is given by the equation (Obahoundje et al., 2018):

$$K = \frac{N\sum_{i=1}^{r} x_{ij} - \sum_{i=1}^{r}(x_{i+} \times x_{+i})}{N^2 - \sum_{i=1}^{r}(x_{i+} \times x_{+i})} \quad \text{.....equation (3.8)}$$

Where, N is the total number of observations, r is the number of rows in the matrix, x_{ij} is the number of observations in row i column j, x_{i+} and x_{+i} are the marginal total of row i and column j

respectively (Amproche et al., 2020). Kappa coefficient, K ranges from zero (0) to one (1), with 0 to 0.40 representing poor accuracy, 0.40 to 0.80 representing moderate accuracy and K greater than 0.80 represents strong accuracy (Obahoundje et al., 2018).

3.3.2.1.3 SCS Curve Number map preparation

The ArcGIS 10.2 software was used to prepare the curve area map of the study area using the land cover map, DEM and Soil data for the study area. Firstly, the original land cover classification was reclassified into four (4) categories; water, medium residential, forest and agricultural. The soil data for Ghana was obtained from http://landscapeportal.org/ and digitized. Hydrological soil group codes (A,B,C,D) were assigned to various hydrological soil types within the soil data. Soil infiltration rates vary greatly and are influenced by both subsurface permeability and surface intake rates. The hydrological soil groups categorize soils based on their minimum infiltration rate, which is determined following extended wetting of bare soil (SDA Conservation Engineering Division, 1986). A new attribute for each polygon within the soil data was created to account for the percentage of each soil group present. The soil and land use data were then merged to create polygons that have both soil and land use information. A curve number look up table (Figure 3.3) was created within the geodatabase to allow the system assign curve numbers to various polygons within the merged soil and land use data. The curve numbers for the CN look up table was obtained from SCS TR55 (1986).

Analysis tools in ArcToolbox was used to merge the soil-land use data to the curve number look up table. HEC-GeoHMS was then used to create a curve number grid for the area. The CN grid was used to create the curve number map of the study area.

Table

CNLookUp

OBJECTID *	LUValue	Description	A	B	C	D
1	1	Water	100	100	100	100
2	2	Medium Residential	57	72	81	86
3	3	Forest	30	58	71	78
4	4	Agricultural	67	77	83	87

1 (0 out of 4 Selected)

CNLookUp

Figure 3. 3: Curve number look up table

The idea of curve numbers represent the continuous rainfall losses after the initial abstraction has been exceeded. The Soil Conservation Service (SCS), now known as the Natural Resource Conservation Service (NRCS), established a curve number (CN) to measure the amount of rainfall that infiltrates into the soil and the amount of surface runoff (Shukur, 2017). Table 3.3 shows the various curve number values assigned to various land use types and hydrological soil groups as established by the NRCS. The curve numbers range from roughly 30, indicating that the soil and land use with very high infiltration rates and 100, which acts as water where all precipitation becomes runoff (Rimfors & Velichkin, 2015).

Table 3. 3: Runoff curve numbers for rural and urban areas (NRCS, 1986)

Land Use description	Curve Numbers for Hydrologic Soil Group			
	A	B	C	D
Fully developed Urban areas (vegetation established)				
Lawns, open spaces, parks, golf courses, cemeteries, etc.				
Good condition: grass cover on 75% or more of the area	39	61	74	80
Fair condition: grass cover on 50% to 75% or less of the area	49	69	79	84
Good condition: grass cover on 50% or less of the area	68	79	86	89
Paved parking lot, roofs, driveways, etc.				
Streets and roads	98	98	98	98
Paved with curbs and storm sewer (excluding right-of-way)	98	98	98	98
Gravel (including right-of-way)	76	85	89	91
Dirt (including right-of-way)	72	82	87	89
Paved with open ditches (including right-of-way)	83	89	92	93
Average % Impervious				
Commercial and Business areas	89	92	94	95
Industrial areas	81	88	91	93
Row houses and residential with lot size 0.05 or less	77	85	90	92
Residential: average lot size				
0.10 ha	61	75	83	87
0.14 ha	57	72	81	86
0.20 ha	54	70	80	85
0.40 ha	51	68	79	84
0.81 ha	46	65	77	82
Developing urban areas (no vegetation established)				
Newly graded area	77	86	91	94
Woods				
Poor-No mulch, small trees or brush	45	66	77	83
Fair -Graded, some mulch	36	60	73	77
Good- Protected from grazing, heavy shrubs cover soil	25	55	70	77
Mixture of woods and grass	30	58	71	78
Cultivated				
Fallow: (plowed. No crop planted, bare soil)	77	86	91	94
Row crop: (Corn, tomatoes, etc.)	72	81	88	91

The Hydrological soil groups are defined by the NRCS as follows:

Group A: Soils with low runoff capacity and high infiltration rate, even when thoroughly wetted. Consists of well drained sands or gravels with high rate of water transmission.

Group B: Soils with moderate infiltration rates when thoroughly wetted and consists of moderately to well drained soils with mid moderately fine to moderately course textures. They have moderate rate of water transmission.

Group C: Soils with slow infiltration rate when thoroughly wetted, consisting predominantly of soils with a layer that impedes the vertical movement of water, with slow infiltration rate, having moderately fine, to fine texture. They have slow rate of water transmission.

Group D: Soils with very high runoff potential and slow infiltration rate when thoroughly wetted. Consists mostly of clays with high swelling potential. These soils have very slow water transmission.

When a sub-basin consists of different land uses and soil types, the curve number is calculated as (Ibrahim-Bathis & Ahmed, 2016);

$$CN_{composite} = \frac{\Sigma A_i CN_i}{\Sigma A_i} \quad \text{..... equation (3.9)}$$

Where, $CN_{composite}$ = the composite curve number used for runoff volume estimation

i = an index of watersheds subdivision having uniform land use and soil type

A_i = drainage area of a certain subdivision i

CN_i = the curve number for subdivision i.

3.3.2.2 Model Development Using HEC-HMS

In order to assess the impacts of rainfall variability on flooding over the Black Volta basin in Ghana, a hydrological model was used to simulate stream flow. Surface run-off, lateral flow, and return flow are all part of stream flow. As a result, land use, soil types, and meteorological conditions in the basin are all expected to have an effect on the hydrological response of the basin.

A substantial amount of spatial and temporal data is required for watershed hydrologic modeling and the associated model calibration and verification. The availability and quality of this data is frequently a problem that must be addressed. Due to a lack of high-resolution data for constructing, calibrating, and verifying a model, it is often necessary to compromise overall modeling quality. To avoid compromising model quality, the Hydrologic Engineering Centre Hydrologic Modelling System (HEC-HMS) model was chosen for this study, to simulate the rainfall-runoff processes of catchments. This is because this model does not require extensive use of data, is free and also easy to use but still capable of effectively simulating complex hydrological systems. Figure 3.4 below shows the step-by-step approach used in achieving this objective.

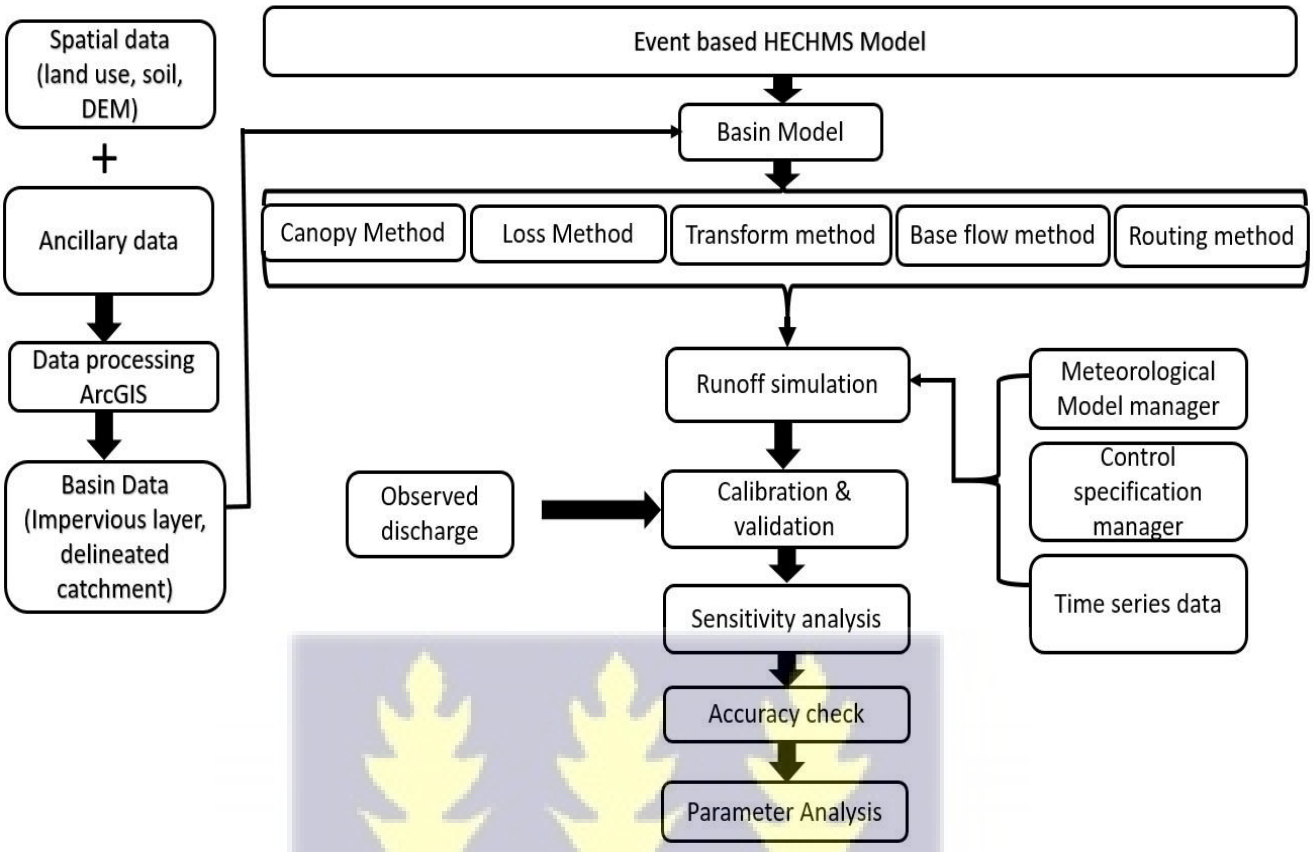

Figure 3. 4: Flow chart for Hydrological model development

3.3.2.2.1 Terrain Preprocessing and Basin Model Preparation

Digital Elevation Model (DEM) of the river basin, land use, soil data and other ancillary data were used to carry out terrain preprocessing and develop the basin model. Terrain preprocessing is a series of steps to derive the drainage network.This was done using HEC-GeoHMS, which is a geospatial hydrology toolkit and an extension for ArcGIS (ESRI) softwareThe program allows users to display geographical data, document watershed conditions, do spatial analysis, and assist in the design of hydrologic model structure and parameter inputs. The HEC-GeoHMS was released by the US Army Corps of Engineers, Hydrologic Engineering Center (HEC) and has been used extensively in basin modelling.

For example, some of the recent applications are Ibrahim-Bathis & Ahmed, (2016), Bhuiyan et al (2017) and Zhou et al (2018). In this study, catchment and stream network delineation was done with terrain preprocessing tools within the HEC-GeoHMS extension tool, and the basin model was exported to the HEC-HMS software according to the procedure provided in the HEC-GeoHMS manual (M. J. Fleming & Doan, 2013). Figure 3.5 shows the various steps within the HEC-GeoHMS tool used in terrain preprocessing, drainage or stream network generation and delineating basin and sub-basin boundaries.

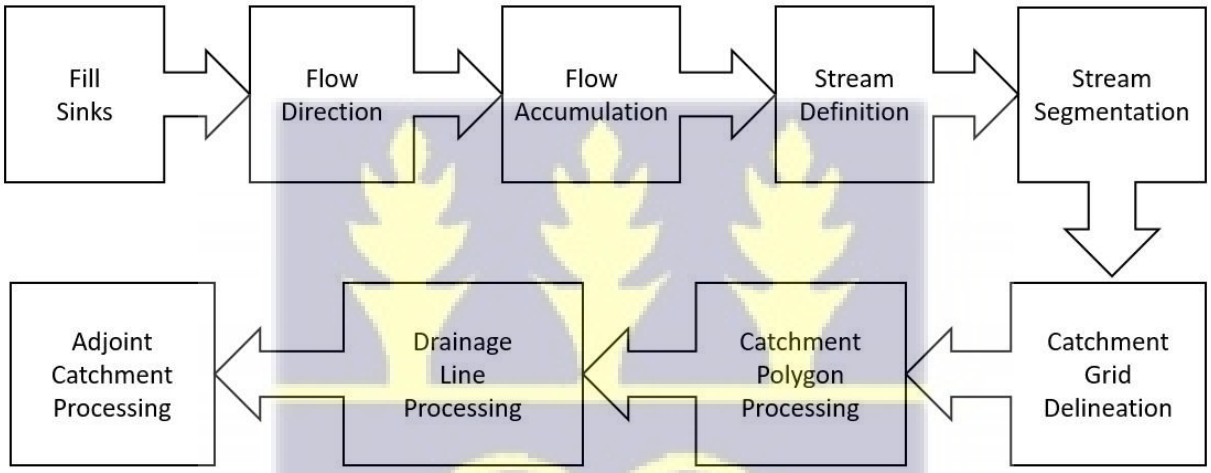

Figure 3. 5: Procedure for basin delineation and terrain pre-processing in HEC-GeoHMS

i. **Fill Sinks**: Sinks or pits are filled by increasing the elevation of the sink cells to the level of the surrounding terrain. This is because these pits are considered to be errors due to re-sampling and interpolating the grid (Meena, 2012).

ii. **Flow Direction & Accumulation:** Flow direction map created to define the sharpest downhill direction for each terrain cell. Using flow direction data as input, a flow accumulation map is created to determine the number of upstream cells draining to a specific cell.

iii. **Stream Definition**: This stage classifies all cells with a flow accumulation greater than the user-specified threshold as cells belonging to the stream network. The user defined threshold can be expressed as a square area, or as number of cells (Meena, 2012). For a stream to be created, the flow accumulation for a certain cell must surpass the user-defined threshold. The default is one percent (1%) of the largest drainage area in the entire DEM (US Army Corps of Engineers, 2010).

iv. **Stream Segmentation**: Stream segmentation divides the waterway into segments that connect junctions, outlets, and drainage divides (Baumbach et al., 2015).

v. **Catchment Grid Delineation**: Flow direction and stream link grids are used to divide the watershed into sub-basins for each stream segment (Meena, 2012).

vi. **Catchment Polygon Processing**: The catchment grid is used to construct vector layers (polygon) of sub-basins (US Army Corps of Engineers, 2010).

vii. **Drainage Line Processing**: Using the stream link and flow direction grid, a vector stream layer is created.

viii. **Adjoint Catchment Processing**: Upstream basins are aggregated at every stream confluence to enhance data extraction when defining a HECGeoHMS Project (US Army Corps of Engineers, 2010).

3.3.2.2.2 Project Generation and Set up

Basin characteristics were extracted using HEC-GeoHMS from the terrain preprocessing dataset. Raw DEM, filled DEM, flow direction grid, flow accumulation grid, stream network, stream link grid, catchment grid, and slope grid are the raster datasets that were obtained, while catchment, drainage line, and adjoint catchment are the vector data. River length, basin slope, basin centroid, longest flow path, and centroid flow path are some of the hydrologic or basin characteristics that was computed.

The outlet point of the target study area was defined at the point where the river drains into the Volta Lake, and the contribution area to this point was extracted from the DEM. The program then defined and created a new basin, based on the specified outlet point.

3.3.2.2.3 HEC-HMS Model Development

The basin model was imported into the HEC-HMS software, which provides a number of options for calculating major basin parameters such as canopy, loss, transform, routing and base flow from a watershed. Specific data such as soil type, land use, and rainfall runoff data recorded at smaller time intervals are not accessible. And according to Nandalal & Ratmayake (2010), calibrating a large number of parameters for improved precision is not justifiable and the same calibrating accuracy can be accomplished with the smallest number of parameters. So for this study, the simplest models with the fewest parameters were used for computing these parameters.

A. Canopy Method

During field visits, it was observed that interception is most likely larger in the lower reaches of the catchment area for the basin. This assumption is because vegetation appears in the upper and middle parts of the catchment area in the form of grass and tiny bushes, whereas vegetation is thicker and larger in the lower portions of the catchment. However, the canopy storage is assumed to play a minor role in the hydrological system of the Black Volta basin in Ghana since the vegetation is so sparse, with thick vegetation at only the lower portions of the basin; hence, the simple canopy method was selected for computing the canopy storage for this study. This method includes 2 parameters to account for water captured by vegetation: initial storage and maximum storage (Rimfors & Velichkin, 2015). The initial storage indicates the proportion of the canopy storage that is filled at the start of the simulation, while the maximum storage represents the canopy storage's maximum capacity in millimeters. In any case, at the start of the simulation, the canopy storage is considered to be entirely filled. Table 3.4 below shows the initial values (before calibration) for the canopy method parameters that were assigned to compute canopy storage for the various sub-basins.

Table 3. 4: Initial values of parameters for canopy method

Sub-basin	Initial storage (%)	Maximum storage (mm)	Crop coefficient
W180	80	0.02	1
W190	80	0.02	1
W200	80	0.02	1
W210	80	0.02	1
W220	80	0.02	1
W230	80	0.02	1
W240	80	0.02	1
W250	80	0.02	1
W260	80	0.02	1
W270	80	0.02	1
W280	80	0.02	1
W290	80	0.02	1
W300	80	0.02	1
W310	80	0.02	1
W320	80	0.02	1
W330	80	0.02	1
W340	80	0.02	1

B. Loss Method

When rain droplets fall to the ground, some of it is lost to infiltration and depression storages. It is necessary to account for these losses. In this study, the SCS Curve Number loss method was used to account for rainfall loss. This method is widely used when modelling rainfall events, because it is straightforward and easy to grasp. The method includes three parameters: initial abstraction, curve number and percent imperviousness

i. Initial abstraction

An amount of precipitation is trapped in cracks, sinks, and other formations or structures at the start of a rainfall event as initial abstraction, preventing initial overland movement. When the initial abstraction is exceeded, all subsequent precipitation skips these storage volumes, leaving

only infiltration and evapotranspiration to affect runoff. Initial abstraction can be calculated as (Ibrahim-Bathis & Ahmed, 2016);

$$I_a = 0.2 \times S \quad \text{..... equation (3.10)}$$

Where I_a = Initial abstraction

S = total maximum retention

After the initial abstraction is satisfied, the remaining amount of soil storage is because of the continuous abstraction, which can be computed as (Ibrahim-Bathis & Ahmed, 2016);

$$F_a = \frac{S(P-I_a)}{P-(I_a+S)} \quad \text{..... equation (3.11)}$$

Where, S = total maximum retention = $\frac{25400}{CN} - 254$

I_a = Initial abstraction

P = Precipitation

CN = Curve number (in mm)

ii. SCS Curve Numbers

The idea of curve numbers represent the continuous rainfall losses after the initial abstraction has been exceeded. The Soil Conservation Service (SCS), now known as the Natural Resource Conservation Service (NRCS), established a curve number (CN) to measure the amount of rainfall that infiltrates into the soil and the amount of surface runoff (Shukur, 2017). The curve numbers range from roughly 30, indicating that the soil and land use have very high infiltration rates and 100, which acts as water where all precipitation becomes runoff (Rimfors & Velichkin, 2015).

When a catchment consists of different land uses and soil types, the curve number is calculated as (Ibrahim-Bathis & Ahmed, 2016);

$$CN_{composite} = \frac{\Sigma A_i CN_i}{\Sigma A_i} \quad \text{..... equation (3.12)}$$

Where, $CN_{composite}$ = the composite curve number used for runoff volume estimation

i = an index of watersheds subdivision having uniform land use and soil type

A_i = drainage area of a certain subdivision i

CN_i = the curve number for subdivision i.

The average curve numbers for the basin were determined through ArcGIS 10.2 by applying a mix of LULC map, soil data, and DEM of the basin. Details of the methods and techniques used to derive the curve numbers for the basin is defined in the section 3.3.2.1.3 (SCS Curve Number map preparation) of this report.

iii. Percent Imperviousness

The percent impervious area is defined as the area of the watershed covered by impervious surfaces directly connected to the sub-basin outlet. Impervious areas are particularly relevant in regions of extreme development and in minor storms where the impervious area runoff volume is disproportionately large in relation to the event precipitation volume. The impervious area for each sub-basin was estimated by using GIS to convert the obtained land use data to a percent impervious grid. Using the sub-basin delineation and the percent impervious grid, the "Zonal Statistics" tool in ArcGIS was used to extract overall percent imperviousness for each sub-basin. Table 3.5 below shows the initial parameter values used to compute the soil loss method.

Table 3. 5: Initial values of parameters for the soil loss method

Sub-basin	Initial abstraction (mm)	Curve number	Imperviousness (%)
W180	21.771	70	12
W190	19.756	72	12
W200	17.849	74	15
W210	14.328	78	15
W220	16.933	75	15
W230	10.405	83	15
W240	8.9647	85	15
W250	18.789	73	20
W260	11.151	82	20
W270	16.042	76	20
W280	15.174	77	25
W290	16.933	75	25
W300	7.5908	87	25
W310	11.916	81	25
W320	14.328	78	30
W330	8.9647	85	25
W340	10.405	83	30

C. Hydrograph Transform Method

This refers to the process used to transform the computed excess precipitation into point runoff. Transform accounts for direct runoff modelling at the outlet of each sub-basin. In this study, the SCS Unit hydrograph model was selected for modeling direct runoff (Rimfors & Velichkin, 2015). The sole input for this technique is the lag time (Tlag). It is computed for each watershed based on the time of concentration from the center of mass of excess rainfall to the hydrograph peak. Tc, as; $T_{lag} = 0.6Tc$. The time of concentration is the time taken for a drop to travel from the farthest point to the sub-basin outlet, while the storage coefficient represents the storage effects (attenuation) of the sub-basin.

Mathematically, the relationship between the peak of the unit hydrograph U_p and the time to reach the peak, T_p is shown by (Rimfors & Velichkin, 2015);

$$U_p = 2.08\frac{A}{T_p} \quad \text{..... equation (3.13)}$$

Where, A = area of the sub-basin, and T_p is calculated as (Rimfors & Velichkin, 2015);

$$T_p = \frac{\Delta t}{2} + t_{lag} \quad \text{..... equation (3.14)}$$

Where, Δt is the excess precipitation duration, and the lag-time t_{lag} is calculated as (Tassew et al., 2019);

$$t_{lag} = 0.6 \times T_c \quad \text{..... equation (3.15)}$$

t_c is the time of concentration.

The time of concentration can be estimated depending on basin characteristics including topography and the length of the reach by Kirpich's formula (Tassew et al., 2019);

$$T_c = 0.0078 \times \left(\frac{L^{0.77}}{S^{0.385}}\right) \quad \text{..... equation (3.16)}$$

In this study, The Tc was calculated using TR-55 method (USDA 1986) for calculating travel times from the hydrological distant point in each sub-basin, which is related to the longest flow path, derived for each sub-basin using HEC-GeoHMS.

The TR-55 technique divides the longest flowpath (generated with HEC-GeoHMS) into three segments: sheet flow, shallow concentrated flow, and channel flow, and computes the required inputs (flowpath length and slope) to determine travel time for each segment. The total time of concentration for the sub-basin was calculated by adding the travel times for each segment. HEC-

GeoHMS was used to exports a Microsoft Excel Spreadsheet that was used to manually complete the Tc computations with user-provided information such as Manning's n-value roughness factors and cross-sectional geometry. This user-provided information were obtained from research and from satellite images. Table 3.6 below shows the initial lag time values assigned for computing the transform method for each sub-basin.

Table 3. 6: Initial parameter values for hydrograph transform method

Sub-basin	Graph type	Lag time
W180	Standard	3104.65814
W190	Standard	5285.55909
W200	Standard	996.682208
W210	Standard	4181.42989
W220	Standard	2589.14329
W230	Standard	3464.37126
W240	Standard	922.333889
W250	Standard	3228.45695
W260	Standard	4004.99568
W270	Standard	339.507583
W280	Standard	1946.5361
W290	Standard	2919.9806
W300	Standard	3691.57766
W310	Standard	12.304
W320	Standard	4176.50269
W330	Standard	2567.58457
W340	Standard	3630.61903

D. Baseflow Method

The sustained or "fair-weather" runoff from previous precipitation that was temporarily stored in the watershed, plus the delayed subsurface runoff from the current storm, is referred to as baseflow (Rimfors & Velichkin, 2015). For event-based hydrological modelling, the base flow component does not play a significant role in the runoff generated. However, for the purpose of model calibration, the recession baseflow method was employed. The recession base flow method was chosen because of its simplicity and is intended to mimic the typical behavior seen in watersheds when channel flow declines exponentially following an event (De Silva et al., 2014). The recession baseflow method consists of three parameters: initial base flow, recession constant, and threshold ratio.

Initial baseflow describes the initial baseflow for each sub-basin. During calibration, initial baseflow was calibrated to observed data for each simulation. The recession constant parameter determines the slope of the baseflow hydrograph's receeding limb. The threshold ratio is the value at which the baseflow will reset when the current flow decreases to the ratio value as related to the peak flow of the event. Table 3.7 shows the initial input values for the initial baseflow, recession constant and threshold ratio.

Table 3. 7: Initial input values for baseflow parameters

Sub-basin	Initial discharge (m3/s)	Recession constant	Threshold type	Ratio to peak
W180	0.02	0.75	Ratio to Peak	0.15
W190	0.02	0.75	Ratio to Peak	0.15
W200	0.02	0.75	Ratio to Peak	0.15
W210	0.02	0.75	Ratio to Peak	0.15
W220	0.02	0.75	Ratio to Peak	0.15
W230	0.02	0.75	Ratio to Peak	0.15
W240	0.02	0.75	Ratio to Peak	0.15
W250	0.02	0.75	Ratio to Peak	0.15
W260	0.02	0.75	Ratio to Peak	0.15
W270	0.02	0.75	Ratio to Peak	0.15
W280	0.02	0.75	Ratio to Peak	0.15
W290	0.02	0.75	Ratio to Peak	0.15
W300	0.02	0.75	Ratio to Peak	0.15
W310	0.02	0.75	Ratio to Peak	0.15
W320	0.02	0.75	Ratio to Peak	0.15
W330	0.02	0.75	Ratio to Peak	0.15
W340	0.02	0.75	Ratio to Peak	0.15

E. Reach Routing Method

The routing method is used to model the flow of runoff along the rivers from the higher catchment to the downstream catchment's outlet. In this study, the Muskingum Cunge method was chosen for modelling the rivers. Muskingum-Cunge is the optimum model for channel routing if no observed hydrograph data is available for calibration in any location. The Muskingum-Cunge routing approach estimates the translation and attenuation of flood hydrographs over the reach using physically based characteristics such as length, slope, Manning's n-values, and cross sectional geometry (Ibrahim-Bathis & Ahmed, 2016). Maps, aerial images, and field surveys can be used to estimate all of the physical parameters required for the Muskingum-Cunge model. Due to field observations, the cross section shape of the rivers was chosen to be rectangular. Satellite images were used to determine the widths of various portions of the rivers. However, the widths of the

rivers are tentative due to image resolution and the river system's dynamic nature, and also due to erosion and sediment transport. A manning's roughness coefficient number for the riverbeds was chosen based on field observations and research. Reach routing lengths and slopes were extracted directly from the SRTM DEM using HECGeoHMS and integrated into the HEC-HMS model. Because of the poor resolution of the digital elevation model, the slopes obtained from the SRTM DEM needed to be modified during calibration. The Muskingum-Cunge method is computed using the following equations (Rimfors & Velichkin, 2015);

$$\frac{\partial Q}{\partial t} + \frac{\partial Q}{\partial x} + \mu \frac{\partial^2 Q}{\partial x^2} + cq_L \quad \text{..... equation (3.17)}$$

Where, q_L = lateral inflow, and c= wave speed, which is given by (Rimfors & Velichkin, 2015);

$$c = \frac{dQ}{dA} \quad \text{..... equation (3.18)}$$

And μ = hydraulic diffusivity, which is given by (Rimfors & Velichkin, 2015);

$$\mu = \frac{Q}{2BS_o} \quad \text{..... equation (3.19)}$$

B is the top width of the river surface and S_o is the river's bottom slope.

Table 3.8 shows initial input values for the reach length, slope and manning's roughness coefficient used to compute the reach routing method.

Table 3. 8: Initial input values for reach routing parameters

Reach	Length (m)	Slope	Manning's n
R10	106629	0.0001	0.03
R30	28738	0.0005	0.03
R50	109667	0.0002	0.03
R80	23908	0.0002	0.03
R90	19961	0.0002	0.03
R110	65.156	0.0001	0.03
R130	82652	0.0004	0.03
R150	65503	0.0006	0.03
R160	184861	0.0001	0.03

Table 3. 9: Summary of HEC-HMS Basin Model Parameters

Modelling Method	Parameters	Description
CANOPY STORAGE		
Simple Canopy	Initial Storage	Initial storage in canopy
	Maximum Storage	Maximum storage in canopy
SOIL LOSS		
SCS Curve Number	Initial abstraction	The fraction of the storm depth after which runoff begins
	Curve number	An empirical parameter for estimating direct runoff or infiltration due to excessive rainfall.
	Impervious layer percentage	Percentage of the sub-basin that is covered by directly connected impermeable surfaces such as concrete, rooftops, and urban development.
HYDROGRAPH TRANSFORMATION		
SCS Unit Hydrograph	Lag Time	Travel time from the most hydrologically remote point in the sub-basin to the watershed outlet
BASEFLOW		
Recession Base flow	Initial Base flow	Base flow at the beginning of the simulation
	Recession Ratio	Rate at which base flow recedes between storm events
	Threshold Ratio	The ratio to the peak flow at which the base flow is reset
REACH ROUTING		
Muskingum-Cunge Routing	Length	Length of reach
	Slope	Slope of reach
	Manning's n-value	The channel's roughness coefficient, as well as the left and right overbanks
	Shape	Shape of the routing reach cross section. For this study, rectangular.

F. Meteorological Model

The meteorological model is an essential component for rainfall-runoff simulations and is a component of the HEC-HMS model that represents precipitation, including rainfall and snow. Within the meteorological model, evapotranspiration rates are also defined.

i. Rainfall

Daily time series of meteorological data comprising of rainfall, temperature, relative humidity, evapotranspiration etc at all available meteorologic stations was acquired from the Ghana Meteorological Agency. In an attempt to rectify the lack of observed meteorological data in areas within the basin where precipitation coverage is sparse, the Inverse Distance precipitation method was applied. By applying an inverse distance squared weighting to all available precipitation gages in the user-specified search radius, the Inverse Distance technique estimates sub-basin average precipitation. The inverse distance precipitation technique assigns an average precipitation to a sub-basin during a defined period by using adjacent precipitation gauges. Weighting is used to apportion precipitation to each sub-basin depending on the distance between the gauge and one or more nodes within each sub-basin. For this study, a single node was defined for each sub-basin and was defined by the centroid of the sub-basin. The closer the gauge is to the sub-basin node, the greater the precipitation in the sub-basin is weighted to that gauge. This method is preferred because it provides the ability to incorporate multiple gauges where available. The technique also allows you to provide a search radius, which will only utilize gauges within that radius, ensuring that remote gauges do not distort the precipitation applied to the sub-basin.

ii. Evapotranspiration

The specified evapotranspiration method was used to represent evapotranspiration rates in the basin. Evapotranspiration is not a critical component for short-term event-based simulations. Although evapotranspiration loss rates are entered as a daily total, HEC-HMS divides the monthly rate to fit the computational time interval selected for the model run. The largest computational time interval for any simulation is 1 hour, resulting in low evapotranspiration rates per simulation time step for the study.

G. Runoff Simulation

The meteorological model manager was used to specify the precipitation gauges, input rainfall data and coordinates of the gauge stations and the methods that was used in the hydrologic model to estimate areal precipitation. The Stream discharge data from Lawra, Chache, Bui and Bamboi discharge stations were entered into the time series model. The data from Lawra station was used to account for inflows from upstream of lawra station, which is outside the Ghana portion of the Black Volta basin, while data from the other three (3) stations were used to calibrate and validate the model. The control specification model was used to define the period of simulation. Control specification defines the simulation process's boundary conditions, such as the start and finish dates of the simulations. The simulation start time was set as 01 July while the end time was set at 30 November.

G. Calibration and Validation

The flood of 1996, 1999, 2007 and 2010 were one of the largest flood events in the stream flow record of the Black Volta basin. Hence, the event of 1996 and 2007 were selected for calibration, and 1999 and 2010 for validation. Other factors that influenced the decision of rainfall events to

use for the calibration and validation includes: rainfall characteristics (magnitude, intensity, duration, as well as temporal and spatial variability), watershed characteristics, availability and completeness of rainfall and stream monitoring data.

The model calibration and validation was carried out based on simulated and observed discharge at the gauging stations. The goal was to get the simulated discharge data to match the observed discharge data in terms of peak value, curve shape, and time of peak while keeping parameter changes within a reasonable range. The model parameters were initially calibrated manually after which it was subjected to the HEC-HMS model's automatic calibration methods. The automatic calibration method uses an iterative process to minimize the objective function, to achieve agreement between simulated and observed discharge flow data (Bhuiyan et al., 2017).

The curve number (CN), initial abstraction and impervious layer percentage in the SCS Curve Number technique were all adjusted. However, parameters related to basin characteristics, such as Manning's coefficient, basin area, slope, and soil type remained unaffected. Optimization trials were carried out to improve results of calibration.

A variety of test criteria has been developed to evaluate the effectiveness of a hydrological model calibration. For this study, the Nash–Sutcliffe (NSE) coefficient of model efficiency, Root Mean Square Error (RMSE), Percent bias (δ_b), Percent Difference in Runoff Volume (VR) and the Percent Difference in Peak Discharge (QP) were used to measure the goodness-of-fit between the observed and simulated flow time series. Description of these statistical criteria have been discussed in chapter two (2) of this report, along with a table showing the general performance rating for the selected statistics (Table 2.2).

H. Sensitivity Analysis

A sensitivity analysis of the model was performed to further comprehend the complicated interactions between model parameters and variables. The sensitivity analysis evaluates which parameters have a substantial impact on model performance (Bhuiyan et al., 2017). Parameter values were changed in the range of ±20% with 5% intervals in order to analyze the sensitivity of the calibration parameters. Parameters such as curve number, initial abstraction, impervious layer percentage and lag time were adjusted to evaluate parameter sensitivity.

3.3.4 APPLICATION OF HYDROLOGIC MODEL FOR FLOOD FORECASTING

3.3.4.1 Forecasting Peak flows using IDF curves

Intensity-Duration-Frequency (IDF) curves for selected stations within the basin were obtained from Ghana Meteorological Agency (GMet). Figures 3.6, 3.7 and 3.8 shows the IDF curves that were used in this study. The IDF curves show the intensity of rainfalls for various rainfall durations expressed in return periods. Rainfall depths were extracted from the IDF curves by multiplying the various intensities by their corresponding durations, and used to create frequency storms as rainfall inputs for simulation.

The Meteorological model manager within the HEC-HMS was used to create a meteorological model. Frequency storm was selected as the type of precipitation. Rainfall depths for 5, 10, 15, 20, 25, 50, 75, and 100 year return periods were used as inputs into the established hydrologic model. The duration was set at 24 hours (1 day) because of the size of the catchment. Large basins have longer time of concentration, hence would take longer time to reach peak discharge. A Control specification file was created to run the simulation for one week.

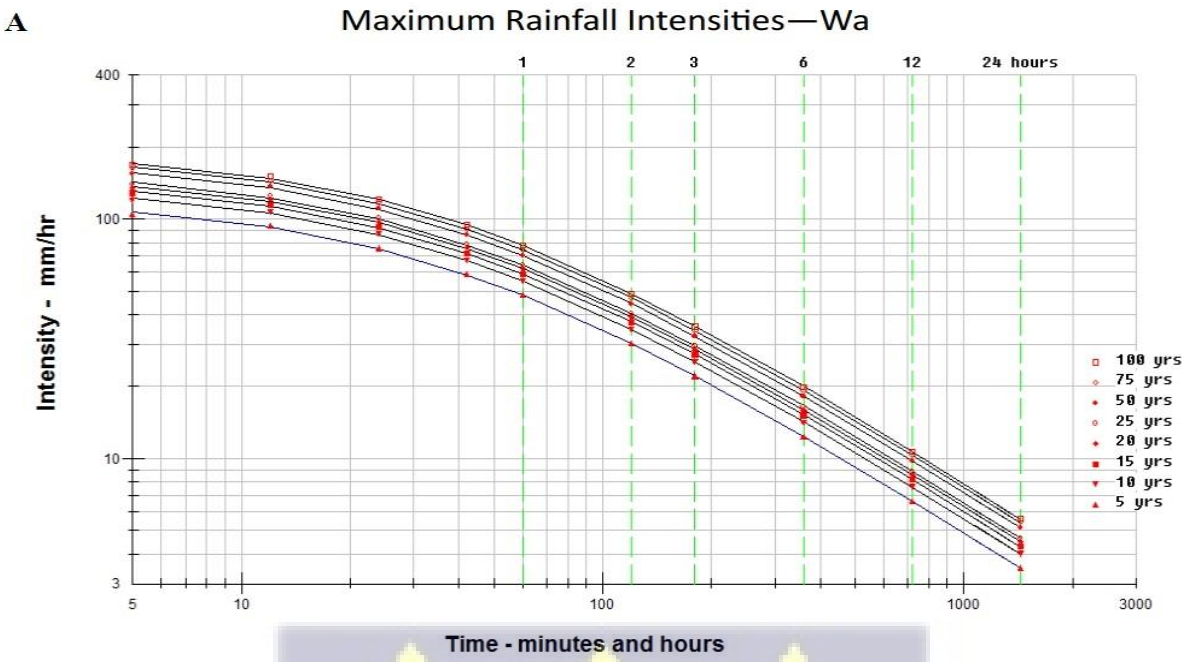

Figure 3. 6: IDF curves of Wa station

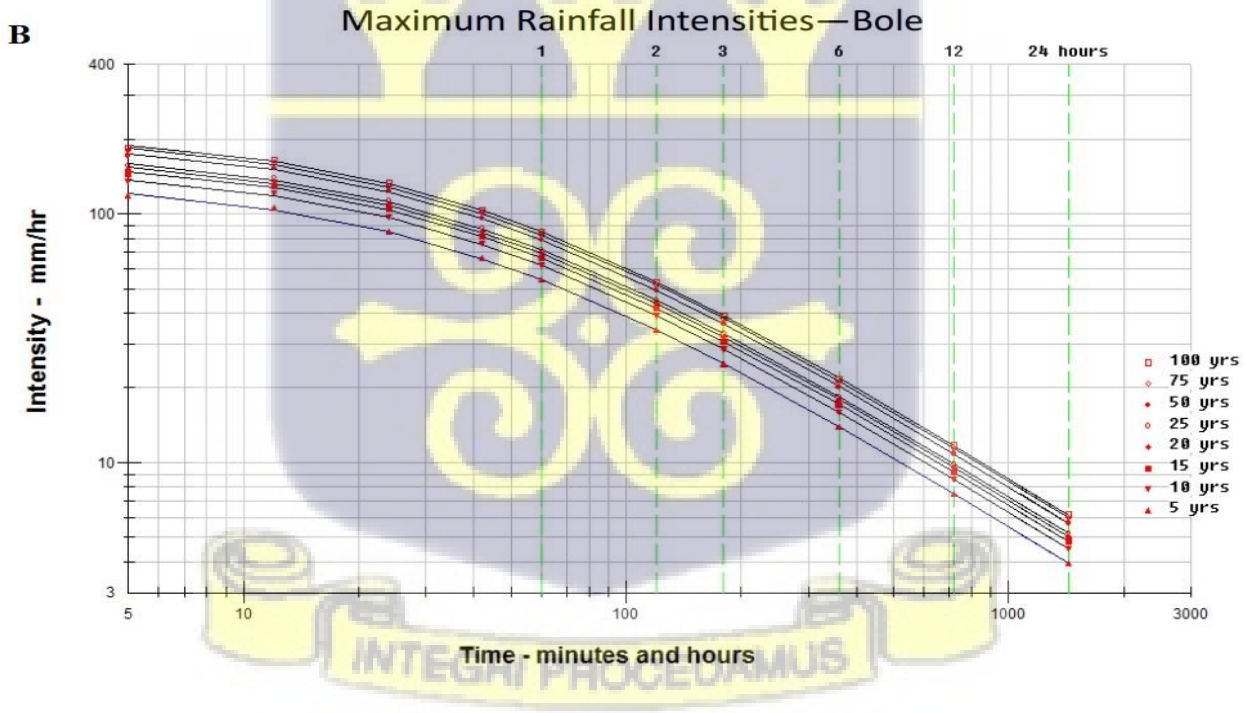

Figure 3. 7: IDF curves of Bole station

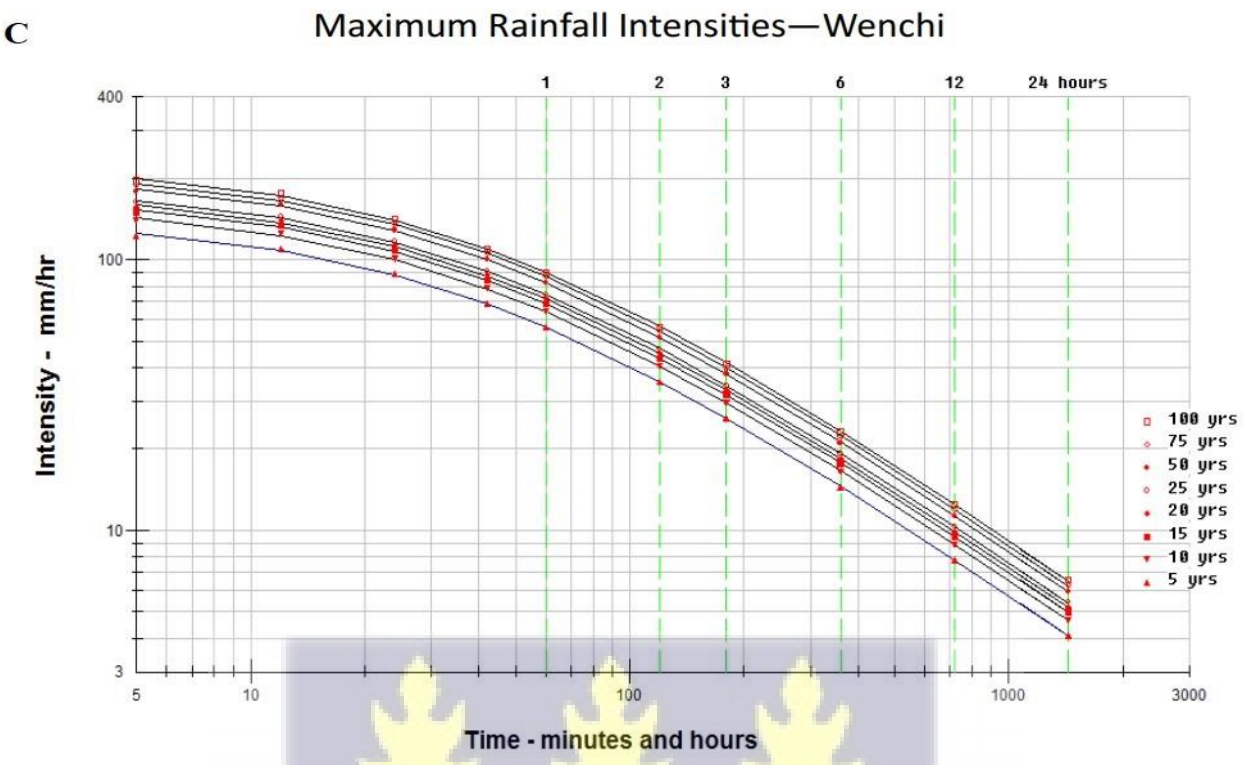

Figure 3. 8: IDF curves of Wenchi station

IDF curve of Wa meteorological station was used to develop frequency storm to simulate peak discharge at Chache discharge station. IDF curve of Bole meteorological station as well as contribution from upstream station (i.e Chache)was used to simulate peak discharge at Bui discharge station , and IDF curve of Wenchi meteorological station as well as contributions from upstream station (i.e Bui) were used to simulate peak flow for Bamboi discharge station.

CHAPTER FOUR

RESULTS AND DISCUSSION

4.1 SPATIO-TEMPORAL RAINFALL TREND ANALYSIS

4.1.1 Descriptive Statistics of Rainfall Amount Time Series

Descriptive statistics were analyzed to assess the distribution of rainfall amount for selected stations within the basin. Results of the descriptive statistics study of the total rainfall amount for the selected stations from 1980 to 2018 are displayed in tables 4.1 and 4.2 respectively. The descriptive statistics was carried out on an annual and monthly scale.

At an annual scale, the recorded minimum and maximum total rainfall amount during the 38 years are respectively; 522.9 mm and 1295.8 mm for Wa station, 832.7 mm and 1826.7 mm for Bui station, 716.3 mm and 1377.9 mm for Damongo station, 762 mm and 1562 mm for Bole station, 807.1 mm and 1499.5 mm for Sunyani station, 849.6 mm and 1726.3 mm for Wenchi station, and 854.80 mm and 2300 mm for Kintampo station. The lowest annual total rainfall of 522.9 mm within the basin for the period was recorded at Wa station, whereas the highest total annual rainfall of 2300 mm was recorded at Kintampo station. This is in concordance with the findings of Klutse et al (2021), who stated that the lowest total annual rainfall within the basin is approximately 500 mm, whereas, the highest total annual rainfall is around 2000mm. Hence, the annual rainfall amount increases from the northern (upstream) parts of the basin to the southern (downstream) parts of the basin. In terms of eco-climatological zones, it can be said that total rainfall amount increases from the Sahel savanna regions to the Guinea Savanna regions.

Table 4. 1: Descriptive Statistics of Total Rainfall amount (mm) for period (1980–2018) for selected stations in Black Volta basin in Ghana

WA						BUI					
	Min (mm)	Max (mm)	Mean (mm)	Std Dev	CV		Min (mm)	Max (mm)	Mean (mm)	Std Dev	CV
Annual	522.90	1295.80	977.28	230.65	0.24	**Annual**	832.7	1826.70	1092.14	267.83	0.25
Jan	0.00	67.50	4.16	13.20	3.17	**Jan**	0.00	93.30	11.49	21.96	1.91
Feb	0.00	93.70	9.46	20.90	2.21	**Feb**	0.00	88.30	21.07	25.28	1.20
Mar	0.00	90.80	23.74	21.57	0.91	**Mar**	0.80	239.90	69.58	57.54	0.83
Apr	11.60	186.90	82.41	43.05	0.52	**Apr**	32.50	223.10	113.30	50.71	0.45
May	30.40	210.90	119.09	45.46	0.38	**May**	66.10	407.50	159.20	69.06	0.43
Jun	48.40	250.20	132.28	53.86	0.41	**Jun**	66.20	315.10	156.58	64.41	0.41
Jul	71.20	237.00	142.22	44.40	0.31	**Jul**	20.00	293.20	124.79	76.20	0.61
Aug	52.00	361.00	211.48	75.93	0.36	**Aug**	39.50	298.80	116.03	62.93	0.54
Sep	63.20	353.30	188.90	64.25	0.34	**Sep**	80.50	308.70	193.08	59.33	0.31
Oct	0.00	191.20	81.21	43.02	0.53	**Oct**	42.20	291.80	134.76	64.29	0.48
Nov	0.00	36.60	6.21	9.24	1.49	**Nov**	0.00	551.20	32.24	92.34	2.86
Dec	0.00	37.00	2.32	7.87	3.39	**Dec**	0.00	439.40	19.03	76.38	4.01
DAMONGO						**BOLE**					
	Min (mm)	Max (mm)	Mean (mm)	Std Dev	CV		Min (mm)	Max (mm)	Mean (mm)	Std Dev	CV
Annual	716.30	1377.90	1077.22	167.80	0.16	**Annual**	762.0	1562.0	1079.37	165.47	0.15
Jan	0.00	63.50	2.49	10.51	4.21	**Jan**	0.0	50.8	2.61	8.92	3.42
Feb	0.00	45.70	8.58	11.97	1.40	**Feb**	0.0	84.9	12.38	18.96	1.53
Mar	0.00	118.20	37.81	26.40	0.70	**Mar**	0.0	155.6	48.40	37.66	0.78
Apr	24.70	235.90	104.96	50.02	0.48	**Apr**	17.0	189.1	99.05	42.61	0.43
May	57.30	223.30	128.87	41.89	0.33	**May**	38.7	390.4	131.93	58.97	0.45
Jun	61.50	281.30	145.14	55.48	0.38	**Jun**	48.0	304.7	147.45	58.65	0.40
Jul	30.50	326.20	150.86	70.89	0.47	**Jul**	49.6	259.8	145.14	57.70	0.40
Aug	27.20	333.20	187.73	65.64	0.35	**Aug**	64.7	268.6	159.86	58.19	0.36
Sep	76.70	363.30	201.33	62.99	0.31	**Sep**	60.8	348.0	205.66	64.31	0.31
Oct	6.30	218.10	97.75	52.12	0.53	**Oct**	31.9	347.5	105.19	63.49	0.60
Nov	0.00	77.80	9.78	15.26	1.56	**Nov**	0.0	74.0	17.01	19.95	1.17
Dec	0.00	29.80	1.98	5.56	2.80	**Dec**	0.0	55.0	4.71	12.44	2.64

Table 4. 2: Statistics of Total Rainfall amount (mm) for period (1980–2018) for selected stations in Black Volta basin in Ghana (continued)

SUNYANI	Min (mm)	Max (mm)	Mean (mm)	Std Dev	CV
Annual	807.10	1499.50	1175.19	189.58	0.16
Jan	0.00	47.60	8.73	12.15	1.39
Feb	0.00	159.80	48.30	41.62	0.86
Mar	17.70	236.40	104.64	52.54	0.50
Apr	32.00	398.60	144.91	70.42	0.49
May	58.60	320.70	151.61	62.79	0.41
Jun	59.50	364.80	182.18	73.58	0.40
Jul	11.50	248.20	100.71	55.40	0.55
Aug	1.50	186.40	68.49	52.94	0.77
Sep	55.40	330.40	159.21	69.34	0.44
Oct	22.80	319.60	160.97	67.10	0.42
Nov	6.40	203.00	46.64	38.47	0.82
Dec	0.00	207.40	15.22	34.46	2.26

WENCHI	Min (mm)	Max (mm)	Mean (mm)	Std dev	CV
Annual	849.60	1726.30	1229.81	183.17	0.15
Jan	0.00	61.10	6.95	13.53	1.95
Feb	0.00	101.10	26.01	25.14	0.97
Mar	0.00	283.00	98.92	65.73	0.66
Apr	34.10	304.80	151.01	53.45	0.35
May	78.10	344.10	161.68	56.89	0.35
Jun	60.90	347.00	147.93	58.73	0.40
Jul	19.00	298.20	123.17	64.31	0.52
Aug	3.10	237.00	94.71	59.09	0.62
Sep	82.50	368.40	182.61	72.26	0.40
Oct	16.00	299.10	175.93	68.29	0.39
Nov	0.30	142.80	49.50	35.82	0.72
Dec	0.00	96.50	11.39	18.92	1.66

KINTAMPO	Min (mm)	Max (mm)	Mean (mm)	Std Dev	CV
Annual	854.80	2300.90	1291.47	256.34	0.20
Jan	0.00	70.80	6.38	14.87	2.33
Feb	0.00	107.70	22.78	23.42	1.03
Mar	0.00	180.60	74.59	44.65	0.60
Apr	29.10	259.70	136.11	56.72	0.42
May	56.90	419.20	166.07	85.24	0.51
Jun	45.00	340.00	178.06	68.14	0.38
Jul	31.30	366.40	145.00	91.48	0.63
Aug	9.20	300.30	121.82	76.53	0.63
Sep	106.70	415.70	232.32	75.24	0.32
Oct	53.70	447.40	180.00	77.44	0.43
Nov	0.00	92.40	35.86	27.78	0.77
Dec	0.00	117.40	9.99	22.58	2.26

On a monthly basis, January, February, March, and December recorded little or no rainfall for the entire basin, hence these months are considered as the dry season months, as supported by studies of (Sanogo et al., 2015). Most of the basin's rainfall occurred between April and October for the period. This is in agreement with the findings of Owusu et al (2008), which states that the rainy season within the Volta basin spans from the month of May to October. Figure 4.1 shows the spatio-temporal variation of mean monthly rainfall time series for the 1980-2018 period.

The coefficient of variation for monthly total rainfall amount varied from 0.24 to 3.39 at Wa station, 0.25 to 4.01 at Bui station, 0.16 to 4.21 at Damongo station, 0.15 to 3.42 for Bole station, 0.16 to 2.26 at Sunyani station, 0.15 and 1.95 at Wenchi station, and 0.20 and 2.33 at Kintampo station. For each of the stations, the dry months such as January, February, November and December recorded higher coefficient of variation values than the wet months (i.e. March to October), this suggests more variable rainfall amounts within the dry months than the wet months. The coefficient of variation also varies spatially within the basin. The rainfall stations at the northern parts of the basin have higher CV values than those stations at the southern portions of the basin for both dry and wet months. This suggests that the upstream part of the basin have more variable monthly rainfall amounts than the downstream portions of the catchment.

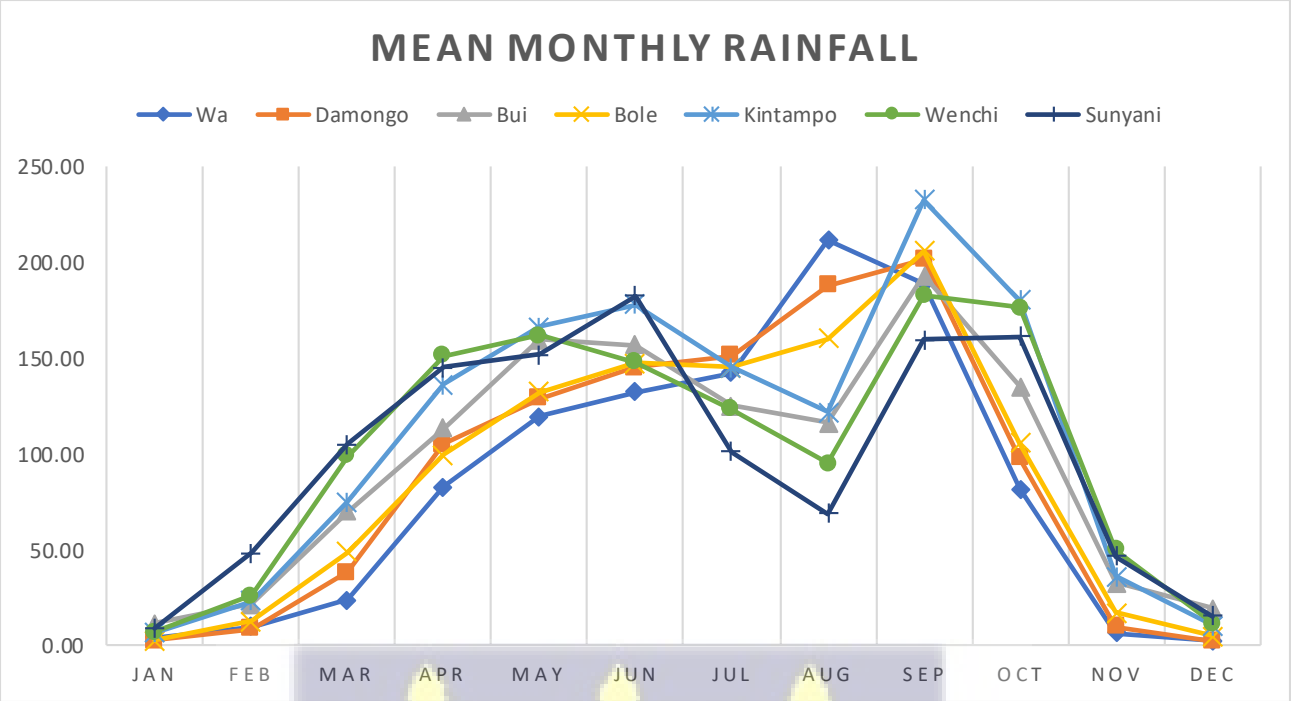

Figure 4. 1: Spatio-temporal variation of mean monthly rainfall

Some of the station exhibit bimodal pattern of rainfall distribution, while others show a unimodal pattern. From figure 4.1, the rainfall stations at the northern parts of the basin exhibit a unimodal distribution of mean monthly rainfall with the peaks occurring in August and September. While the stations at the southern portions show a bimodal distribution, with peak mean monthly rainfall occurring in May/June and September. This result is in agreement with the findings of Ilori & Ajayi (2020), which observed a unimodal distribution of mean annual rainfall for rainfall stations within the Sudan savanna with peak occurring in August, and a bimodal distribution for stations within the Guinea Savanna, with peak in June and September.

4.1.2 Descriptive Statistics of Decadal Rainfall Amount

Table 4.3 shows the results of descriptive statistics of decadal annual rainfall amount. From the table, Wa station recorded its minimum and maximum annual rainfall amount between 2010 and 2018. This suggests severe intra-annual variability of rainfall at Wa station within 2010 and 2018. At Bui, Bole and Sunyani stations, the minimum annual rainfall amount was recorded within 1980-1989, whereas the maximum annual rainfall amount was recorded within 2010-2018. Damongo station recorded its minimum annual rainfall amount within the 1990-1999 period and its maximum annual rainfall amount within 2000-2009. The period 1980-1989 recorded both minimum and maximum annual rainfall amounts for Wenchi Station, suggesting intra-annual rainfall variability. Kintampo station recorded minimum annual rainfall amount within the period 1990-1999 and maximum annual rainfall amount within the 2010-2018 period. Overall, it can be inferred that the period 1980 to 1989 recorded the minimum annual rainfall amount for most of the stations. This is in concordance with the findings of Aziz & Obuobie (2017). The descriptive statistics of decadal monthly total rainfall amount is shown in Appendix A to G.

Analysis of the mean annual rainfall for the selected stations on a decadal scale reveals the inter-decadal distribution and variation of mean annual rainfall within the basin (Figure 4.2).

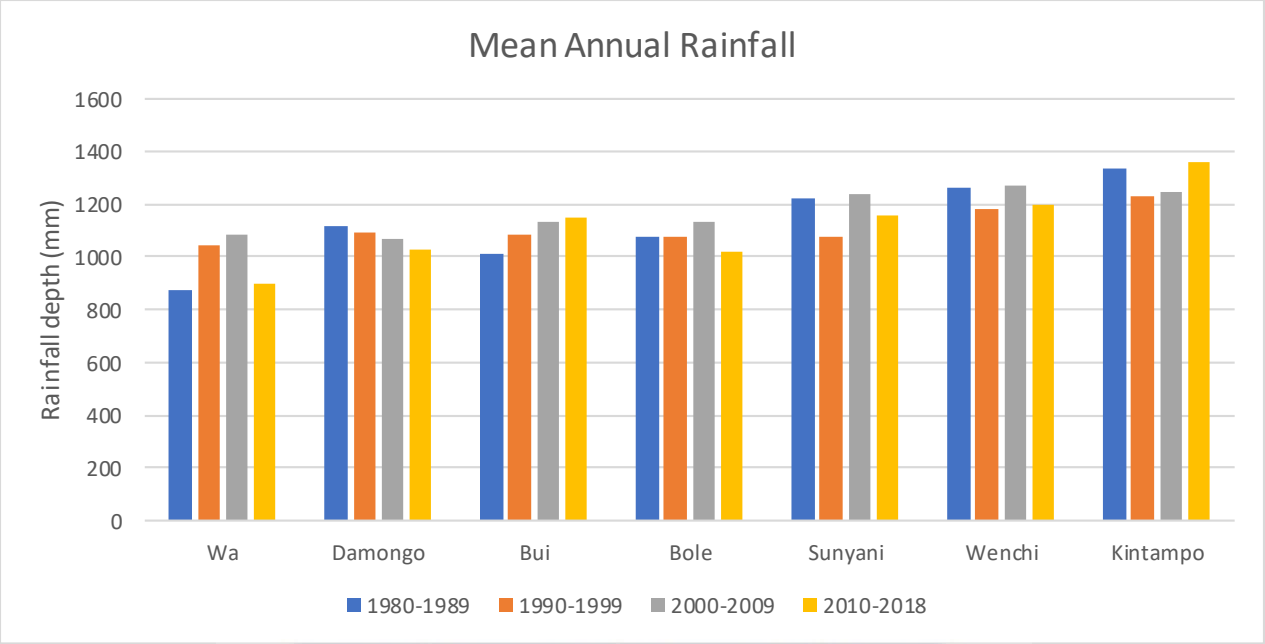

Figure 4. 2: Mean Annual rainfall for the period of 1980-1989, 1990-1999, 2000-2010, and 2010-2018 for the selected stations

Wa and Bole stations show increasing mean annual rainfall from 1980-1989, 1990-1999, 200-2009 and then the mean annual rainfall declines from 2010-2018. At Damongo station, the mean annual rainfall decreases steadily from 1980-1989 to 1990-1999 to 200-2009 and then to 2010-2018. Bui station on the other hand shows a steady increase in mean annual rainfall from 1980-1989 to 1990-1999 to 200-2009 and then to 2010-2018. Sunyani and Wenchi Stations behave similarly with high mean annual rainfall for 1980-1989, low mean annual rainfall for 1990-1999, high mean annual rainfall for 2000-2009 and low mean annual rainfall for 2010-2018. At Kintampo station, the mean annual rainfall decreases from 1980-1989 to 1990-1999 and then rises steadily from 2000-2010 and then 2010-2018, with 2010-2018 recording the highest mean annual rainfall for the station.

Table 4. 3: Descriptive Statistics of Decadal Annual Rainfall amount (mm) for various stations in Black Volta basin in Ghana

1980-1989						1990-1999					
Station	**Min (mm)**	**Max (mm)**	**Mean (mm)**	**Std. dev**	**CV**	**Station**	**Min (mm)**	**Max (mm)**	**Mean (mm)**	**Std. dev**	**CV**
Wa	522.90	1104.00	871.91	186.63	0.21	**Wa**	767.30	1290.40	1040.92	182.00	0.17
Damongo	800.10	1276.20	1118.58	158.71	0.14	**Damongo**	716.30	1317.70	1091.05	199.81	0.18
Bui	489.50	1387.60	1009.67	299.66	0.30	**Bui**	833.10	1553.80	1084.59	204.63	0.19
Bole	762.00	1330.60	1078.52	162.59	0.15	**Bole**	821.90	1562.00	1079.56	193.69	0.18
Sunyani	812.10	1499.50	1222.01	229.67	0.19	**Sunyani**	811.70	1401.60	1075.19	183.42	0.17
Wenchi	849.60	1726.30	1261.50	248.36	0.20	**Wenchi**	918.60	1408.30	1182.05	158.94	0.13
Kintampo	993.20	1496.50	1333.64	151.85	0.11	**Kintampo**	854.80	1650.10	1229.06	231.84	0.19
2000-2009						**2010-2018**					
Station	**Min (mm)**	**Max (mm)**	**Mean (mm)**	**Std. dev**	**CV**	**Station**	**Min (mm)**	**Max (mm)**	**Mean (mm)**	**Std. dev**	**CV**
Wa	913.80	1273.10	1082.35	107.63	0.10	**Wa**	61.40	1295.80	898.10	366.52	0.41
Damongo	746.50	1377.90	1065.61	159.54	0.15	**Damongo**	766.40	1290.20	1028.78	163.34	0.16
Bui	955.00	1328.40	1130.81	130.45	0.12	**Bui**	530.20	1826.70	1146.03	419.86	0.37
Bole	904.40	1251.30	1131.65	120.85	0.11	**Bole**	777.80	1403.60	1022.02	185.90	0.18
Sunyani	1017.60	1458.40	1241.06	128.35	0.10	**Sunyani**	807.10	1408.90	1161.11	184.71	0.16
Wenchi	987.00	1413.00	1271.87	129.74	0.10	**Wenchi**	971.40	1549.00	1200.94	188.03	0.16
Kintampo	868.80	1635.10	1250.80	227.10	0.18	**Kintampo**	1033.90	2300.90	1359.13	391.63	0.29

4.1.3 Descriptive Statistics of Rainfall Intensity Time Series

The daily maximum rainfall (intensity) was estimated to assess rainfall intensity within the basin. The recorded minimum and maximum rainfall intensity at an annual scale during the period respectively, are; 31 mm and 142 mm for Wa station, 47 mm and 439.4 mm for Bui station, 53.8 mm and 129.5 mm for Damongo station, 50 mm and 131.5 mm for Bole station, 39.1 mm and 204 mm for Sunyani station, 46.1 mm and 143.3 mm for Wenchi station, and 50.4 mm and 223.6 mm for Kintampo station. This suggests that Bui station recorded the highest rainfall intensity for the period (1980-2018) within the basin, while Wa station recorded the least rainfall intensity. The results show increasing rainfall intensity from the middle portions of the basin to the northern and southern portions of the basin. Tables 4.4 and 4.5 shows results of descriptive statistics for daily maximum rainfall (intensities) for the period (1980-2018) within the basin.

Table 4. 4: Statistics of Daily Maximum rainfall / Intensities (mm) for period (1980–2018) for selected stations in Black Volta basin in Ghana

	WA						BUI				
	Min	**Max**	**Mean**	**Std. dev**	**CV**		**Min**	**Max**	**Mean**	**Std. dev**	**CV**
Annual	31.00	142.40	69.11	23.35	0.34	**Annual**	47.00	439.40	87.73	61.86	0.71
Jan	0.00	36.90	3.32	9.57	2.88	**Jan**	0.00	69.60	9.46	16.38	1.73
Feb	0.00	80.20	8.83	19.35	2.19	**Feb**	0.00	76.20	16.43	19.43	1.18
Mar	0.00	42.90	14.31	12.47	0.87	**Mar**	0.80	80.00	31.46	21.28	0.68
Apr	11.50	72.50	36.99	15.61	0.42	**Apr**	12.40	82.70	39.78	19.32	0.49
May	8.80	126.00	39.13	20.05	0.51	**May**	20.20	105.50	49.07	19.70	0.40
Jun	16.90	90.20	38.68	17.16	0.44	**Jun**	19.10	95.00	45.24	19.18	0.42
Jul	17.40	72.40	39.73	13.22	0.33	**Jul**	7.40	116.30	42.85	23.97	0.56
Aug	21.60	142.40	54.35	24.85	0.46	**Aug**	16.40	89.70	40.98	18.11	0.44
Sep	14.00	101.70	43.37	17.87	0.41	**Sep**	15.80	111.30	51.42	21.95	0.43
Oct	0.00	68.00	28.47	14.39	0.51	**Oct**	11.30	112.70	40.72	23.77	0.58
Nov	0.00	24.40	4.65	6.65	1.43	**Nov**	0.00	368.30	21.66	61.66	2.85
Dec	0.00	37.00	2.29	7.84	3.43	**Dec**	0.00	439.40	17.62	76.12	4.32
	DAMONGO						**BOLE**				
	Min	**Max**	**Mean**	**Std. dev**	**CV**		**Min**	**Max**	**Mean**	**Std. dev**	**CV**
Annual	53.80	129.50	74.48	17.31	0.23	**Annual**	50.00	131.50	79.26	20.51	0.26
Jan	0.00	63.50	2.34	10.44	4.46	**Jan**	0.00	37.10	2.21	7.01	3.17
Feb	0.00	45.30	6.84	9.88	1.45	**Feb**	0.00	79.80	10.68	17.50	1.64
Mar	0.00	76.20	21.42	16.75	0.78	**Mar**	0.00	110.30	27.38	23.63	0.86
Apr	11.80	79.70	40.69	16.11	0.40	**Apr**	12.20	81.30	40.54	18.39	0.45
May	14.00	98.40	46.42	20.27	0.44	**May**	15.80	92.60	41.08	16.59	0.40
Jun	16.80	99.20	43.98	16.18	0.37	**Jun**	18.80	101.10	43.79	20.53	0.47
Jul	8.50	117.10	47.00	19.97	0.42	**Jul**	12.10	130.10	46.75	22.68	0.49
Aug	10.40	129.50	57.00	21.93	0.38	**Aug**	16.00	122.00	51.47	22.88	0.44
Sep	17.40	93.40	48.76	17.88	0.37	**Sep**	13.60	131.50	49.82	23.93	0.48
Oct	6.30	92.10	34.55	17.69	0.51	**Oct**	13.20	94.70	34.87	19.88	0.57
Nov	0.00	55.30	7.17	10.54	1.47	**Nov**	0.00	74.00	12.02	15.63	1.30
Dec	0.00	21.20	1.58	4.09	2.59	**Dec**	0.00	45.30	3.60	9.44	2.62

Table 4. 5: Statistics of Daily Maximum rainfall / Intensities (mm) for period (1980–2018) for selected stations in Black Volta basin in Ghana (continued)

	SUNYANI						WENCHI				
	Min	**Max**	**Mean**	**Std. dev**	**CV**		**Min**	**Max**	**Mean**	**Std. dev**	**CV**
Annual	39.10	204.00	82.55	27.74	0.34	**Annual**	46.10	143.30	82.60	23.33	0.28
Jan	0.00	47.20	7.94	11.63	1.46	**Jan**	0.00	29.00	5.23	8.63	1.65
Feb	0.00	118.10	29.05	26.52	0.91	**Feb**	0.00	55.60	14.63	12.92	0.88
Mar	10.10	76.10	39.12	16.03	0.41	**Mar**	0.00	143.30	41.29	28.83	0.70
Apr	23.00	91.40	46.52	20.39	0.44	**Apr**	15.00	118.00	49.87	22.57	0.45
May	13.80	93.40	43.19	18.18	0.42	**May**	20.50	99.40	45.38	18.59	0.41
Jun	17.80	204.00	55.76	33.28	0.60	**Jun**	17.10	118.40	41.66	23.90	0.57
Jul	8.40	96.00	40.01	22.82	0.57	**Jul**	9.60	102.20	47.35	22.25	0.47
Aug	1.40	103.00	26.42	20.39	0.77	**Aug**	2.50	96.10	37.68	21.75	0.58
Sep	17.00	97.80	46.96	23.03	0.49	**Sep**	16.50	137.50	47.83	26.62	0.56
Oct	4.00	102.60	38.47	20.74	0.54	**Oct**	9.60	94.30	40.63	18.53	0.46
Nov	3.50	45.60	19.04	10.64	0.56	**Nov**	0.30	51.70	19.37	12.74	0.66
Dec	0.00	56.00	8.44	11.53	1.37	**Dec**	0.00	32.70	7.39	10.23	1.38

	KINTAMPO				
	Min	**Max**	**Mean**	**Std. dev**	**CV**
Annual	50.40	223.60	84.72	36.65	0.43
Jan	0.00	67.40	5.18	12.54	2.42
Feb	0.00	51.60	14.74	13.72	0.93
Mar	0.00	115.00	35.99	23.23	0.65
Apr	12.70	109.20	49.02	24.12	0.49
May	12.70	223.60	53.15	40.22	0.76
Jun	23.10	111.20	49.81	20.71	0.42
Jul	9.40	223.60	47.17	34.99	0.74
Aug	4.30	116.20	41.70	23.46	0.56
Sep	25.60	135.50	53.07	20.93	0.39
Oct	20.50	191.30	47.41	29.65	0.63
Nov	0.00	47.50	19.18	13.42	0.70
Dec	0.00	59.20	6.31	12.84	2.04

On a monthly scale the rainfall intensities behaves differently from the total monthly rainfall amount for the stations except for Bole and Wa. The months of August and September recorded the highest rainfall intensities for Wa and Bole stations respectively, which agrees with the maximum total rainfall amount for these stations. Bui recorded its maximum rainfall intensity in December; this could be attributed to the occurrence of short duration high intensity rainfall at the station due to climate change (Sanogo et al., 2015), since December is usually a dry season month. Damongo recorded maximum rainfall intensity in August, Sunyani in June, and Kintampo in July. Wenchi station recorded its maximum rainfall intensity in March; this is a rainfall anomaly and could be attributed to changing climate.

4.1.4 Mann Kendall Trend Analysis of Rainfall

The Mann-Kendall trend test and Sen's estimator was applied to the set of rainfall data for seven stations to reveal rainfall variability and possible rainfall trends within the area. The Kendall tau, the p-value and the Sen's slope are statistical indicators of the trend for this test.

The Kendall tau measures the correlation between variables, in this case, rainfall and time. A positive ($z > 0$) Kendall tau value shows an increasing trend in the data set, and vice versa. The p-value shows the significance of trends. For this study, a 5% significance level was used to compute the trend analysis. Hence, trends with p-values less than 0.05 will be considered significant and vice versa. The Sen's slope estimates the magnitude of the trends. In a time series, a Sen's slope estimator $\beta > 0$ implies an upward trend, otherwise the data shows a downward trend.

The test Mann Kendall test was performed based on the daily maximum rainfall (Intensity), annual and monthly total rainfall from 1980 to 2018. A decadal trend analysis was also performed to estimate decadal trends in rainfall within the basin.

4.1.5 Trend Analysis of Annual and Monthly Total Rainfall

The results of Mann-Kendall trend analysis and Sen's slope estimator showed that approximately 30% (2 out of 7) of the stations recorded increasing trend in annual rainfall amount while approximately 70% (5 out of 7) presented a decreasing trend in precipitation for the period 1980-2018. However, none of these trends are statistically significant. Figures 4.3 and 4.4 shows the trend of annual rainfall amount for the various stations within the period. This suggests that the basin recorded a general decreasing trend in rainfall amount for the period of 1980 to 2018. This is consistent with the findings of Odoulami & Akinsanola (2018), which used Mann-Kendall trend test to analyze the trend of annual rainfall in the West African sub-region for the period of 1998 to 2013. Their study recorded a decreasing trend of annual rainfall amount in the Guinea savanna of the region. The aforementioned study stated that the region

experienced localized increasing trends of rainfall within some parts of the Sahelian regions. Similar study by Ilori & Ajayi (2020) also reported a statistically non-significant decreasing trend of rainfall amount over the climatic zones of West Africa over the period 1961 to 2000. A study by Owusu et al (2008), also reported similar results of decreasing trend of annual rainfall amount for the period of 1951 to 2000 for the West African sub-region. However, the aforementioned study used Gridded monthly precipitation data from Global Precipitation Climatology Centre and not historical rainfall gauge data.

Some studies however, reported opposing results. For example, a study by Akpoti et al (2016), using Mann-Kendall trend test to assess the trend of total rainfall amount within the Black Volta basin in West Africa, reported a decreasing trend of annual rainfall amount for gauge stations within Ghana except Bui for the period of 1976 to 2011. Aziz et al (2019) also analyzed trend of annual rainfall within the Black Volta basin for the period 1981 to 2010 using Mann-Kendall trend test. The study recorded and increasing trend of annual rainfall within the basin. These conflicting results could be as a result in the difference in the investigation period used for the analysis and also the size of the area considered (Sanogo et al., 2015).

Positive slope of 2.24 mm/year and 4.06 mm/year were obtained for Bui and Wa stations respectively suggesting an increasing trend in annual total rainfall amount for the 38 years period. However, the p-values of 0.76 and 0.13 for Bui and Wa stations respectively suggest that the trends are statistically insignificant. Similar studies by Gbangou et al (2020) and Subaar et al (2018), also recorded significant increasing trend of annual rainfall amount for Wa station for the period of 1980 to 2018. Table 4.6 shows the results of Mann Kendal trend test and Sen's slope estimation for annual and monthly total rainfall for the selected period within the basin.

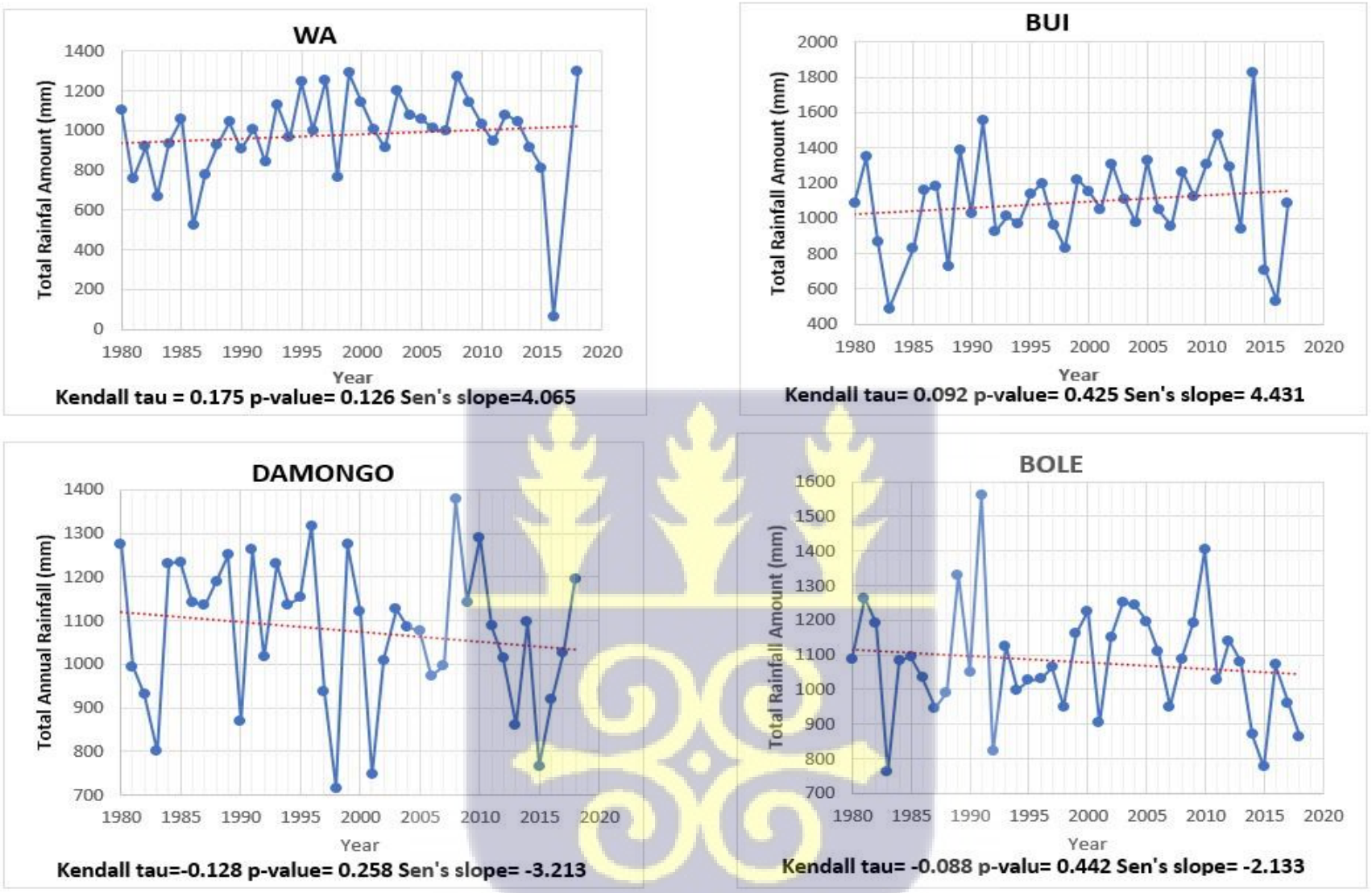

Figure 4. 3: Trend of annual rainfall amount for Wa, Bui, Damongo and Bole

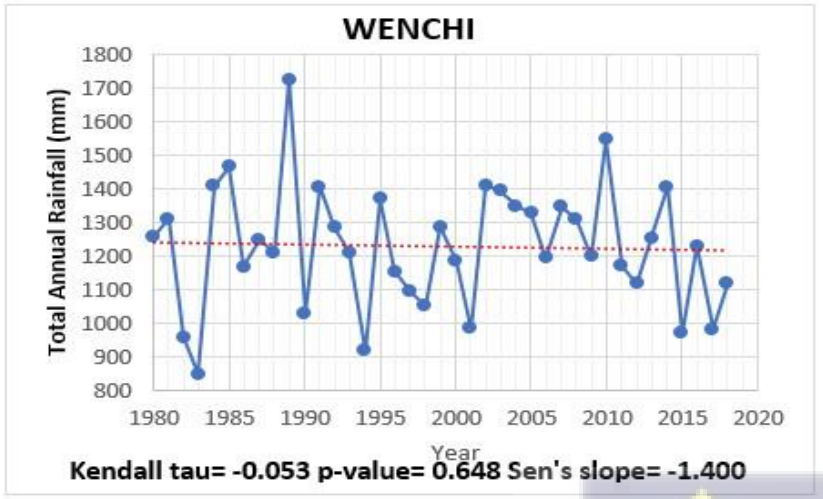

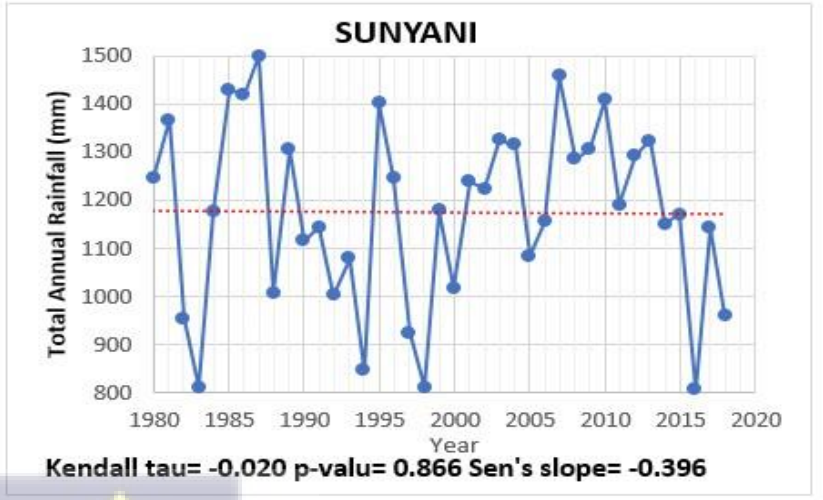

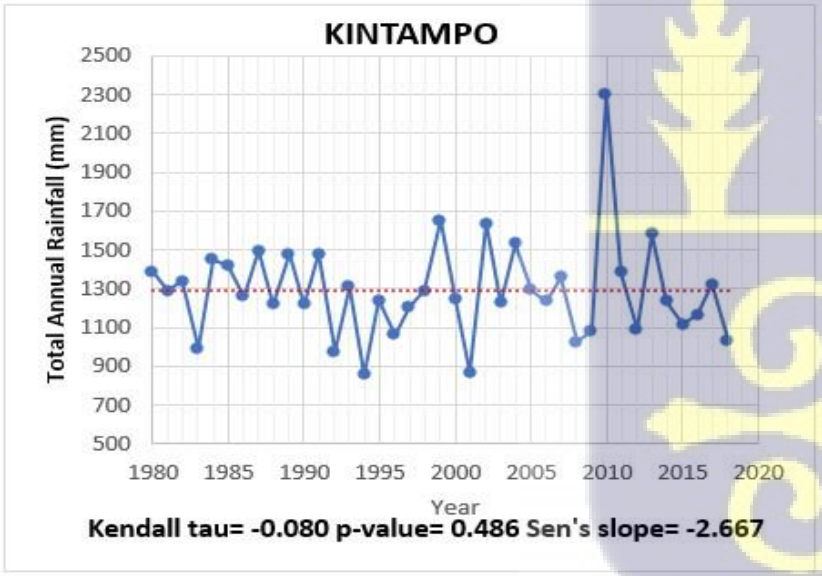

Figure 4. 4: Trend of annual rainfall amount for Sunyani, Wenchi and Kintampo

Table 4. 6: Mann–Kendal trend statistics for annual and monthly total rainfall amount (5% significance level)

WA				BUI				DAMONGO				BOLE			
Series	Kendall's tau	p-value	Sen's slope	Series	Kendall's tau	p-value	Sen's slope	Series	Kendall's tau	p-value	Sen's slope	Series	Kendall's tau	p-value	Sen's slope
Annual	0.17	0.13	4.06	**Annual**	0.03	0.76	2.24	**Annual**	-0.13	0.26	-3.21	**Annual**	-0.09	0.44	-2.13
Jan	-0.02	0.89	0.00	**Jan**	0.09	0.46	0.00	**Jan**	0.20	0.13	0.00	**Jan**	0.01	0.92	0.00
Feb	0.13	0.28	0.00	**Feb**	-0.11	0.36	0.00	**Feb**	0.30	**0.01**	0.14	**Feb**	0.09	0.42	0.00
Mar	-0.01	0.91	0.00	**Mar**	-0.19	0.11	-1.19	**Mar**	-0.11	0.33	-0.29	**Mar**	-0.10	0.35	-0.39
Apr	0.06	0.62	0.40	**Apr**	0.19	0.12	1.41	**Apr**	-0.04	0.69	-0.28	**Apr**	0.11	0.32	0.59
May	0.07	0.58	0.46	**May**	0.14	0.25	1.08	**May**	-0.06	0.56	-0.38	**May**	-0.12	0.30	-0.78
Jun	0.10	0.41	0.82	**Jun**	-0.04	0.77	-0.35	**Jun**	0.09	0.41	0.72	**Jun**	0.08	0.50	0.41
Jul	-0.18	0.11	-0.98	**Jul**	-0.08	0.50	-0.75	**Jul**	-0.12	0.30	-0.97	**Jul**	-0.14	0.21	-1.01
Aug	0.21	0.07	2.48	**Aug**	-0.13	0.30	-1.05	**Aug**	-0.01	0.94	-0.12	**Aug**	0.01	0.92	0.09
Sep	0.22	0.06	2.02	**Sep**	-0.10	0.39	-0.74	**Sep**	-0.11	0.32	-0.81	**Sep**	-0.10	0.36	-1.07
Oct	0.18	0.13	0.92	**Oct**	-0.09	0.47	-0.84	**Oct**	-0.02	0.87	-0.15	**Oct**	0.04	0.70	0.21
Nov	-0.04	0.75	0.00	**Nov**	0.16	0.18	0.31	**Nov**	-0.02	0.88	0.00	**Nov**	0.02	0.89	0.00
Dec	-0.27	0.05	0.00	**Dec**	0.17	0.20	0.00	**Dec**	0.08	0.51	0.00	**Dec**	-0.12	0.33	0.00

SUNYANI				WENCHI				KINTAMPO			
Series	Kendall's tau	p-value	Sen's slope	Series	Kendall's tau	p-value	Sen's slope	Series	Kendall's tau	p-value	Sen's slope
Annual	-0.02	0.87	-0.40	**Annual**	-0.05	0.65	-1.40	**Annual**	-0.08	0.49	-2.67
Jan	0.02	0.90	0.00	**Jan**	0.05	0.68	0.00	**Jan**	0.08	0.50	0.00
Feb	0.09	0.46	0.52	**Feb**	0.20	0.07	0.55	**Feb**	0.14	0.21	0.33
Mar	-0.14	0.21	-1.20	**Mar**	-0.15	0.18	-1.45	**Mar**	-0.03	0.82	-0.26
Apr	0.07	0.56	0.52	**Apr**	-0.13	0.26	-1.05	**Apr**	-0.09	0.43	-0.75
May	-0.01	0.94	-0.18	**May**	0.08	0.50	0.67	**May**	0.29	**0.01**	2.37
Jun	0.12	0.29	1.42	**Jun**	0.15	0.18	0.85	**Jun**	-0.04	0.75	-0.20
Jul	-0.07	0.51	-0.60	**Jul**	-0.08	0.50	-0.71	**Jul**	-0.12	0.27	-1.66
Aug	-0.11	0.32	-0.84	**Aug**	-0.09	0.40	-0.90	**Aug**	-0.21	0.07	-1.87
Sep	-0.04	0.71	-0.35	**Sep**	-0.08	0.50	-0.69	**Sep**	-0.03	0.83	-0.27
Oct	0.05	0.68	0.22	**Oct**	0.14	0.23	1.32	**Oct**	0.24	**0.04**	2.26
Nov	0.23	**0.04**	0.95	**Nov**	0.13	0.24	0.53	**Nov**	0.07	0.52	0.22
Dec	-0.10	0.38	0.00	**Dec**	0.03	0.81	0.00	**Dec**	-0.07	0.58	0.00

On a monthly scale, the month of February recorded a statistically significant increasing rainfall trend for Damongo (p-value of 0.01) station. Kintampo station showed significant decreasing rainfall trends in the moths of May (p-value of 0.01) and a significant decreasing rainfall trend for the month of October (p-value of 0.04). A significant increasing rainfall trend was recorded for Sunyani station (p-value of 0.04) for the month of November. The month of July showed a decreasing rainfall trend for all the stations within the basin, this could be attributed to climate change causing a shift in the rainy season. Abungba et al (2020) also recorded decreasing trend of rainfall for the month of July in the basin for the period of 1961 to 2016, using Mann-Kendall trend test which he attributed to impacts of climate change. Ilori & Ajayi (2020) also pointed out that the decreasing trends of annual rainfall over West Africa is due to climate change as a result of global warming.

When using long term trends, there is underestimation of trends with high slope values (Ackom et al., 2020). Hence, there is the need for a decadal trend analysis because it provides more details about Spatio-temporal trends in an area. Kpanou et al (2021) also stated that Ghana has strong inter annual and decadal variability of rainfall. Ergo, the decadal trend analysis of rainfall amount for the basin was assessed and is discussed in the next section of this report.

4.1.6 Trend Analysis of Decadal Annual and Monthly Rainfall Amount

The decadal rainfall amount trend analysis for Wa station is illustrated in table 4.7. The results revealed an increasing rainfall trend for the periods 1980-1989, 1990-1999, and 2000-2009, which agrees with the studies of (Gbangou et al., 2020). Whereas, the period 2010-2018 showed a decreasing trend. However, none of these trends is statistically significant. Within the 1980-1989 period, the months of June recorded an increasing trend of rainfall amount. Whereas, within 2000-2009, March showed significant increasing trend of rainfall amount.

Table 4. 7: Decadal Mann–Kendal trend statistics for annual and monthly total rainfall amount for Wa station (5% significance level)

WA						
	1980-1989			1990-1999		
	Kendall's tau	p-value	Sen's slope	Kendall's tau	p-value	Sen's slope
Annual	0.02	1.00	1.85	0.33	0.22	31.00
Jan	-0.47	0.12	0.00	0.45	0.12	0.00
Feb	-0.49	0.08	-0.73	0.38	0.15	0.40
Mar	-0.11	0.73	-1.48	0.40	0.12	3.52
Apr	-0.38	0.16	-8.90	-0.11	0.73	-2.56
May	-0.07	0.86	-3.78	-0.20	0.48	-5.87
Jun	0.47	0.07	8.97	0.24	0.38	6.41
Jul	-0.07	0.86	-0.36	-0.29	0.29	-7.21
Aug	0.16	0.60	2.92	0.11	0.73	0.95
Sep	0.20	0.48	7.20	0.51	0.05	24.53
Oct	0.06	0.92	1.44	0.20	0.48	1.85
Nov	-0.26	0.34	-0.93	-0.03	0.92	0.00
Dec	0.04	0.88	0.00	-0.25	0.36	0.00
	2000-2009			2010-2018		
	Kendall's tau	p-value	Sen's slope	Kendall's tau	p-value	Sen's slope
Annual	0.11	0.73	12.30	-0.21	0.55	-33.90
Jan	-0.24	0.37	0.00			
Feb	0.27	0.31	0.00	-0.04	0.90	-0.20
Mar	0.64	**0.01**	4.02	0.36	0.28	3.68
Apr	-0.07	0.86	-0.53	-0.29	0.40	-12.13
May	-0.16	0.60	-3.70	-0.52	0.14	-13.25
Jun	-0.24	0.38	-9.68	0.33	0.38	10.54
Jul	0.24	0.38	3.35	-0.24	0.56	-3.24
Aug	0.11	0.73	4.76	-0.05	1.00	-0.50
Sep	0.16	0.60	4.30	0.05	1.00	2.63
Oct	0.51	0.05	9.78	0.24	0.56	7.05
Nov	0.13	0.63	0.00	-0.10	0.76	-0.25

The decadal trend analysis for total rainfall amount for Bui station is shown in table 4.8. The result revealed an increasing rainfall trend for the periods 1980-1989. The periods 1990-1999, 2000-2009 and 2010-2018 showed a decreasing trend. However, none of these trends is statistically significant. There was also no significant monthly trends for the station. Comparing this result to the result of the trend test for the whole period (1980-2018) which showed increasing trend, it could be said that even though three (3) decades showed decreasing trend, overall the station still records an increasing trend of total rainfall amount.

Table 4. 8: Decadal Mann–Kendal trend statistics for annual and monthly total rainfall amount for Bui station (5% significance level).

BUI						
	1980-1989			1990-1999		
	Kendall's tau	p-value	Sen's slope	Kendall's tau	p-value	Sen's slope
Annual	0.11	0.76	14.76	-0.07	0.86	-5.20
Jan	-0.58	0.14	0.00	0.17	0.52	0.01
Feb	-0.49	0.13	-6.70	0.00	1.00	0.00
Mar	-0.24	0.56	-3.35	-0.20	0.48	-7.90
Apr	-0.07	0.90	-1.23	-0.02	1.00	-0.55
May	-0.07	0.90	-1.75	-0.11	0.73	-3.45
Jun	0.47	0.27	20.50	0.02	1.00	1.90
Jul	0.36	0.28	8.63	0.11	0.73	2.22
Aug	0.36	0.28	2.31	-0.02	1.00	-0.10
Sep	0.07	0.90	2.54	0.29	0.29	9.38
Oct	0.14	0.72	5.78	0.20	0.48	10.70
Nov	-0.49	0.13	-2.42	-0.27	0.28	-3.43
Dec				-0.38	0.15	-0.34
	2000-2009			2010-2018		
	Kendall's tau	p-value	Sen's slope	Kendall's tau	p-value	Sen's slope
Annual	-0.11	0.73	-7.10	-0.43	0.18	-119.60
Jan	-0.21	0.40	-0.20	-0.40	0.18	-3.43
Feb	0.22	0.42	0.00	-0.26	0.34	-2.75
Mar	0.02	1.00	0.68	0.24	0.56	3.21
Apr	-0.16	0.60	-7.13	-0.07	1.00	-0.40
May	-0.16	0.60	-0.48	-0.21	0.55	-9.83
Jun	-0.24	0.38	-10.86	-0.50	0.11	-15.87
Jul	0.16	0.60	5.50	-0.52	0.14	-22.97
Aug	0.16	0.60	3.32	-0.24	0.56	-6.79
Sep	-0.38	0.16	-3.91	-0.11	0.71	-2.70
Oct	0.29	0.29	9.11	-0.36	0.28	-14.94
Nov	0.11	0.73	1.55	0.14	0.72	2.42
Dec	-0.08	0.77	0.00	0.10	0.75	0.00

The decadal trend analysis for rainfall amount for Damongo station (Table 4.9) revealed an increasing rainfall trend for the periods 1980-1989, 1990-1999 and 2000-2009, whereas the periods 2010-2018 showed a decreasing trend. However, none of these trends is statistically significant. Comparing this result to the result of the trend test for the whole period (1980-2018) which showed decreasing trend, it could be said that even though three (3) decades showed increasing trend, overall the station still records a decreasing trend of total rainfall amount.

Table 4. 9: Decadal Mann–Kendal trend statistics for annual and monthly total rainfall amount for Damongo station (5% significance level)

DAMONGO						
	1980-1989			1990-1999		
	Kendall's tau	p-value	Sen's slope	Kendall's tau	p-value	Sen's slope
Annual	0.16	0.60	23.35	0.07	0.86	7.57
Jan				0.47	0.12	0.00
Feb	-0.38	0.15	0.00	0.33	0.21	0.88
Mar	0.02	1.00	0.10	-0.20	0.48	-2.88
Apr	-0.16	0.60	-3.53	0.07	0.86	2.11
May	-0.07	0.86	-4.48	-0.24	0.38	-7.89
Jun	0.38	0.16	11.64	-0.07	0.86	-2.63
Jul	-0.16	0.60	-3.19	-0.16	0.60	-4.43
Aug	0.29	0.29	8.86	0.24	0.38	3.90
Sep	0.07	0.86	1.83	0.07	0.86	1.54
Oct	-0.07	0.86	-1.85	-0.02	1.00	-0.20
Nov	-0.02	0.93	0.00	-0.03	0.92	0.00
Dec	-0.04	0.90	0.00	-0.49	0.07	0.00
	2000-2009			2010-2018		
	Kendall's tau	p-value	Sen's slope	Kendall's tau	p-value	Sen's slope
Annual	0.20	0.48	16.35	-0.11	0.76	-17.61
Jan	-0.33	0.22	0.00	0.04	0.88	0.00
Feb	0.31	0.23	0.36	-0.06	0.92	-0.55
Mar	0.33	0.22	3.63	0.28	0.36	3.39
Apr	-0.07	0.86	-1.53	0.33	0.26	7.51
May	0.29	0.29	5.40	0.06	0.92	2.43
Jun	-0.29	0.29	-5.47	-0.22	0.48	-8.12
Jul	0.24	0.38	8.88	0.22	0.48	4.11
Aug	0.07	0.86	1.59	-0.06	0.92	-2.99
Sep	0.07	0.86	3.48	-0.17	0.61	-6.56
Oct	0.42	0.11	10.01	-0.33	0.26	-6.15
Nov	-0.09	0.72	-0.16	-0.09	0.75	-0.08
Dec	0.00	1.00	0.00	-0.26	0.36	0.00

The decadal trend analysis for rainfall amount for Bole station (Table 4.10) revealed an increasing rainfall trend for the periods 1990-1999 whereas the periods 1980-1989, 2000-2009 and 2010-2018 showed a decreasing trend. However, only the trend recorded during the 2010-2018 period is statistically significant. The monthly trends showed a statistically significant increasing trend for June within the 1980-1989 period, and September within the 2010-2018 period.

Table 4. 10: Decadal Mann–Kendal trend statistics for annual and monthly total rainfall amount for Bole station (5% significance level)

BOLE						
	1980-1989			**1990-1999**		
	Kendall's tau	**p-value**	**Sen's slope**	**Kendall's tau**	**p-value**	**Sen's slope**
Annual	-0.16	0.60	-19.93	0.02	1.00	1.73
Jan	-0.45	0.12	0.00	0.37	0.18	0.00
Feb	-0.48	0.06	-1.52	0.31	0.23	2.50
Mar	-0.42	0.11	-6.84	-0.13	0.59	-2.18
Apr	-0.02	1.00	-1.32	-0.02	1.00	-0.10
May	-0.24	0.38	-6.00	-0.20	0.48	-6.88
Jun	0.78	**0.00**	21.48	0.38	0.16	7.83
Jul	-0.42	0.11	-9.20	-0.47	0.07	-8.93
Aug	-0.07	0.86	-2.19	0.24	0.38	8.18
Sep	0.02	1.00	0.02	0.02	1.00	1.50
Oct	0.16	0.60	1.09	-0.16	0.60	-5.50
Nov	-0.04	0.86	-0.25	-0.09	0.72	-1.20
Dec	-0.18	0.50	0.00	-0.33	0.22	0.00
	2000-2009			**2010-2018**		
	Kendall's tau	**p-value**	**Sen's slope**	**Kendall's tau**	**p-value**	**Sen's slope**
Annual	-0.20	0.48	-9.55	-0.56	**0.04**	-53.89
Jan	-0.24	0.37	0.00	0.00	1.00	0.00
Feb	0.28	0.29	0.94	-0.14	0.60	-0.70
Mar	0.02	1.00	0.47	-0.11	0.76	-1.44
Apr	0.02	1.00	0.50	-0.28	0.36	-2.99
May	-0.33	0.22	-7.73	0.17	0.61	4.73
Jun	-0.20	0.48	-3.43	-0.33	0.26	-9.35
Jul	0.11	0.73	2.20	0.44	0.12	12.41
Aug	0.11	0.73	5.50	-0.39	0.18	-14.37
Sep	-0.20	0.48	-6.26	-0.56	**0.04**	-13.91
Oct	0.29	0.29	6.47	-0.39	0.18	-11.63
Nov	-0.45	0.07	-3.28	0.11	0.76	1.51
Dec	0.22	0.42	0.00	-0.24	0.44	0.00

The trend analysis for decadal rainfall amount for Sunyani station (Table 4.11) revealed an increasing rainfall trend for the periods 1980-1989 and 2000-2009, whereas the periods 1990-1999 and 2010-2018 showed a decreasing trend. However, only the trend recorded during the 2010-2018 period is statistically significant. The monthly trends were statistically insignificant throughout the period.

Table 4. 11: Decadal Mann–Kendal trend statistics for annual and monthly total rainfall amount for Sunyani station (5% significance level)

SUNYANI						
	1980-1989			**1990-1999**		
	Kendall's tau	**p-value**	**Sen's slope**	**Kendall's tau**	**p-value**	**Sen's slope**
Annual	0.20	0.48	22.12	-0.11	0.73	-15.84
Jan	-0.51	0.13	-1.73	0.33	0.21	0.70
Feb	-0.17	0.61	-2.61	-0.16	0.60	-3.15
Mar	0.16	0.60	6.01	0.20	0.48	5.34
Apr	-0.16	0.60	-2.26	-0.20	0.48	-6.01
May	-0.29	0.29	-11.15	-0.17	0.61	-4.81
Jun	0.33	0.22	15.00	0.20	0.48	5.03
Jul	0.07	0.86	3.47	-0.02	1.00	-0.82
Aug	0.33	0.22	11.18	0.29	0.29	7.13
Sep	0.02	1.00	2.83	-0.11	0.76	-1.66
Oct	-0.07	0.86	-1.08	0.42	0.11	5.73
Nov	-0.38	0.16	-2.07	-0.24	0.38	-6.30
Dec	-0.20	0.46	-0.77	-0.22	0.37	-1.38
	2000-2009			**2010-2018**		
	Kendall's tau	**p-value**	**Sen's slope**	**Kendall's tau**	**p-value**	**Sen's slope**
Annual	0.29	0.29	23.12	-0.67	**0.01**	-47.72
Jan	-0.41	0.10	-3.04	0.00	1.00	0.00
Feb	0.22	0.48	3.04	-0.11	0.76	-1.25
Mar	0.16	0.60	2.66	-0.17	0.61	-2.08
Apr	-0.42	0.11	-15.44	-0.11	0.76	-3.57
May	0.20	0.48	3.51	-0.33	0.26	-4.79
Jun	0.02	1.00	0.28	-0.50	0.11	-30.48
Jul	0.20	0.48	6.46	-0.17	0.61	-6.48
Aug	-0.07	0.86	-2.27	0.11	0.76	5.47
Sep	0.20	0.48	9.80	0.00	0.92	-1.52
Oct	0.24	0.38	11.40	-0.25	0.35	-11.51
Nov	0.02	1.00	1.40	0.06	0.92	1.77
Dec	0.31	0.23	1.27	-0.30	0.27	-0.32

The trend analysis for decadal rainfall amount for Wenchi station (Table 4.12) revealed an increasing rainfall trend for the period 1980-1989, whereas the periods 1990-1999, 2000-2009 and 2010-2018 showed a decreasing trend. However, none of the trends is statistically significant. The monthly trends were statistically insignificant throughout the period. Overall, the station recorded a decreasing trend of annual total rainfall amount for the selected period (1980-2018), this is in line with the studies of (Owusu & Waylen, 2013).

Table 4. 12: Decadal Mann–Kendal trend statistics for annual and monthly total rainfall amount for Wenchi station (5% significance level)

WENCHI						
	1980-1989			**1990-1999**		
	Kendall's tau	**p-value**	**Sen's slope**	**Kendall's tau**	**p-value**	**Sen's slope**
Annual	0.20	0.48	41.50	-0.11	0.73	-18.90
Jan	0.00	1.00	0.00	0.13	0.63	0.00
Feb	-0.02	1.00	-0.10	-0.24	0.38	-1.87
Mar	0.16	0.60	8.35	0.16	0.60	8.25
Apr	-0.29	0.29	-4.35	0.20	0.48	2.56
May	0.07	0.86	3.55	-0.20	0.48	-5.98
Jun	0.51	0.05	10.70	0.11	0.73	3.50
Jul	0.16	0.60	3.12	-0.07	0.86	-1.20
Aug	0.24	0.38	9.68	0.02	1.00	1.33
Sep	0.20	0.48	10.80	-0.29	0.29	-12.10
Oct	0.07	0.86	2.89	0.42	0.11	11.77
Nov	-0.11	0.73	-2.80	-0.20	0.48	-6.21
Dec	0.05	0.84	0.00	-0.36	0.16	-3.10
	2000-2009			**2010-2018**		
	Kendall's tau	**p-value**	**Sen's slope**	**Kendall's tau**	**p-value**	**Sen's slope**
Annual	-0.11	0.73	-9.70	-0.33	0.26	-42.08
Jan	-0.23	0.36	-1.63	-0.26	0.36	0.00
Feb	0.18	0.47	1.16	-0.33	0.26	-2.70
Mar	0.42	0.11	9.05	0.22	0.48	5.83
Apr	-0.42	0.11	-4.57	-0.28	0.36	-11.17
May	-0.11	0.73	-0.88	-0.39	0.18	-11.97
Jun	-0.47	0.07	-14.10	-0.11	0.76	-4.15
Jul	0.16	0.60	4.35	-0.17	0.61	-6.53
Aug	0.31	0.21	3.10	0.28	0.36	13.18
Sep	0.29	0.29	7.30	-0.28	0.36	-9.66
Oct	0.47	0.07	14.07	-0.33	0.26	-11.64
Nov	0.09	0.72	1.33	-0.28	0.36	-2.83
Dec	0.31	0.21	1.04	-0.26	0.36	0.00

The trend analysis for decadal rainfall amount for Kintampo station (Table 4.13) revealed an increasing rainfall trend for the period 1980-1989 and 1990-1999 whereas the periods 2000-2009 and 2010-2018 showed a decreasing trend. However, none of the trends is statistically significant. The monthly trends revealed a statistically significant increasing trend of rainfall for June within the 1980-1989 period and March within the 2000-2009 period. The 2010-2018 period recorded a significant decreasing trend of rainfall for the months May, October and December.

Table 4. 13: Decadal Mann–Kendal trend statistics for annual and monthly total rainfall amount for Kintampo station (5% significance level)

KINTAMPO						
	1980-1989			**1990-1999**		
	Kendall's tau	**p-value**	**Sen's slope**	**Kendall's tau**	**p-value**	**Sen's slope**
Annual	0.16	0.60	14.88	0.16	0.60	20.88
Jan	-0.49	0.07	0.00	0.33	0.24	0.00
Feb	-0.09	0.72	-0.27	0.22	0.37	1.80
Mar	0.28	0.36	7.39	-0.18	0.47	-2.03
Apr	-0.11	0.73	-3.02	0.16	0.60	3.32
May	-0.24	0.38	-2.53	0.20	0.48	5.67
Jun	0.63	**0.01**	16.60	0.42	0.11	9.68
Jul	-0.13	0.59	-12.97	0.07	0.86	1.22
Aug	0.13	0.59	14.63	0.02	1.00	0.15
Sep	0.02	1.00	3.43	-0.16	0.60	-6.68
Oct	-0.22	0.48	-8.06	0.38	0.16	10.20
Nov	0.02	1.00	0.44	0.02	1.00	0.06
Dec	-0.55	0.06	-0.23	-0.33	0.21	-0.85
	2000-2009			**2010-2018**		
	Kendall's tau	**p-value**	**Sen's slope**	**Kendall's tau**	**p-value**	**Sen's slope**
Annual	-0.16	0.60	-23.93	-0.44	0.12	-57.44
Jan	-0.38	0.15	-1.10	-0.18	0.57	0.00
Feb	0.26	0.31	3.72	-0.50	0.08	-5.35
Mar	0.64	**0.01**	9.70	0.17	0.61	6.83
Apr	-0.16	0.60	-4.84	0.11	0.76	1.46
May	0.11	0.76	6.41	-0.56	**0.04**	-23.08
Jun	-0.38	0.16	-11.40	-0.17	0.61	-10.83
Jul	0.16	0.60	5.55	-0.44	0.12	-13.36
Aug	-0.16	0.60	-6.24	0.17	0.61	9.02
Sep	0.20	0.48	3.52	-0.33	0.26	-12.91
Oct	0.11	0.73	2.00	-0.71	**0.01**	-33.40
Nov	-0.11	0.73	-0.90	-0.36	0.28	-4.01
Dec	0.24	0.38	0.48	-0.72	**0.04**	-0.50

4.1.7 Trend Analysis of Annual and Monthly Rainfall Intensity

On an annual scale, all the stations recorded increasing rainfall intensity trends except Damongo station, which had a Sen's slope of -0.028mm/year with a p-value of 0.88, suggesting a decreasing trend, however, statistically insignificant. This suggests an overall increasing rainfall intensity trend in the basin. This is consistent with a study conducted by Tabari (2020), who suggested an increasing trend of precipitation intensity across all climatic regions globally in response to global warming. Similar study by Ackom et al (2020) in the Odaw river basin of Ghana, also recorded increasing rainfall intensities for all the station within the basin. Increasing rainfall intensity is becoming more common as a result of climate change, and this raises the potential of devastating flood events that endanger both people and property (Mensah & Ahadzie, 2020). A study conducted by Karamage et al (2018) to assess the relationship between precipitation and runoff in Africa concluded that, humid tropical basins and nations with high rainfall intensity have higher runoff depths and runoff coefficients which could lead to severe flash floods in those regions. Atanga & Tankpa (2021) in their study concluded that flash floods are common in Ghana, they occur annually and may occur several times throughout the wet season, and are caused by increasing rainfall intensity. Manzanas et al (2014), assessed precipitation variability and trends in Ghana using Mann-Kendall trend test, and observed increasing rainfall intensity from 1986 to 2010. The results of Mann Kendall trend analysis for annual and monthly rainfall intensities for the period 1980-2018 is shown in Table 4.14.

Table 4. 14: Mann–Kendal trend statistics for annual and monthly daily maximum rainfall (intensities) (5% significance level)

	WA				BUI				DAMONGO				BOLE		
	Kendall's tau	p-value	Sen's slope		Kendall's tau	p-value	Sen's slope		Kendall's tau	p-value	Sen's slope		Kendall's tau	p-value	Sen's slope
Annual	0.26	**0.02**	0.81	**Annual**	0.15	0.19	0.42	**Annual**	-0.02	0.89	-0.03	**Annual**	0.14	0.20	0.32
Jan	-0.02	0.89	0.00	**Jan**	0.10	0.45	0.00	**Jan**	0.21	0.12	0.00	**Jan**	0.02	0.89	0.00
Feb	0.14	0.26	0.00	**Feb**	-0.04	0.74	0.00	**Feb**	0.27	**0.02**	0.10	**Feb**	0.10	0.40	0.00
Mar	-0.01	0.91	0.00	**Mar**	-0.21	0.09	-0.55	**Mar**	-0.09	0.40	-0.16	**Mar**	-0.07	0.55	-0.17
Apr	0.11	0.34	0.28	**Apr**	0.27	**0.03**	0.71	**Apr**	-0.10	0.37	-0.25	**Apr**	0.12	0.28	0.28
May	0.12	0.31	0.21	**May**	0.12	0.31	0.31	**May**	-0.02	0.88	-0.04	**May**	-0.01	0.94	-0.03
Jun	0.13	0.27	0.32	**Jun**	-0.06	0.66	-0.13	**Jun**	0.14	0.21	0.29	**Jun**	0.15	0.19	0.35
Jul	-0.09	0.46	-0.16	**Jul**	-0.06	0.63	-0.18	**Jul**	-0.06	0.57	-0.14	**Jul**	-0.10	0.36	-0.27
Aug	0.31	**0.01**	0.75	**Aug**	-0.06	0.65	-0.13	**Aug**	-0.03	0.80	-0.04	**Aug**	0.09	0.41	0.28
Sep	0.22	0.06	0.36	**Sep**	0.04	0.73	0.13	**Sep**	-0.16	0.17	-0.32	**Sep**	-0.04	0.75	-0.08
Oct	0.05	0.64	0.09	**Oct**	-0.16	0.19	-0.38	**Oct**	-0.06	0.56	-0.12	**Oct**	0.01	0.90	0.04
Nov	-0.06	0.65	0.00	**Nov**	0.16	0.17	0.20	**Nov**	-0.04	0.71	0.00	**Nov**	0.01	0.90	0.00
Dec	-0.27	0.05	0.00	**Dec**	0.18	0.17	0.00	**Dec**	0.09	0.48	0.00	**Dec**	-0.12	0.33	0.00

	SUNYANI				WENCHI				KINTAMPO		
	Kendall's tau	p-value	Sen's slope		Kendall's tau	p-value	Sen's slope		Kendall's tau	p-value	Sen's slope
Annual	0.03	0.79	0.10	**Annual**	0.00	1.00	0.00	**Annual**	0.05	0.67	0.10
Jan	0.01	0.93	0.00	**Jan**	0.04	0.72	0.00	**Jan**	0.08	0.52	0.00
Feb	0.09	0.42	0.31	**Feb**	0.21	0.06	0.28	**Feb**	0.20	0.07	0.27
Mar	-0.22	0.05	-0.38	**Mar**	-0.13	0.24	-0.50	**Mar**	0.00	0.98	0.00
Apr	0.03	0.81	0.08	**Apr**	0.02	0.88	0.04	**Apr**	-0.02	0.84	-0.06
May	0.20	0.07	0.48	**May**	-0.05	0.65	-0.12	**May**	0.20	0.07	0.62
Jun	0.06	0.59	0.17	**Jun**	0.09	0.44	0.23	**Jun**	-0.07	0.55	-0.18
Jul	-0.09	0.44	-0.23	**Jul**	-0.04	0.69	-0.13	**Jul**	-0.04	0.73	-0.11
Aug	-0.10	0.36	-0.22	**Aug**	-0.02	0.83	-0.05	**Aug**	-0.13	0.25	-0.30
Sep	-0.10	0.37	-0.27	**Sep**	-0.06	0.62	-0.12	**Sep**	-0.01	0.93	-0.02
Oct	0.04	0.72	0.07	**Oct**	-0.03	0.80	-0.05	**Oct**	0.24	**0.03**	0.42
Nov	0.20	0.07	0.29	**Nov**	0.09	0.43	0.14	**Nov**	0.09	0.44	0.18
Dec	-0.12	0.32	0.00	**Dec**	0.05	0.64	0.00	**Dec**	-0.07	0.58	0.00

Positive slope of 0.81 mm/year was obtained for Wa, with a p-value of 0.02 suggesting a statistically significant increasing trend in annual rainfall intensity for the period.

On a monthly scale, Damongo station recorded a significant increasing trend of rainfall intensity for the month of February. A significant increasing trend was recorded at Bui Station for April, and at Wa station for August, and at Kintampo station for October.

From the results of the trend analysis for annual rainfall amount and annual rainfall intensity, the annual rainfall amount shows a general decreasing trend for the basin, while the annual rainfall intensity shows an increasing trend. Hence, it can be inferred that flooding within the Black Volta basin is associated with increasing intensity of rainfall within the region.

According to Tabari (2020), the increasing rainfall intensity trend and the projected decrease in total precipitation supports the "it never rains, but it pours" trend.

4.1.8 Decadal Annual and Monthly Rainfall Intensities Trend Analysis

The trend of decadal rainfall Intensity for Wa station is shown in table 4.15. The results revealed a decreasing trend of rainfall intensity for the periods 1980-1989 and 2010-2018. Whereas, the 1990-1999 and 2000-2009 period showed an increasing trend. However, none of these trends is statistically significant. Within the 1990-1999 period, the months of April recorded a statistically significant increasing trend of rainfall amount. Within 2000-2009 also, March and October showed significant increasing trend of rainfall Intensity.

Table 4. 15: Decadal Mann–Kendal trend statistics for annual and monthly rainfall Intensity for Wa station (5% significance level)

WA	1980-1989			1990-1999		
	Kendall's tau	p-value	Sen's slope	Kendall's tau	p-value	Sen's slope
Annual	-0.022	1.000	-0.411	0.111	0.721	0.967
Jan	-0.471	0.121	0.000	0.447	0.117	0.000
Feb	-0.487	0.080	-0.621	0.378	0.150	0.400
Mar	-0.156	0.601	-1.400	0.368	0.146	1.900
Apr	-0.200	0.484	-0.650	-0.511	**0.047**	-4.025
May	-0.200	0.484	-0.922	-0.156	0.601	-1.050
Jun	0.244	0.381	0.700	0.156	0.601	1.400
Jul	0.067	0.862	0.450	-0.289	0.291	-1.086
Aug	0.244	0.381	1.443	-0.135	0.590	-1.380
Sep	-0.225	0.369	-0.660	0.467	0.073	6.020
Oct	0.056	0.919	1.044	-0.022	1.000	-0.240
Nov	-0.319	0.242	-0.825	0.029	0.915	0.000
Dec	0.043	0.885	0.000	-0.253	0.365	0.000
	2000-2009			**2010-2018**		
	Kendall's tau	p-value	Sen's slope	Kendall's tau	p-value	Sen's slope
Annual	0.378	1.700	0.152	-0.143	0.711	-5.487
Jan	-0.243	0.373	0.000			
Feb	0.272	0.309	0.000	-0.036	0.901	-0.200
Mar	0.644	**0.009**	1.975	0.286	0.399	1.386
Apr	0.333	0.216	2.133	-0.429	0.179	-4.933
May	0.111	0.727	0.575	-0.429	0.239	-2.100
Jun	-0.200	0.484	-1.300	0.333	0.381	2.500
Jul	0.200	0.484	1.938	-0.524	0.136	-1.900
Aug	0.156	0.601	1.100	-0.048	1.000	-1.000
Sep	-0.067	0.862	-0.233	-0.048	1.000	-0.025
Oct	0.511	**0.047**	3.700	0.619	0.069	3.350
Nov	0.076	0.773	0.000	-0.098	0.761	-0.250

The trend of decadal rainfall Intensity for Bui station on an annual scale (table 4.16) revealed an increasing rainfall trend for the periods 1980-1989 and 2000-2009. Whereas, the 1990-1999 and 2010-2018 period showed a decreasing trend. However, none of these trends is statistically significant. None of the months showed any significant decadal trend.

Table 4. 16: Decadal Mann–Kendal trend statistics for annual and monthly rainfall Intensity for Bui station (5% significance level)

BUI	1980-1989			1990-1999		
	Kendall's tau	p-value	Sen's slope	Kendall's tau	p-value	Sen's slope
Annual	0.254	0.402	2.763	-0.022	1.000	-0.171
Jan	-0.577	0.143	0.000	0.167	0.516	0.014
Feb	-0.488	0.129	-4.225	0.000	1.000	0.000
Mar	-0.143	0.773	-1.480	-0.111	0.727	-1.700
Apr	0.286	0.399	2.250	0.022	1.000	0.250
May	-0.143	0.720	-1.209	0.022	1.000	0.250
Jun	0.467	0.272	4.733	0.022	1.000	0.363
Jul	0.327	0.262	1.674	0.156	0.601	2.967
Aug	0.143	0.720	1.413	0.067	0.862	1.143
Sep	0.000	0.905	0.033	0.378	0.156	5.100
Oct	0.214	0.548	3.050	0.156	0.601	2.233
Nov	-0.293	0.362	-1.300	-0.315	0.209	-3.433
Dec				-0.378	0.150	-0.340
	2000-2009			**2010-2018**		
	Kendall's tau	p-value	Sen's slope	Kendall's tau	p-value	Sen's slope
Annual	0.111	0.721	0.675	-0.214	0.536	-1.465
Jan	-0.215	0.404	-0.200	-0.403	0.184	-3.425
Feb	0.218	0.416	0.000	-0.109	0.708	-2.383
Mar	-0.067	0.862	-0.660	0.238	0.562	1.400
Apr	-0.200	0.484	-0.975	0.333	0.469	2.350
May	-0.200	0.484	-2.517	-0.214	0.548	-3.413
Jun	-0.022	1.000	-0.100	0.000	0.905	-0.002
Jul	0.111	0.727	1.129	-0.524	0.136	-4.525
Aug	0.378	0.156	3.300	-0.048	1.000	-0.875
Sep	0.022	1.000	1.200	0.255	0.383	1.807
Oct	0.333	0.216	1.543	-0.357	0.275	-2.258
Nov	0.067	0.862	0.420	0.143	0.720	1.360
Dec	-0.025	0.923	0.000	0.103	0.754	0.000

The trend of decadal rainfall Intensity for Damongo station on an annual scale (table 4.17) revealed a decreasing rainfall trend for the periods 1980-1989, 2000-2009 and 2010-2018. Whereas, the 1990-1999 period showed an increasing trend. However, none of these trends is statistically significant. None of the months showed any significant decadal trend.

Table 4. 17: Decadal Mann–Kendal trend statistics for annual and monthly rainfall Intensity for Damongo station (5% significance level)

DAMONGO	1980-1989			1990-1999		
	Kendall's tau	p-value	Sen's slope	Kendall's tau	p-value	Sen's slope
Annual	-0.156	0.592	-0.867	0.422	0.107	5.500
Jan				0.471	0.121	0.000
Feb	-0.381	0.154	0.000	0.378	0.150	0.863
Mar	-0.067	0.862	-0.900	-0.111	0.727	-0.800
Apr	0.022	1.000	0.017	0.022	1.000	0.462
May	-0.067	0.862	-0.667	-0.111	0.727	-0.829
Jun	0.378	0.156	2.150	-0.156	0.601	-1.533
Jul	-0.156	0.601	-1.200	-0.378	0.156	-2.100
Aug	0.156	0.601	1.957	0.422	0.108	7.800
Sep	0.200	0.484	2.000	0.067	0.862	0.744
Oct	-0.244	0.381	-3.757	-0.200	0.484	-1.733
Nov	-0.024	0.926	0.000	-0.025	0.923	0.000
Dec	-0.036	0.897	0.000	-0.487	0.075	0.000
	2000-2009			**2010-2018**		
	Kendall's tau	p-value	Sen's slope	Kendall's tau	p-value	Sen's slope
Annual	-0.111	0.721	-0.600	-0.111	0.755	-1.092
Jan	-0.272	0.309	0.000	0.043	0.885	0.000
Feb	0.263	0.308	0.286	-0.056	0.919	-0.508
Mar	0.422	0.108	1.800	0.111	0.761	0.871
Apr	-0.156	0.601	-0.280	0.222	0.477	3.250
May	0.333	0.216	3.300	-0.028	0.917	-0.050
Jun	-0.156	0.601	-1.375	-0.222	0.477	-4.427
Jul	0.111	0.727	1.400	0.222	0.477	2.583
Aug	-0.156	0.601	-1.350	-0.111	0.761	-1.106
Sep	-0.244	0.381	-0.725	-0.222	0.477	-1.867
Oct	0.405	0.106	2.875	-0.333	0.260	-2.017
Nov	-0.184	0.468	-0.475	-0.087	0.750	-0.167
Dec	0.000	1.000	0.000	-0.261	0.357	0.000

The trend of decadal rainfall Intensity for Bole station on an annual scale (table 4.18) revealed a decreasing non-significant rainfall trend for the period 1980-1989 and a statistically significant decreasing trend for the periods 1990-1999 and 2010-2018. Whereas, the 2000-2009 period showed an increasing trend, which is not statistically significant. The month of June within the 1980-1989 decade showed a statistically significant increasing trend of rainfall intensity. Within the 2010-2018 period, the months of June and July showed significant decreasing and increasing rainfall intensity respectively.

Table 4. 18: Decadal Mann–Kendal trend statistics for annual and monthly rainfall Intensity for Bole station (5% significance level)

BOLE	**1980-1989**			**1990-1999**		
	Kendall's tau	**p-value**	**Sen's slope**	**Kendall's tau**	**p-value**	**Sen's slope**
Annual	-0.225	0.419	-2.600	-0.511	**0.049**	-7.140
Jan	-0.447	0.117	0.000	0.365	0.182	0.000
Feb	-0.484	0.063	-0.833	0.358	0.164	1.400
Mar	-0.289	0.291	-1.620	-0.180	0.472	-1.100
Apr	-0.378	0.156	-2.000	0.022	1.000	0.200
May	0.180	0.472	0.900	-0.200	0.484	-1.280
Jun	0.822	**0.000**	4.050	0.333	0.216	1.000
Jul	-0.378	0.156	-3.722	-0.244	0.381	-3.533
Aug	-0.067	0.862	-1.133	-0.022	1.000	-0.060
Sep	0.022	1.000	0.500	0.333	0.216	2.000
Oct	0.000	1.000	0.000	-0.244	0.381	-2.900
Nov	-0.090	0.719	-0.278	-0.092	0.717	-0.763
Dec	-0.183	0.504	0.000	-0.327	0.222	0.000
	2000-2009			**2010-2018**		
	Kendall's tau	**p-value**	**Sen's slope**	**Kendall's tau**	**p-value**	**Sen's slope**
Annual	0.244	0.371	2.533	-0.556	**0.032**	-2.383
Jan	-0.243	0.373	0.000	0.253	0.365	0.000
Feb	0.277	0.291	0.940	0.000	1.000	0.000
Mar	-0.067	0.862	-0.200	-0.244	0.381	-1.250
Apr	0.111	0.727	1.450	-0.333	0.216	-3.060
May	-0.067	0.862	-1.817	0.156	0.601	1.117
Jun	0.200	0.484	0.729	-0.556	**0.029**	-8.600
Jul	-0.022	1.000	-0.286	0.511	**0.047**	3.250
Aug	0.225	0.369	2.611	-0.422	0.108	-4.378
Sep	-0.111	0.727	-1.267	-0.315	0.209	-1.850
Oct	-0.045	0.857	-0.350	-0.022	1.000	-0.550
Nov	-0.432	0.087	-2.167	0.111	0.727	0.325
Dec	0.218	0.416	0.000	-0.248	0.384	0.000

The trend of decadal rainfall Intensity for Sunyani station on an annual scale (table 4.19) revealed an increasing non-significant rainfall trend for the period 1980-1989. Whereas, the periods 1990-1999, 2000-2009 and 2010-2018 showed a decreasing trend, which is not statistically significant. The month of October within the 2010-2018 period, showed a statistically significant decreasing trend of rainfall intensity.

Table 4. 19: Decadal Mann–Kendal trend statistics for annual and monthly rainfall Intensity for Sunyani station (5% significance level)

SUNYANI	1980-1989			1990-1999		
	Kendall's tau	p-value	Sen's slope	Kendall's tau	p-value	Sen's slope
Annual	0.022	1.000	0.600	-0.467	0.074	-3.700
Jan	-0.394	0.241	-1.029	0.277	0.291	0.700
Feb	-0.222	0.477	-2.218	-0.111	0.727	-1.040
Mar	0.360	0.151	1.400	0.000	1.000	0.000
Apr	-0.244	0.381	-1.520	-0.022	1.000	-0.533
May	-0.200	0.484	-0.967	0.111	0.761	0.868
Jun	0.244	0.381	1.250	-0.135	0.590	-1.133
Jul	0.156	0.601	2.440	-0.200	0.484	-0.550
Aug	0.422	0.108	4.060	0.467	0.073	2.500
Sep	0.022	1.000	0.320	-0.278	0.358	-2.592
Oct	-0.022	1.000	-0.014	-0.156	0.601	-1.050
Nov	-0.333	0.216	-1.711	-0.022	1.000	-0.040
Dec	-0.261	0.338	-0.933	-0.360	0.151	-2.214
	2000-2010			**2010-2018**		
	Kendall's tau	p-value	Sen's slope	Kendall's tau	p-value	Sen's slope
Annual	-0.289	0.283	-1.967	-0.022	1.000	-0.878
Jan	-0.396	0.121	-3.044	0.000	1.000	0.000
Feb	0.222	0.477	1.550	-0.056	0.919	-1.782
Mar	0.022	1.000	0.325	-0.197	0.463	-1.504
Apr	-0.289	0.291	-4.717	0.056	0.919	0.460
May	0.200	0.484	0.922	-0.167	0.612	-2.490
Jun	0.333	0.216	3.440	-0.143	0.720	-1.473
Jul	-0.022	1.000	-0.111	-0.333	0.260	-3.544
Aug	-0.111	0.727	-1.440	0.222	0.477	3.613
Sep	0.156	0.601	1.067	-0.111	0.761	-0.397
Oct	0.244	0.381	1.200	-0.611	**0.025**	-4.700
Nov	-0.022	1.000	-0.140	0.278	0.358	1.193
Dec	0.310	0.228	1.267	-0.243	0.381	-0.318

The trend of decadal rainfall Intensity for Wenchi station on an annual scale (table 4.20) revealed an increasing non-significant rainfall trend for the period 1980-1989, 2000-2009 and 2010-2018. Whereas, the periods 1990-1999 showed a decreasing trend, which is not statistically significant. None of the months showed any significant decadal trends.

Table 4. 20: Decadal Mann–Kendal trend statistics for annual and monthly rainfall Intensity for Wenchi station (5% significance level)

WENCHI	1980-1989			1990-1999		
	Kendall's tau	p-value	Sen's slope	Kendall's tau	p-value	Sen's slope
Annual	0.111	0.721	1.500	-0.333	0.211	-6.614
Jan	-0.261	0.357	0.000	0.126	0.631	0.000
Feb	-0.333	0.260	-1.983	-0.111	0.727	-0.788
Mar	0.333	0.260	3.058	0.200	0.484	1.767
Apr	-0.389	0.180	-3.075	0.200	0.484	2.063
May	-0.222	0.477	-1.171	0.067	0.862	0.388
Jun	-0.278	0.358	-4.108	-0.289	0.291	-1.400
Jul	0.056	0.919	0.925	-0.289	0.291	-2.714
Aug	0.222	0.477	3.996	-0.022	1.000	-0.088
Sep	-0.111	0.761	-0.913	-0.333	0.216	-3.920
Oct	-0.444	0.119	-3.831	0.244	0.381	2.350
Nov	0.000	0.919	-0.250	-0.333	0.216	-1.929
Dec	-0.261	0.357	0.000	-0.263	0.308	-1.650
	2000-2009			2010-2018		
	Kendall's tau	p-value	Sen's slope	Kendall's tau	p-value	Sen's slope
Annual	0.022	1.000	0.067	0.067	0.858	0.375
Jan	-0.230	0.364	-1.400	-0.261	0.357	0.000
Feb	0.184	0.468	0.960	-0.333	0.260	-1.983
Mar	0.422	0.108	3.050	0.333	0.260	3.058
Apr	0.045	0.857	0.167	-0.389	0.180	-3.075
May	-0.111	0.727	-1.213	-0.222	0.477	-1.171
Jun	-0.422	0.108	-4.320	-0.278	0.358	-4.108
Jul	-0.156	0.601	-1.060	0.056	0.919	0.925
Aug	0.422	0.108	3.767	0.222	0.477	3.996
Sep	0.333	0.216	2.567	-0.111	0.761	-0.913
Oct	0.022	1.000	0.250	-0.444	0.119	-3.831
Nov	-0.022	1.000	-0.200	0.000	0.919	-0.250
Dec	0.315	0.209	1.100	-0.261	0.357	0.000

The trend of decadal rainfall Intensity for Kintampo station on an annual scale (table 4.21) revealed an increasing non-significant rainfall trend for the period 1980-1989 and 2010-2018. Whereas, the periods 1990-1999 and 2000-2009 showed a decreasing trend. The decreasing trend of 1990-1999 is statistically significant at 95% confidence level. Within 1980-1989, the months of May and June recorded significant decreasing and increasing trends respectively. Within 1990-1999, the month of June showed a significant increase in trend of rainfall intensity. The month of December recorded a significant decreasing trend of rainfall within the 2010-2018 period.

Table 4. 21: Decadal Mann–Kendal trend statistics for annual and monthly rainfall Intensity for Kintampo station (5% significance level)

KINTAMPO	**1980-1989**			**1990-1999**		
	Kendall's tau	**p-value**	**Sen's slope**	**Kendall's tau**	**p-value**	**Sen's slope**
Annual	0.333	0.211	0.971	-0.556	**0.032**	-1.917
Jan	-0.487	0.075	0.000	0.325	0.244	0.000
Feb	-0.046	0.856	0.000	0.180	0.472	1.100
Mar	0.333	0.260	2.802	-0.159	0.528	-1.517
Apr	0.156	0.601	1.257	-0.200	0.484	-1.371
May	-0.494	**0.048**	-4.383	0.200	0.484	2.333
Jun	0.629	**0.012**	4.960	0.511	**0.047**	5.140
Jul	-0.360	0.151	-2.767	0.156	0.601	0.900
Aug	0.270	0.281	1.750	-0.111	0.727	-1.780
Sep	0.111	0.727	1.420	0.022	1.000	0.567
Oct	-0.389	0.180	-2.517	-0.378	0.156	-2.325
Nov	0.022	1.000	0.438	-0.022	1.000	-0.100
Dec	-0.546	0.060	-0.156	-0.378	0.150	-0.700
	2000-2009			**2010-2018**		
	Kendall's tau	**p-value**	**Sen's slope**	**Kendall's tau**	**p-value**	**Sen's slope**
Annual	-0.422	0.107	-4.500	0.045	0.928	0.025
Jan	-0.378	0.150	-1.050	-0.178	0.566	0.000
Feb	0.119	0.643	0.000	-0.389	0.180	-2.180
Mar	0.467	0.073	4.400	0.278	0.358	1.900
Apr	-0.022	1.000	-0.080	0.423	0.116	6.242
May	-0.056	0.919	-0.229	-0.056	0.919	-0.088
Jun	-0.378	0.156	-4.650	-0.111	0.761	-0.500
Jul	0.289	0.291	2.550	-0.500	0.075	-5.565
Aug	-0.378	0.156	-2.457	-0.056	0.919	-0.925
Sep	0.467	0.073	2.660	-0.444	0.119	-4.733
Oct	0.244	0.381	3.786	-0.429	0.179	-3.767
Nov	-0.200	0.484	-1.014	-0.071	0.905	-0.775
Dec	0.183	0.511	0.225	-0.724	**0.037**	-0.500

Table 4.22 presents a summary of the decadal trend analysis for annual rainfall amount and rainfall intensity. According to Nouaceur & Murarescu (2020), West Africa's rainy season is associated with the transfer of oceanic moisture to the mainland (the West African monsoon). This is regulated by a northward translation of the meteorological Equator and its low-pressure corridor (Intertropical Convergence Zone—ITCZ) due to the attraction of Saharan thermal depressions and the strengthening of anticyclonic nuclei in the southern hemisphere in winter. Hence, West Africa's rainfall shows variable annual and decadal trends (Zhang et al., 2021).

Table 4. 22: Summary of decadal trend analysis for annual rainfall amount

STATION	1980-1989	1990-1999	2000-2009	2010-2018
Wa	↑↓	↑↑	↑↑	↓↓
Bui	↑↑	↓↓	↓↑	↓↓
Damongo	↑↓	↑↑	↑↓	↓↓
Bole	↓↓	↑↓*	↓↑	↓*↓*
Sunyani	↑↑	↓↓	↓↓	↓*↓
Wenchi	↑↑	↓↓	↓↑	↓↑
Kintampo	↑↑	↑↓*	↓↓	↓↑*

↑ = Increasing trend of rainfall amount, ↓ = Decreasing trend of rainfall amount, * = Significant at 95% confidence level, ↑ = Increasing trend of rainfall intensity, ↓ = Decreasing trend of rainfall intensity, * = Significant at 95% confidence level.

Within 1980-1989, all the stations showed increasing trend of annual rainfall amount except for Bole station. Hence, there was an overall increasing trend within the basin. This is consistent with a similar study conducted by Sanogo et al (2015) who assessed the spatio-temporal characteristics of rainfall in West Africa. The aforementioned study recorded increasing rainfall trend from 1980

to 1990. Within the 1990-1999 decade, Bui, Sunyani and Wenchi stations recorded decreasing trend of annual rainfall amount. These stations are at the middle to lower portions of the basin. Odoulami & Akinsanola (2018) in their study, which assessed daily rainfall trends of West African summer monsoon, also got similar results of decreasing trend of rainfall amount for the 1990-1999 period. Whereas the upstream stations recorded increasing trend of annual rainfall amount. During 2000-2009, Wa and Damongo stations which are upstream stations recorded non-significant increasing trend of rainfall amount, while the rest of the station recorded decreasing trends. Nouaceur & Murarescu (2020) also recorded increasing trend of rainfall amount from the year 2000 to 2010 for the upstream parts of the Sahel savanna in West Africa. Between 2010 and 2018, there has been a general decrease in trend of annual rainfall amount within the basin. With Bole and Sunyani stations recording significant decreasing trends at 95% confidence level. This is consistent with results of Nouaceur & Murarescu (2020) which observed a decreasing trend of rainfall amount from 2010 within Senegal, Mauritania and Burkina Faso in the West African region. The results of the decadal trend of annual rainfall as compared to the long-term trend analysis suggest that even though there has been inter-decadal decreasing and increasing trends of annual rainfall amount for various stations within the basin, there is a general downward trend in rainfall amount experienced in the basin since 1980.

The trend of decadal rainfall intensity within the basin behaved like that of the annual rainfall amount for some stations and contrary for other stations. Within 1980-1989, upstream stations Wa, Damongo and Bole recorded decreasing trend of rainfall intensity, while the middle to downstream stations Bui, Sunyani, Wenchi and Kintampo stations showed increasing trend of rainfall intensity. Within 1990-1999, Wa and Damongo stations at the upstream portions of the basin recorded increasing trend of rainfall intensity, which is in accordance with the trend of annual rainfall

amount for those stations. Whereas the other five stations showed decreasing trend. Hence, the flood events of 1996 and 1999 at the upstream could be attributed to increasing rainfall amounts and intensity in those parts. The 2000-2009 decade recorded varying increasing and decreasing trends of rainfall intensity that had no spatial pattern. Wa, Bui, Bole and Wenchi stations showed increasing trend of rainfall intensity, while Damongo, Sunyani and Kintampo stations exhibited decreasing trends. However, none of the trends is statistically significant. Within the 2010-2018 period, Wenchi and Kintampo stations recorded increasing trend of rainfall intensity, which could lead to flash floods. The trend at Kintampo station is statistically significant. The other stations showed decreasing trend of rainfall intensity, which is in line with the general decreasing trend of annual rainfall amount for the period. There is a gap in literature on the analysis of decadal trend of rainfall intensity in the West African sub-region. Hence, it is recommended that more research should be conducted in this wise.

The variability of decadal trend of annual rainfall amount and intensity in the area can be attributed to rising temperatures as an effect of climate change on the West African Monsoon, as supported by a recent study by Ilori & Ajayi (2020). The aforementioned study concluded that rainfall anomaly in the West African region, indicates that the Sahel would continue to get less rainfall amounts as the annual mean temperature rises in all three climatic zones of West Africa through the end of the twenty-first century, with increasing intensity.

Since 70% of the stations within the study basin shows a decreasing trend of total annual rainfall amount, it is inferred that the study basin has an overall decreasing trend of rainfall amount, Whereas rainfall intensity in the basin has an increasing trend. This is consistent with the results of Abungba et al (2020) which recorded decreasing trend of rainfall amount for both dry and wet seasons within the Ghana portion of the Black Volta basin. The study reported that the decreasing

trend of rainfall amount, implied a reduction in water availability for both seasons in the Basin's upstream catchments, and because the Basin is agrarian in nature, with most farmers relying on rain-fed agriculture, this decrease in trend will affect crop patterns and, ultimately, crop yields in the basin. Consistently, a study conducted by Mouhamed et al (2013) revealed that while the basin has a general trend of decreased annual total rainfall and the maximum number of consecutive wet days, the cumulated rainfall of extremely wet days shows a positive trend in most locations. Similarly, Agyekum et al (2018), in their study observed a significant decreasing seasonal (dry and rainy season) precipitation trend across the Volta Basin. In another study by Kabo-Bah et al (2016), historical rainfall and temperature data from 22 Ghanaian stations were examined to better understand spatial and location-specific trends over time. The results of hydro-met stations across the country revealed an increasing trend of higher temperatures, and declining rainfall trend in various stations affecting water availability and accessibility, however, the rainfall trends are expected to become more erratic.

4.1.9 Spatial Distribution of Rainfall

The spatial distribution of mean annual rainfall amount from 1980-2018 is shown in Figure 4.5 Throughout the 38 years, the highest mean annual total rainfall occurred at the southern (lowland) parts of the basin around Wenchi and Kintampo stations with a mean annual rainfall ranging between 1198 mm to 1292 mm. The northern parts of the basin recorded low mean annual rainfall ranging between 772 mm to 925 mm. The mean annual total rainfall increases from north to south in the basin, from sudan savanna, to guinea savanna and then to the transition eco-climatic zones, as reported by Incoom et al (2020). This implies that the downstream portions would receive more rain, and hence would generate more runoff in the basin.

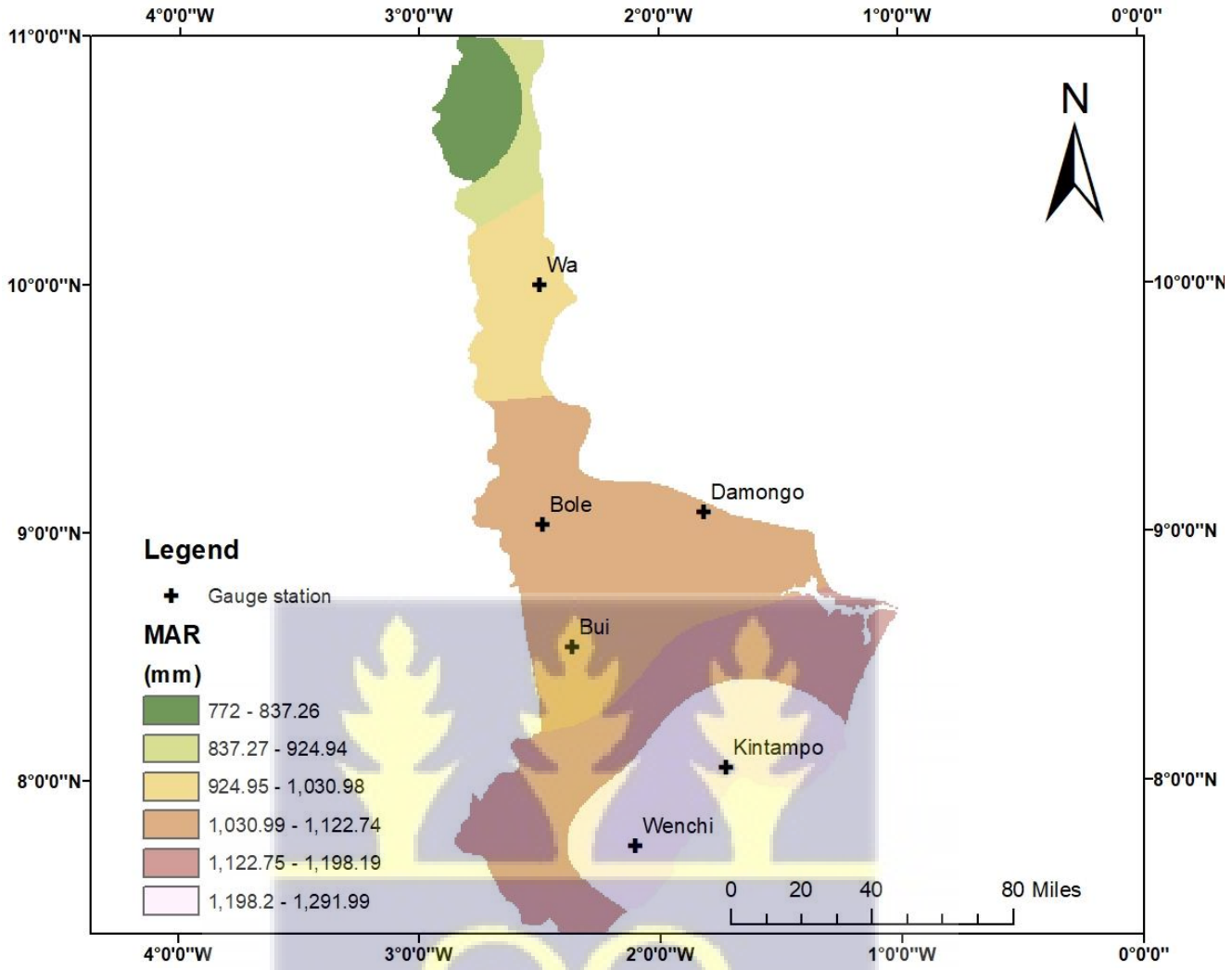

Figure 4. 5: Spatial distribution of mean annual rainfall amount

The annual daily maximum rainfall (intensities) recorded within the basin for the 38 years period ranges from 130 mm/day to 439 mm/day. The highest average daily maximum rainfall was recorded in the middle portions of the basin, while low values of daily maximum rainfall were recorded at the upstream and downstream parts of the basin. Figure 4.6 shows the spatial distribution of average maximum daily rainfall within the study area.

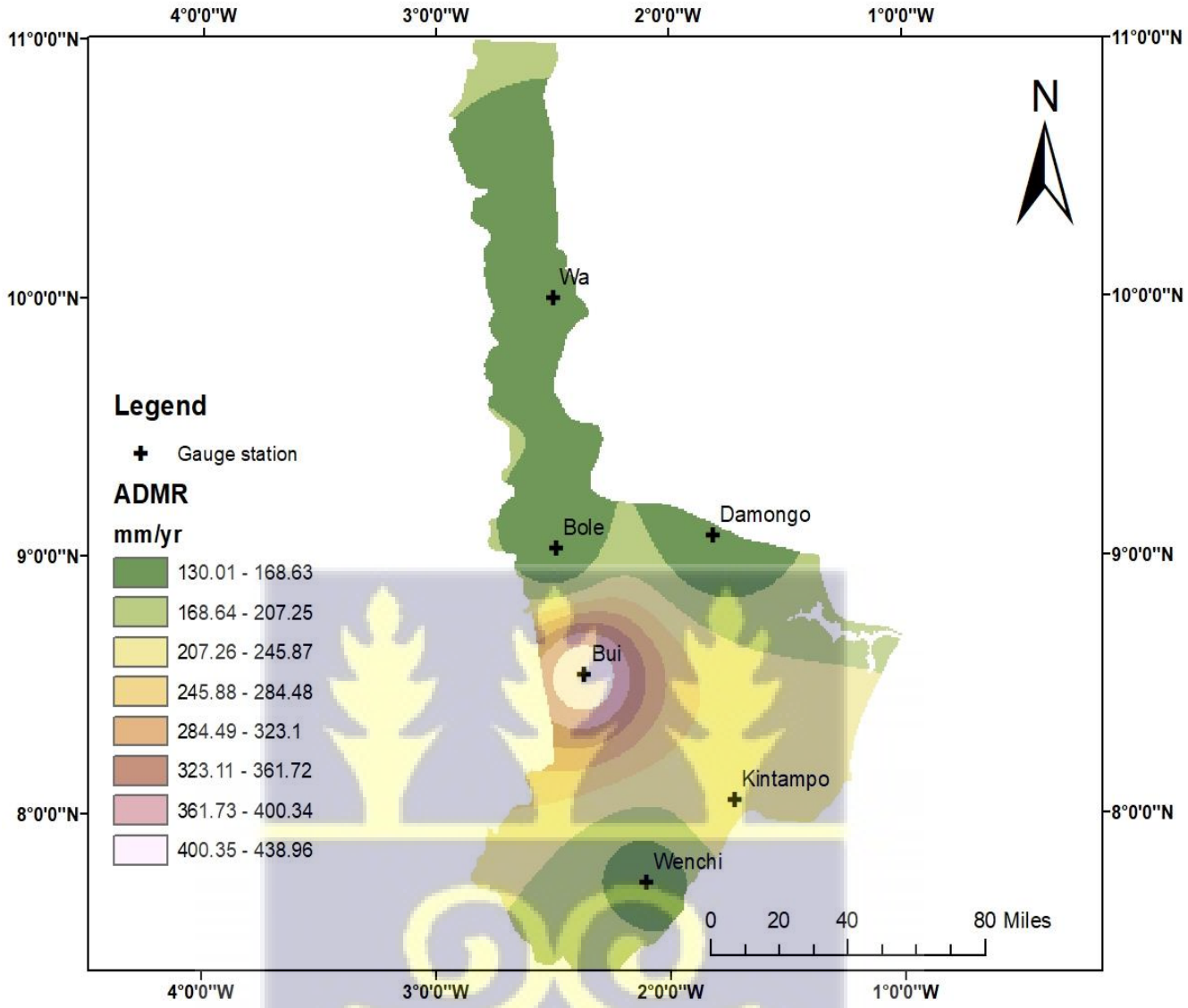

Figure 4. 6: Spatial distribution of annual daily maximum rainfall (Intensities)

4.2 LAND USE CLASSIFICATION

Land use land cover of the Black Volta basin was studied for the year 2011 to determine the various land uses types in the catchment. The present study revealed five land use and land cover categories: settlement, vegetation, bare land, forest and water, as the main land use and land cover types in the catchment area as seen in figure 4.7 below. For this study, only the Ghana portion of the Black Volta basin was considered for classification. However, because the Black Volta River passes through the boundary between Ghana and Ivory Coast, some parts of Ivory Coast had to be included.

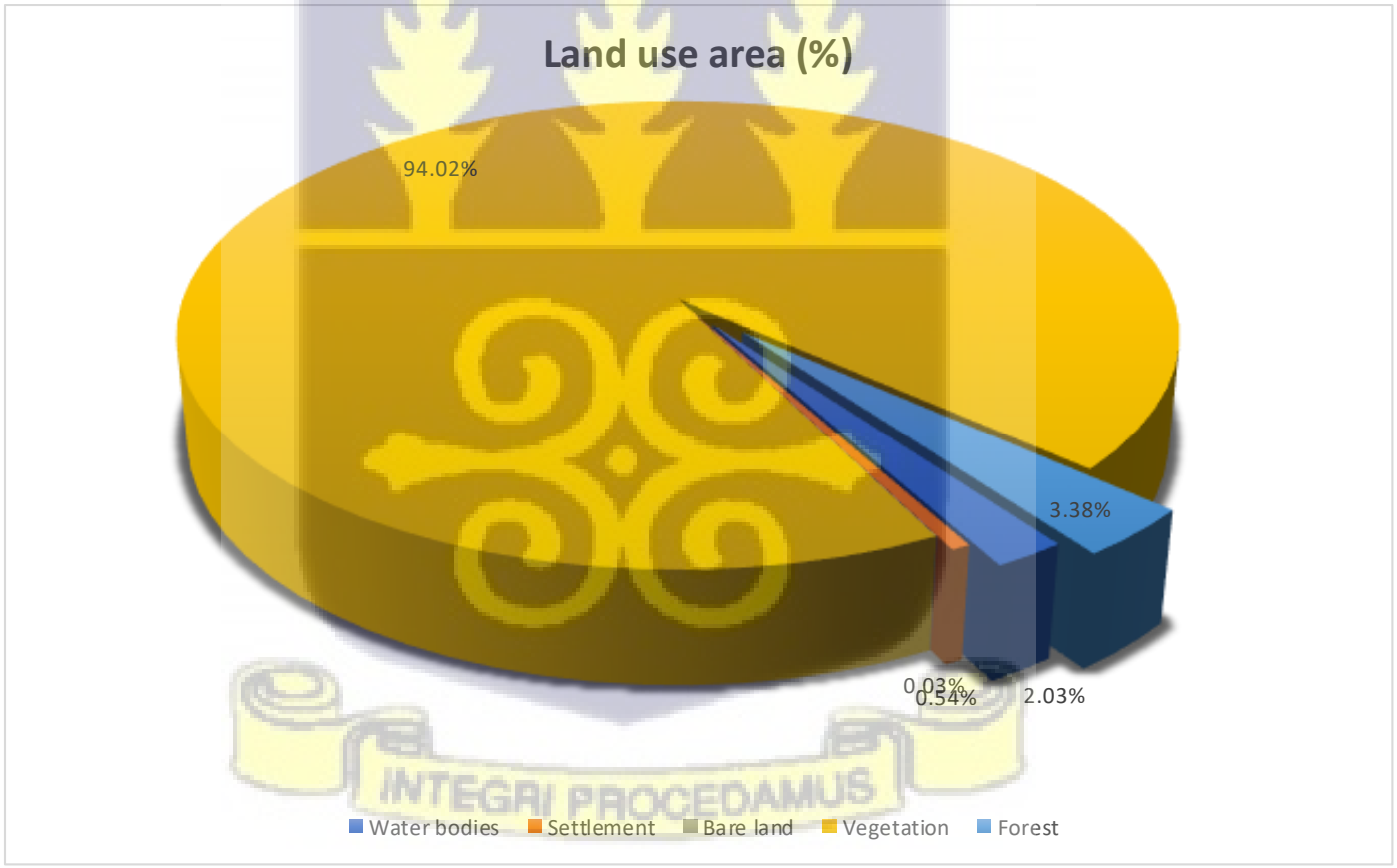

Figure 4. 7: Percentage of land area occupied by classified land use types

The study area or basin area was predominantly occupied by vegetation (45457.4 km^2) representing 94% of the land area, with forest (1632.7 km^2) constituting 3.38% being the second dominant land use type in the study area. Water bodies and settlements occupied 2.03% (983.7 km^2) and 0.54% (260.7 km^2) of the basin area respectively as seen in figure 4.7. Bare land occupied the smallest portion (12.21 km^2) representing 0.03% of the catchment area during the same period. Vegetation accounts for all forms of agricultural land, shrub land, herbaceous savanna, cropland and pastures; however, agricultural land was the predominant vegetation type in the study area. The forest constitutes evergreen lands and deciduous forests. The water bodies represents streams, small reservoirs, lakes and dams in the area. The bare land represents exposed soil and areas without any form of vegetation such as tarred roads and footpaths. The total area of land is 48,346.78 km^2. These results are consistent with results obtained by Amproche et al (2020), however the study subdivided vegetation into three sub-categories: Closed savanna, open savanna and agriculture. Figure 4.8 below shows the classified land use map of the Black Volta basin in Ghana for 2011. Akpoti et al (2016) in their study also reported the dominance of agricultural land as the major land use type in the Black Volta basin for the year 2013.

Different forms of land use influence runoff production and behavior (Khaleghi, 2017). In a variety of settings, when the percentage of forest cover rises, both runoff generation and sediment loss decrease exponentially (Nunes et al., 2011). Hence, intensive cultivation is an important factor runoff generation. According to Liu et al (2006), soil compaction and the loss of natural vegetation which reduce soil infiltration capacity, are the primary causes of increased runoff from agricultural land. From the results of this study, the dominant land use type in the basin is vegetation (94%), with agricultural land being the most predominant vegetation cover type. This implies that the Black Volta basin in Ghana is likely to produce a lot of runoff. Nunes et al (2011) studied the

impacts of land use types on runoff and soil erosion in Portugal and inferred that agricultural land uses have the largest runoff and erosion yield in the region. Guzha (2018) also deducted that forestlands had considerably lower runoff coefficients when compared to land plots under agriculture and grazing fields, when he studied the impacts of land use on surface runoff in Kenya, East Africa.

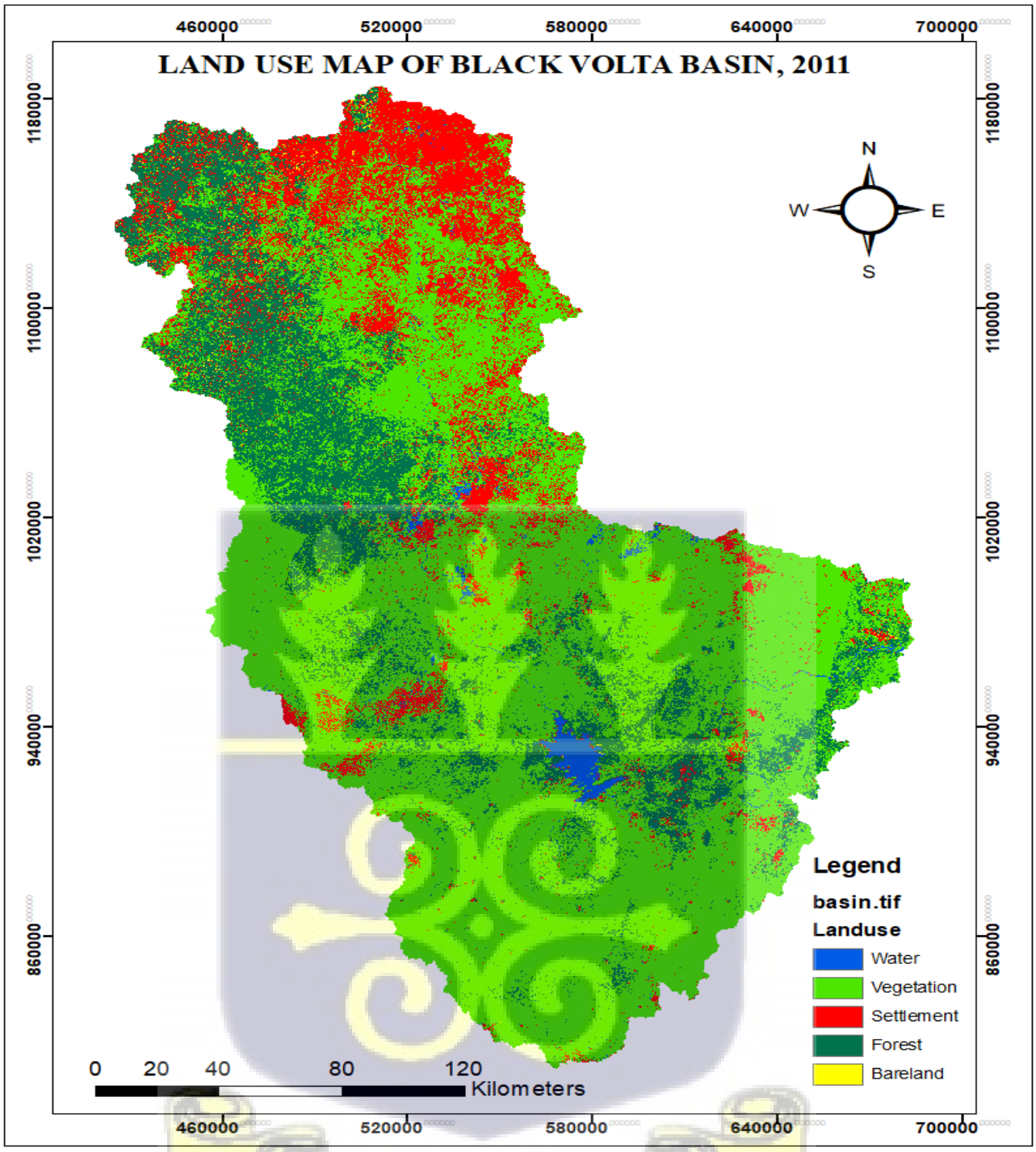

Figure 4. 8: Classified land use map of the Black Volta basin in Ghana, 2011

4.2.1 ACCURACY ASSESSMENT

Results of land use classification is summarized in table 4.23The quality of a land use classification is determined by its accuracy using error matrices. Producer's accuracy, user's accuracy, overall accuracy and kappa statistics were computed. The overall accuracy for 2020 was 91.10%. The Kappa coefficient of the 2011 multispectral classified image was 0.87. The Kappa coefficient indicates that the classification method very well captured the dynamics of the land use of the area of interest.

Table 4. 23: Accuracy matrices for Black Volta basin catchment in Ghana land use classification, 2011

Class	Settlement	Vegetation	Bare land	Forest	Water	Ground Truth	Producer's Accuracy	User's Accuracy
Settlement	120	0	11	0	10	141	97.56%	85.11%
Vegetation	0	124	6	8	13	151	89.21%	82.12%
Bare land	2	10	30	0	2	44	61.22%	68.18%
Forest	0	3	1	109	0	113	91.60%	96.46%
Water	1	2	1	2	354	360	93.40%	98.33%
TOTAL	123	139	49	119	379	809		

Overall Accuracy for 2020 = 91.10%, Kappa coefficient = 0.87

For the image classification, the error matrix in Table 4.23 illustrates classification accuracy of five features. The Producer's accuracy ranges from 97.56% (settlement), 93.40% (water bodies), 91.60% (forest), 89.21% (vegetation), and 61.22% (bare land). On the other hand, the percentage of user's accuracy ranges from 98.33% (water body), 96.46% (forest), 85.11% (settlement), 82.12% (vegetation), and 68.18% (bare land). The results of the error matrix suggest good accuracy of land use classification for the period.

4.2.2 CURVE NUMBER MAP

The SCS curve number is an empirical parameter used to predict direct runoff or infiltration from excess rainfall. The curve number characterizes the runoff properties for a particular soil type and land cover. Analysis tools in ArcToolbox and HEC-GeoHMS was used to merge the soil-land use data to derive the curve number grid for the area. A weighted curve number was calculated to assign curve numbers to individual sub-basins within the catchment. As shown in figure (4.9) the results of curve number preparation gave a weighted area curve number ranging from 70 to 87. However, these initial curve number values were adjusted during hydrologic model calibration. The results showed a general increasing curve numbers from north to south of the study area. Low curve numbers indicate high infiltration and vice versa. Hence, it can be deduced that the northern parts of the study area has higher infiltration as compared to the southern parts. Therefore, the southern parts would generate more surface runoff.

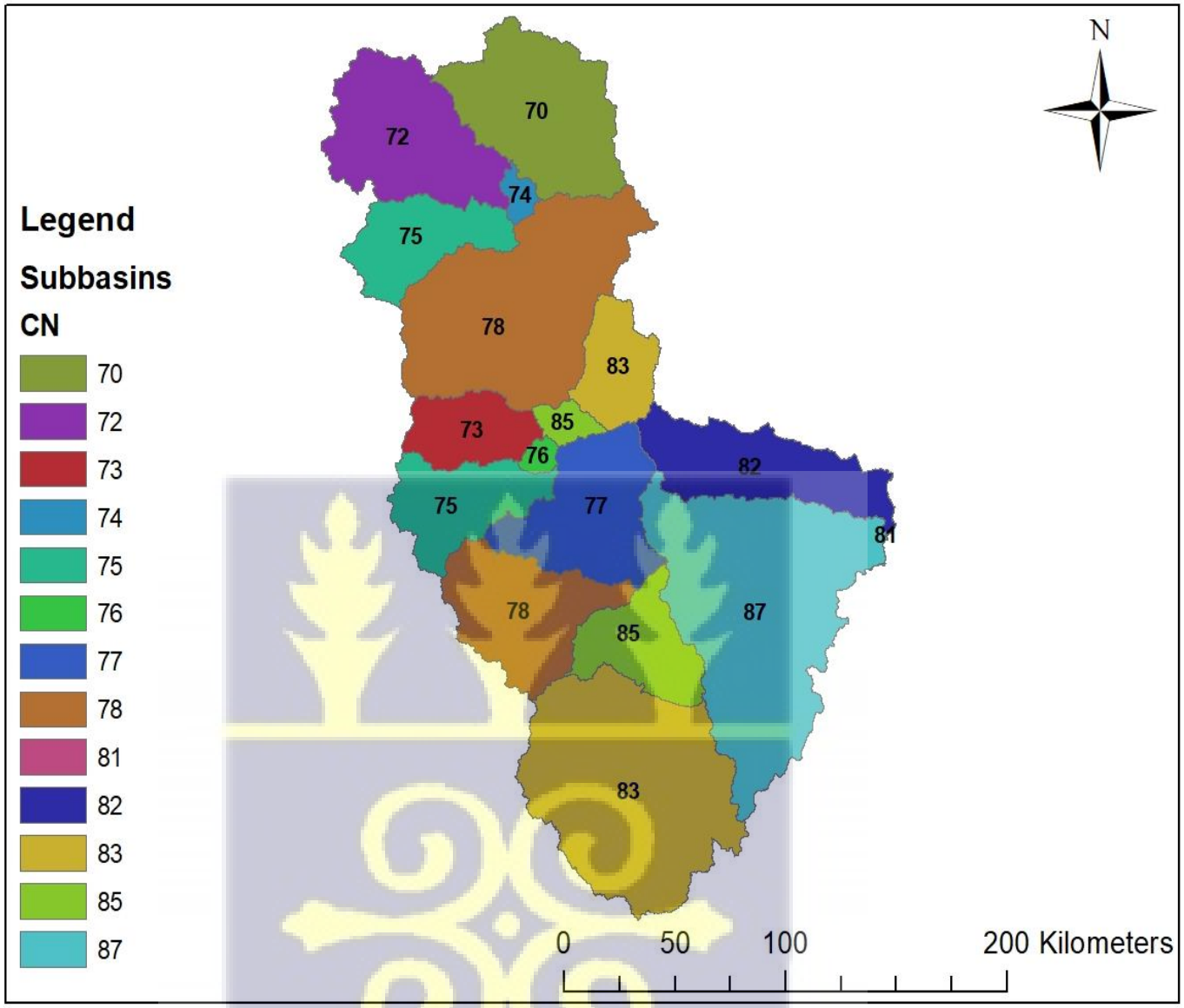

Figure 4. 9: Curve number map of study area

4.3 HYDROLOGICAL MODELLING USING HEC-HMS

4.3.1 Terrain Preprocessing and Basin Model Preparation

Seventeen (17) sub-basins were created using HECGeo-HMS, and each sub-basin was assumed to be internally homogenous, but distinct from each other. Each sub-basins contain information such as area, slope, shape, lag-times and soil properties. The river network was also divided into river sections, with homogenous conditions within one section. Each rivers section contains information such as slope, length, elevation and cross sectional shape. Figure 4.10 below show the output of the terrain preprocessing and basin model preparation.

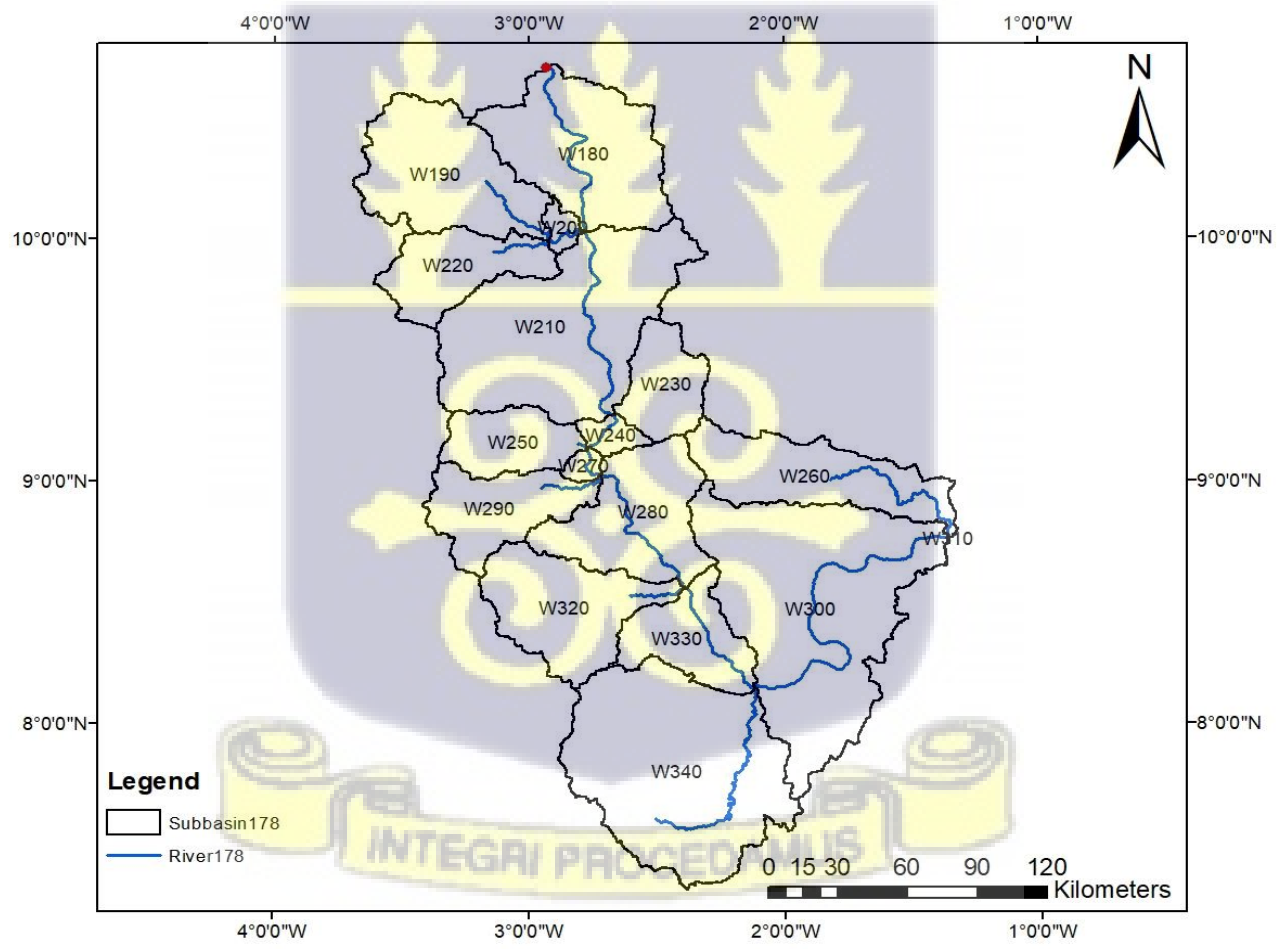

Figure 4. 10: Basin model showing sub-basins and stream network

4.3.2 Project Generation and Set Up

The HECGeo-HMS software was used to create the project for the basin as well as gather input data sets for the HECHMS modeling. The project basin model contains the hydrologic elements and their connectivity in the project basin model indicate the flow of water through the drainage system. Figure 4.11 shows the basin model generated for this study using HECGeo-HMS

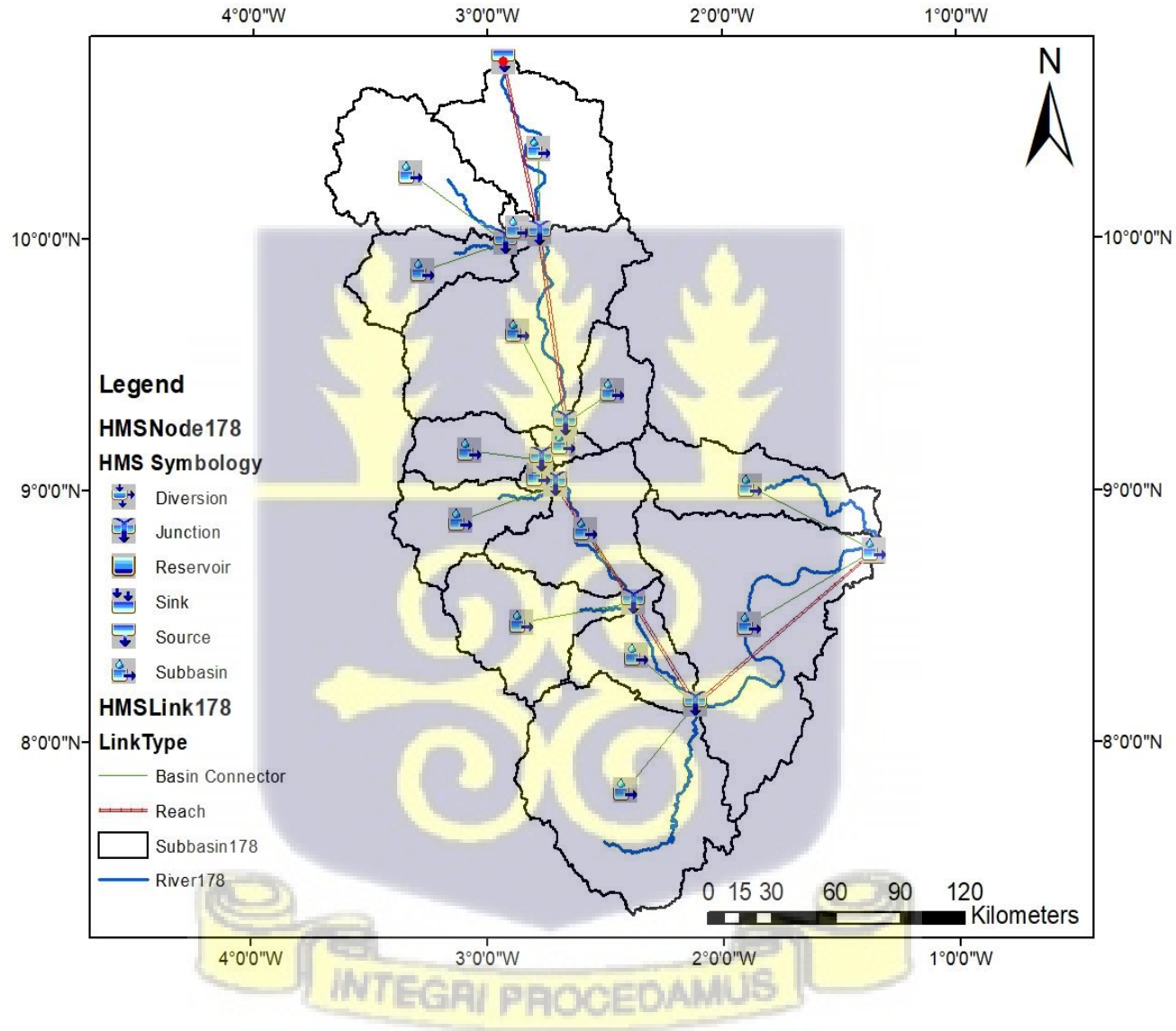

Figure 4. 11: Black Volta basin project developed using HECGeo-HMS

Various studies such as; Skhakhfa & Ouerdachi (2016), Ramly & Tahir (2016), Ibrahim-Bathis & Ahmed (2016), Bhuiyan et al (2017) and Tassew et al (2019) also used HECGeo-HMS for terrain pre-processing, project generation and extraction of basin parameter characteristics as inputs for HEC-HMS. Other studies like Ismael et al (2017) and Bai et al (2019) used the Arc Hydro tools within ArcGIS for pre-processing and generation of basin project, this method required that that the curve numbers for the sub-basins was estimated manually by using the tables used for computations found in the Technical Release Number 55 (SDA Conservation Engineering Division, 1986).

4.3.3 Simulation, Sensitivity Analysis and Calibration

The flood events of September 1996 and 2007 were calibrated based on general shape of the hydrographs, runoff volume and peak flow values. The peak flow, which corresponds to the maximum downstream flooding, is the most significant feature of the hydrograph when assessing a flood event. Data for flood events on all the hydrologic gauge stations (Chache, Bui and Bamboi) were only available in daily averages and not hourly averages; therefore, this distorts the Nash-Sutcliffe efficiency and Root Mean Square error for these events. However, the results of the hydrologic model showed a sound fit between the simulation and the observation after optimization, and the model works well across a range of events. Even though the model tended to overestimate the runoff before optimization, the shape of the hydrograph and time of peaks matches suitably. Figure 4.12 depicts a map of the hydrologic stations used for calibration across the basin. The red points indicate where the discharge gauges are located in the basin.

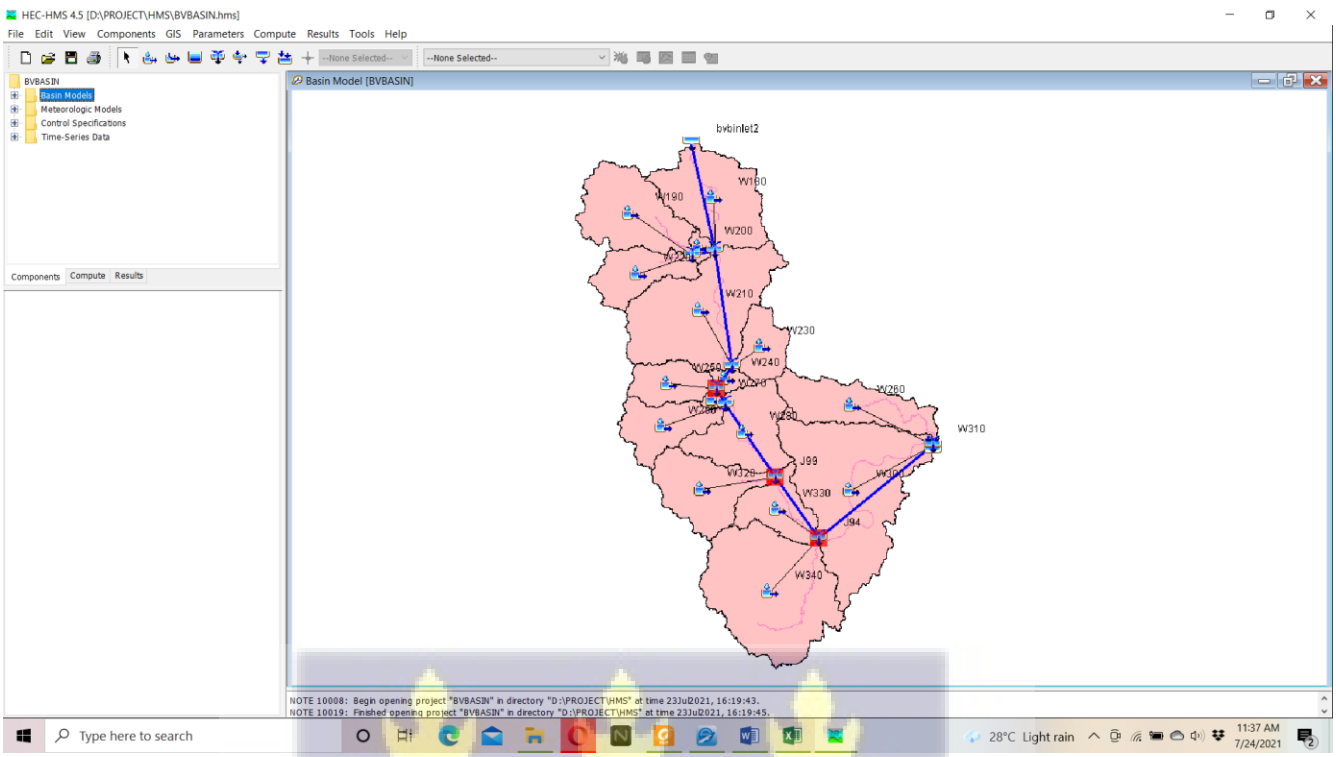

Figure 4. 12: Modelling in HEC-HMS

Model calibration quality was dependent on the accuracy and availability of precipitation data. Figures 4.13 to 4.17 shows hydrographs of simulated and observed discharges for the three stations within the basin for the calibration period. As mentioned earlier, the shape of the simulated and observed hydrographs and peak flows matched suitably. However, there is a lag in the time of peak for the Chache event of 1996 and the Bui event of 1996. The sensitivity analysis for the loss, transform, and routing methods revealed that the curve number, initial abstraction, and lag time were shown to be most sensitive, less sensitive and least sensitive model parameters, respectively. Tassew et al (2019) in their study conducted sensitivity analysis of parameters by changing parameter values in the range ±20 with 5% intervals until best fit was obtained between observed and simulated parameters. The study found curve number which is a function of soil storage and soil infiltration to be the most sensitive parameter in the Upper Blue Nile basin in Ethiopia.

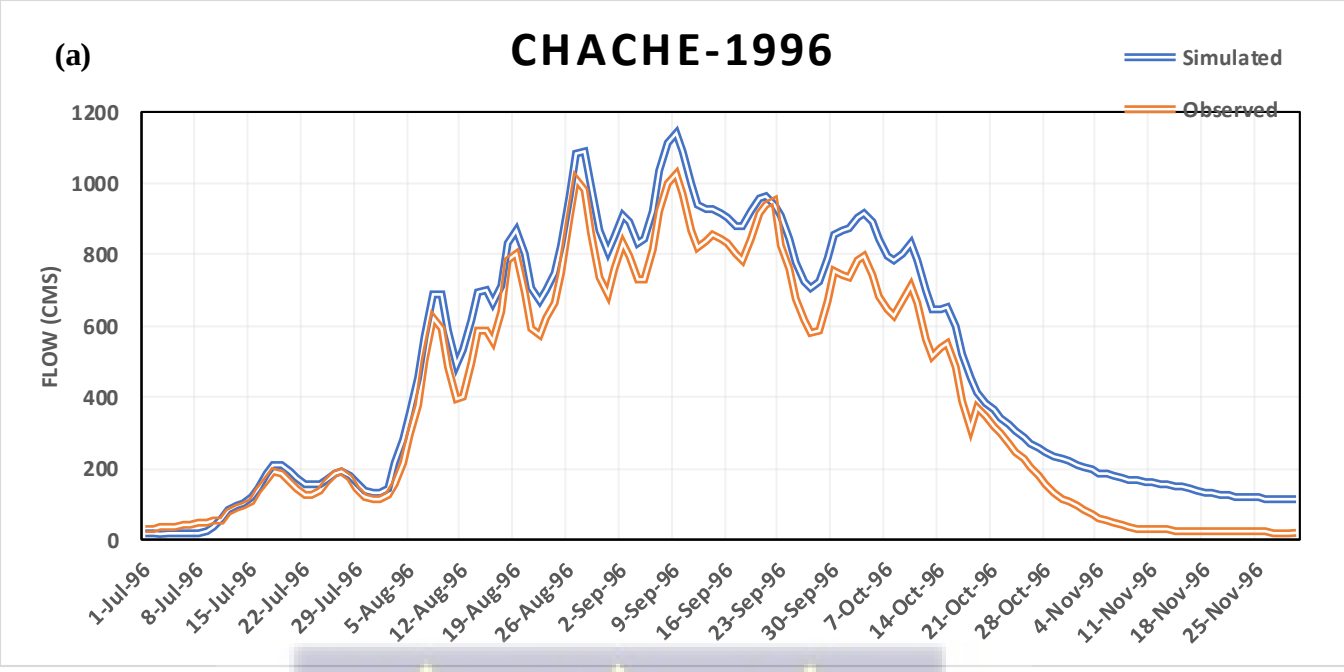

Figure 4. 13: Simulated and observed hydrographs for calibration period at Chache station for 1996 event

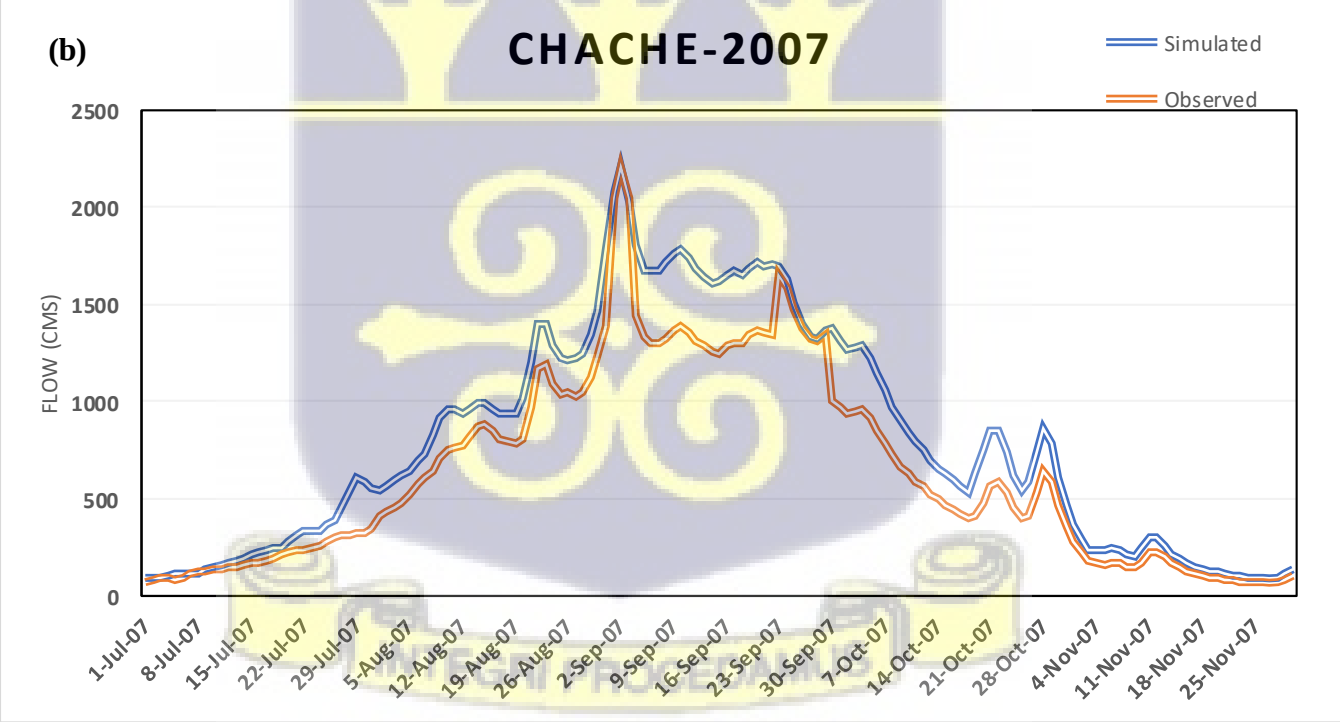

Figure 4. 14: Simulated and observed hydrographs for calibration period at Chache station for 2007 event

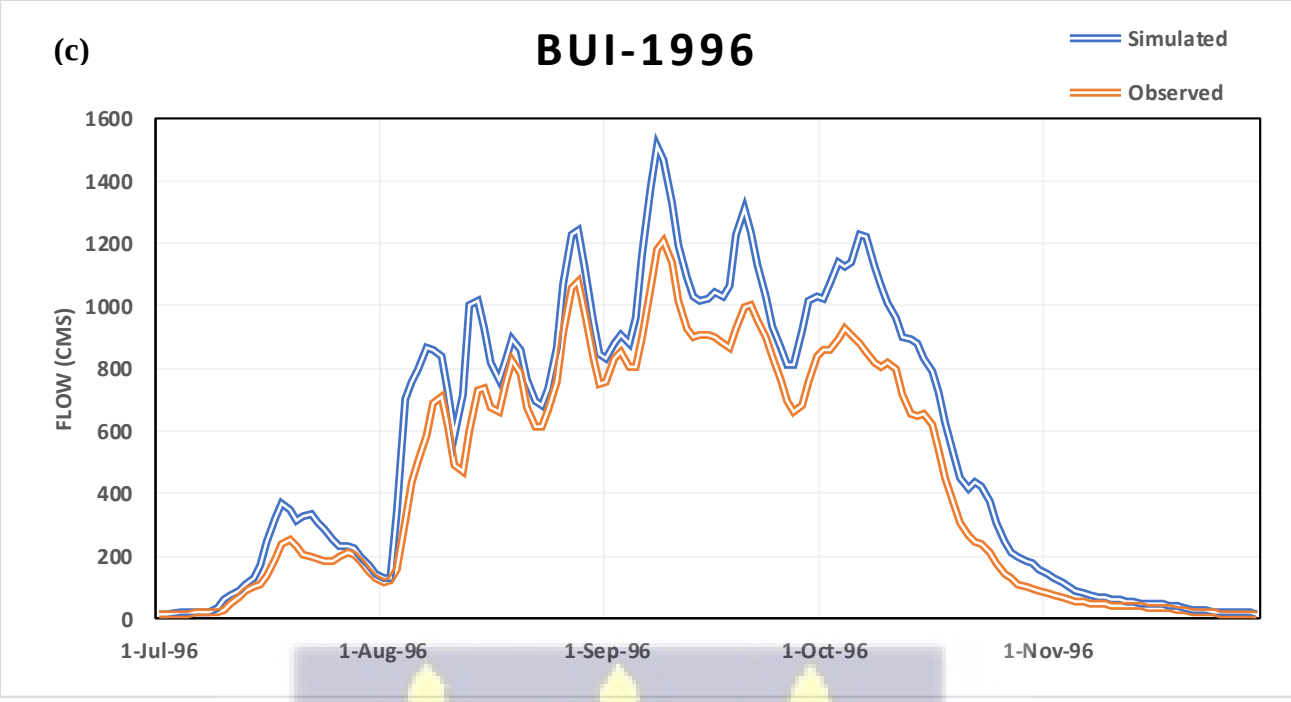

Figure 4. 15: Simulated and observed hydrographs for calibration period at Bui station for 1996 event

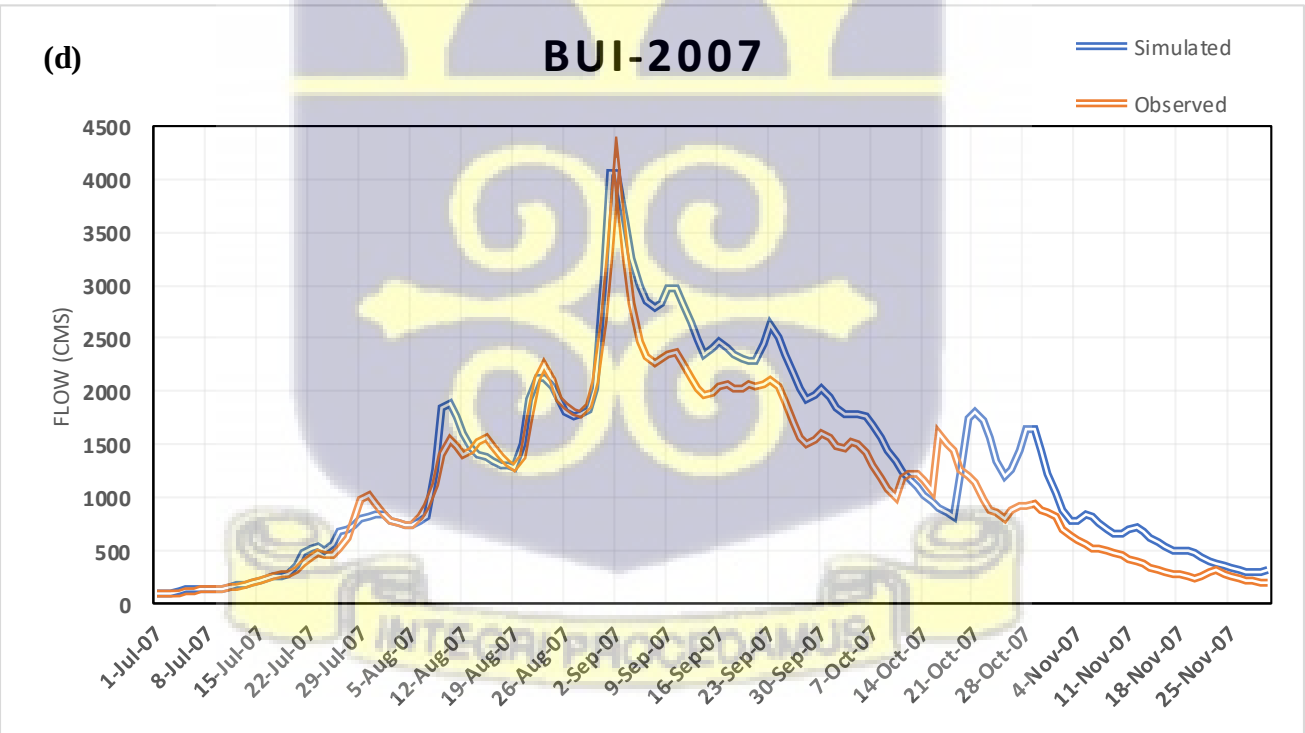

Figure 4. 16: Simulated and observed hydrographs for calibration period at Bui station for 2007 event

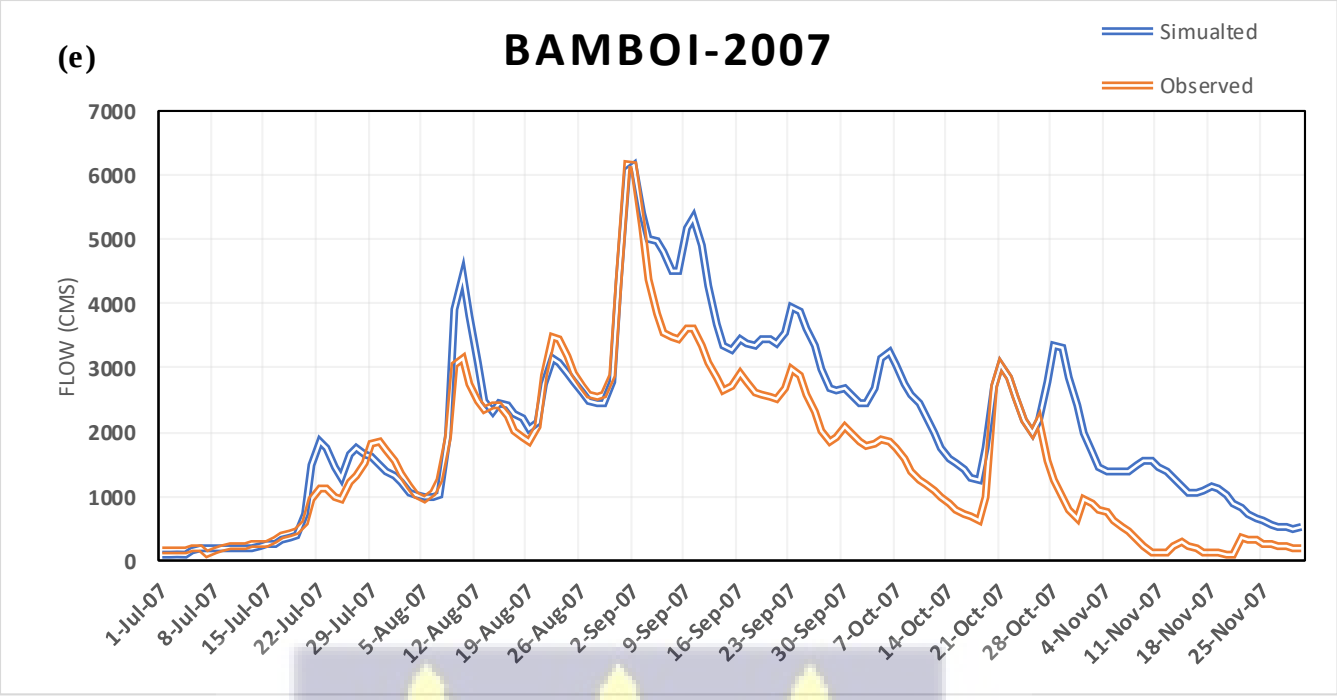

Figure 4. 17: Simulated and observed hydrographs for calibration period at Bamboi station for 2007 event

The modelling results of peak discharge, total volume, and their relative errors in comparison to observed data, the Nash Sutcliffe Efficiency and Root mean Square error values during calibration are shown in Table 4.24.

Table 4. 24: Simulated and observed peak discharges, total volume and error functions

Gage	**Event**	**Observed**		**Computed**		**Peak Q Percent Diff.**	**Volume Percent Diff.**	**Nash-Sutcliffe Efficiency**	**% Bias**	**RMSE**
		Peak Q (cms)	*Volume ($1000m^3$)*	*Peak Q (cms)*	*Volume ($1000m^3$)*					
CHACHE	Sept 1996	1026.0	5232178.6	1140.4	6283088.9	11.1	20.1	0.919	20.14	0.3
	Sept 2007	2205.6	8418454.2	2208.7	10431889.9	0.1	23.9	0.851	23.92	0.4
BUI	Sept 1996	1207.3	5842895.0	1506.2	7213075.5	24.8	23.5	0.855	23.45	0.4
	Sept 2007	4100.0	14740469.6	4057.6	15728462.4	-1.0	6.7	0.901	6.70	0.3
BAMBOI	Sept 2007	6158.9	21171052.7	6149.3	25316540.4	-0.2	19.6	0.789	19.57	0.5

The Percent difference in runoff volume ranges between 6.7%, which is considered very good and 23.9%, which is considered satisfactory based on the general performance rating (table 2.2). From the low values of percent difference in runoff volume and the shapes of the hydrographs (figure 4.13 to 4.17), it is reasonable to assume that runoff in all the events was generated by a mix of infiltration and saturation excess caused by high-intensity rainfall (Tassew et al., 2019). The percent difference in peak discharge obtained ranges between -0.2% considered as very good and 24.8%, which is considered as satisfactory. The NSE ranges from 0.789 (at Bamboi in September 2007) to 0.919 (at Chache in September 1996). This indicated a very good agreement between the observed and simulated runoff based on the recommended NSE values above 0.65 by (Hagen et al., 2020) for flood forecasting in Africa. The percentage bias gave unsatisfactory performances except for the September 2007 event at Bui which gave a percentage bias of 6.70%, which is considered good. The RMSE ranges from 0.3 to 0.5 indicating good model performance. Overall, the model performs well with good simulation between the estimated and observed values.

During optimization, initial basin parameter values are automatically adjusted to give a good agreement between simulated and observed discharge values. The Initial discharge, ratio to peak and recession constant values for the recession baseflow method were adjusted, the curve numbers and initial abstraction values for the loss method were adjusted. For the transform method, the lag time was the only adjusted parameter, whereas the initial and maximum storage for the canopy method was adjusted and the manning's coefficient was adjusted for the reach routing. These adjustments were done for each sub-basin within the catchment. The optimized parameter values were used for model validation. Tables 4.25 and 4.26 shows the initial values assigned to various basin parameters and their corresponding optimized values (after optimization) used for the model validation.

Table 4. 25: Calculated and optimized basin parameters of catchment for calibration and validation (1996)

	Baseflow						Loss			
	Initial Discharge		Ratio to Peak		Recession Constant		Curve Number		Initial Abstraction	
Sub-basin	Initial	optimized	Initial	Optimized	Initial	Optimized	Initial	Optimized	Optimized	Initial
W180	0.02	0.07	0.15	0.20	0.75	0.80	40	43	82.00	76.20
W190	0.02	0.30	0.15	0.37	0.75	0.92	42	48	78.32	70.15
W200	0.02	0.12	0.15	0.24	0.75	0.84	44	48	69.86	64.66
W210	0.02	0.08	0.15	0.20	0.75	0.80	48	50	66.18	55.03
W220	0.02	0.06	0.15	0.17	0.75	0.75	60	60	34.34	33.87
W230	0.02	0.20	0.15	0.33	0.75	0.92	68	79	27.75	23.91
W240	0.02	0.11	0.15	0.23	0.75	0.82	70	75	23.09	21.77
W250	0.02	0.15	0.15	0.28	0.75	0.87	58	65	40.99	36.79
W270	0.02	0.05	0.15	0.17	0.75	0.77	51	52	49.90	48.81
W280	0.02	0.03	0.15	0.16	0.75	0.76	67	67	25.12	25.02
W290	0.02	0.05	0.15	0.18	0.75	0.77	65	67	28.10	27.35
W320	0.02	0.02	0.15	0.15	0.75	0.75	68	68	24.02	23.91

	Transform		Canopy				Routing		
	Lag Time		Initial Storage		Max Storage			Manning's n	
Sub-basin	Initial	Optimized	Initial	Optimized	Initial	Optimized	Reaches	Initial	Optimized
W180	3104.7	3381	80	88	0.02	0.13	R10	0.03	0.0997
W190	5285.6	5792	80	85	0.02	0.08	R130	0.03	0.0438
W200	996.7	1072	80	86	0.02	0.10	R30	0.03	0.0741
W210	4181.4	5042	80	96	0.02	0.21	R50	0.03	0.0958
W220	2589.1	2654	80	82	0.02	0.06	R80	0.03	0.1629
W230	3464.4	4002	80	92	0.02	0.16	R90	0.03	0.0668
W240	922.3	974.4	80	84	0.02	0.06			
W250	3228.5	3570	80	88	0.02	0.11			
W270	339.5	346.3	80	81	0.02	0.03			
W280	1946.5	1950	80	80	0.02	0.02			
W290	2920.0	3004	80	82	0.02	0.05			
W320	4176.5	4200	80	80	0.02	0.02			

Table 4. 26: Calculated and optimized basin parameters of catchment for calibration and validation (2007)

	Baseflow						Loss			
	Initial Discharge		Ratio to Peak		Recession Constant		SCS Curve Number		Initial Abstraction	
Sub-basins	Initial	Optimized	Initial	Optimized	Initial	Optimized	Initial	Optimized	Initial	Optimized
W180	0.02	0.15	0.15	0.27	0.75	0.86	40	44	76.20	84.63
W190	0.02	0.34	0.15	0.46	0.75	0.95	42	54	70.15	89.27
W200	0.02	0.11	0.15	0.23	0.75	0.82	44	47	64.66	69.94
W210	0.02	0.13	0.15	0.27	0.75	0.87	48	54	55.03	62.71
W220	0.02	0.24	0.15	0.36	0.75	0.95	60	71	33.87	39.88
W230	0.02	0.14	0.15	0.27	0.75	0.87	68	77	23.91	27.23
W240	0.02	0.13	0.15	0.26	0.75	0.86	70	77	21.77	23.96
W250	0.02	0.15	0.15	0.28	0.75	0.88	58	65	36.79	41.55
W270	0.02	0.22	0.15	0.34	0.75	0.94	51	60	48.81	57.46
W280	0.04	0.29	0.15	0.34	0.75	0.93	60	66	36.17	40.73
W290	0.02	0.25	0.15	0.38	0.75	0.97	65	79	27.35	33.40
W320	0.02	0.16	0.15	0.29	0.75	0.88	68	77	23.91	26.82
W330	0.02	0.05	0.15	0.17	0.75	0.77	90	91	5.64	5.72
W340	0.02	0.08	0.15	0.20	0.75	0.80	88	92	6.93	7.21

	Transform		Canopy				Routing		
	Lag Time		Initial Storage		Max Storage			Manning's n	
Sub-basins	Initial	Optimized	Initial	Optimized	Initial	Optimized	Reaches	Initial	Optimized
W180	3104.7	3470.6	80	89	0.02	0.12	R10	0.03	0.13
W190	5285.6	6657.9	80	94	0.02	0.25	R130	0.03	0.19
W200	996.7	1080.2	80	87	0.02	0.11	R150	0.03	0.09
W210	4181.4	4800.9	80	91	0.02	0.15	R30	0.03	0.17
W220	2589.1	3026.1	80	93	0.02	0.17	R50	0.03	0.13
W230	3464.4	3981.0	80	91	0.02	0.16	R80	0.03	0.17
W240	922.3	1163.6	80	95	0.02	0.27	R90	0.03	0.27
W250	3228.5	3643.1	80	90	0.02	0.14			
W270	339.5	397.3	80	93	0.02	0.18			
W280	3893.1	4318.6	80	92	0.02	0.25			
W290	2920.0	3571.0	80	97	0.02	0.23			
W320	4176.5	4666.0	80	89	0.02	0.12			
W330	2567.6	2594.0	80	81	0.02	0.03			
W340	3630.6	3768.5	80	83	0.02	0.05			

4.3.4 Model Validation

The flood events of September 1999 and 2010 were used for the model validation. The selection of the events were based on factors such as rainfall characteristics, basin characteristics and availability and completeness of rainfall and discharge data. The optimized parameters from the calibration stage were used to simulate flood events for 1999 and 2010 in the study area. The validation of the simulated findings of peak discharge, total volume, and relative errors with respect to observed data, as well as the Nash–Sutcliffe Efficiency (NSE) and Root Mean Square error values, are listed in table 4.27.

Table 4. 27: Simulated and observed peak discharge, total volume and error functions during validation

Gage	**Event**	**Observed**		**Computed**		**Peak Q % Diff.**	**Volume % Diff.**	**Nash-Sutcliffe Efficiency**	**% Bias**	**RMSE**
		Peak Q (cms)	*Volume ($1000m^3$)*	*Peak Q (cms)*	*Volume ($1000m^3$)*					
CHACHE	Sept 1999	1811.6	8469728.5	1534.8	7969675.8	15.3	5.9	0.965	-5.90	0.2
	Sept 2010	2814.0	11595578.3	2519.8	14301160.0	10.45	-23.3	0.773	23.36	0.5
BUI	Sept 1999	2971.8	14415359.8	4495.3	19927618.8	-51	-38.2	0.505	38.23	0.7
	Sept 2010	4200.0	19785346.3	4169.2	25562583.8	0.73	-29.2	0.655	29.20	0.6
BAMBOI	Sept 2010	8680.2	43356893.4	7018.5	44048321.2	19.1	-1.6	0.627	1.64	0.6

The peak discharge of all the events were slightly overestimated except for the September 1999 event at Bui station, which was underestimated. The percent difference in peak discharge ranges from -51% to 19.1%. The total volume was underestimated for all events except for September 1999 at Chache, which was slightly overestimated. The percent difference in runoff volume ranges from -23.3% to 5.9%. Considering the Nash–Sutcliffe Efficiency (NSE) criteria, good results were obtained between the observed and simulated values with NSE values ranging from 0.505 to 0.965. The total simulation results of the events chosen for validation suggest that the HEC-HMS model has the potential to perform well in predicting peak flows and runoff volume in the Black Volta basin using SCS-CURVE Number and SCS Unit hydrograph methods. Figure 4.18 to 4.22 shows the hydrographs of observed and simulated discharges for the three stations within the basin for the validation period.

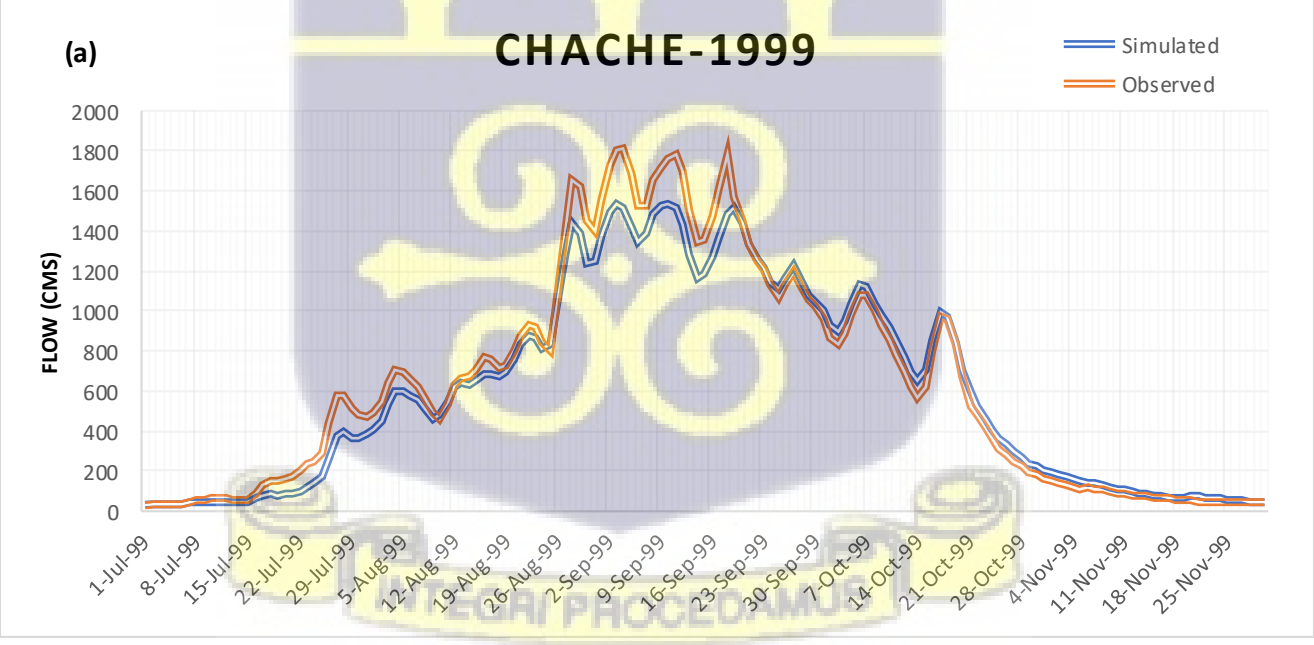

Figure 4. 18: Simulated and observed hydrographs for validation period at Chache station for 1999 event

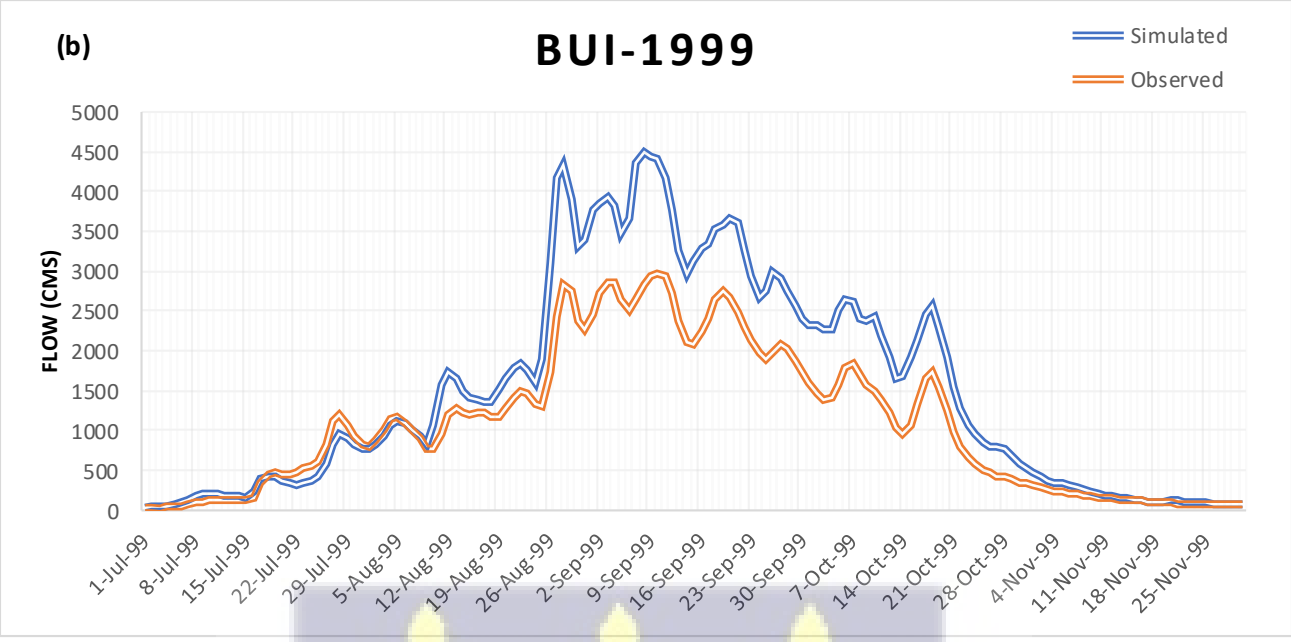

Figure 4. 19: Simulated and observed hydrographs for validation period at Bui station for 1999 event

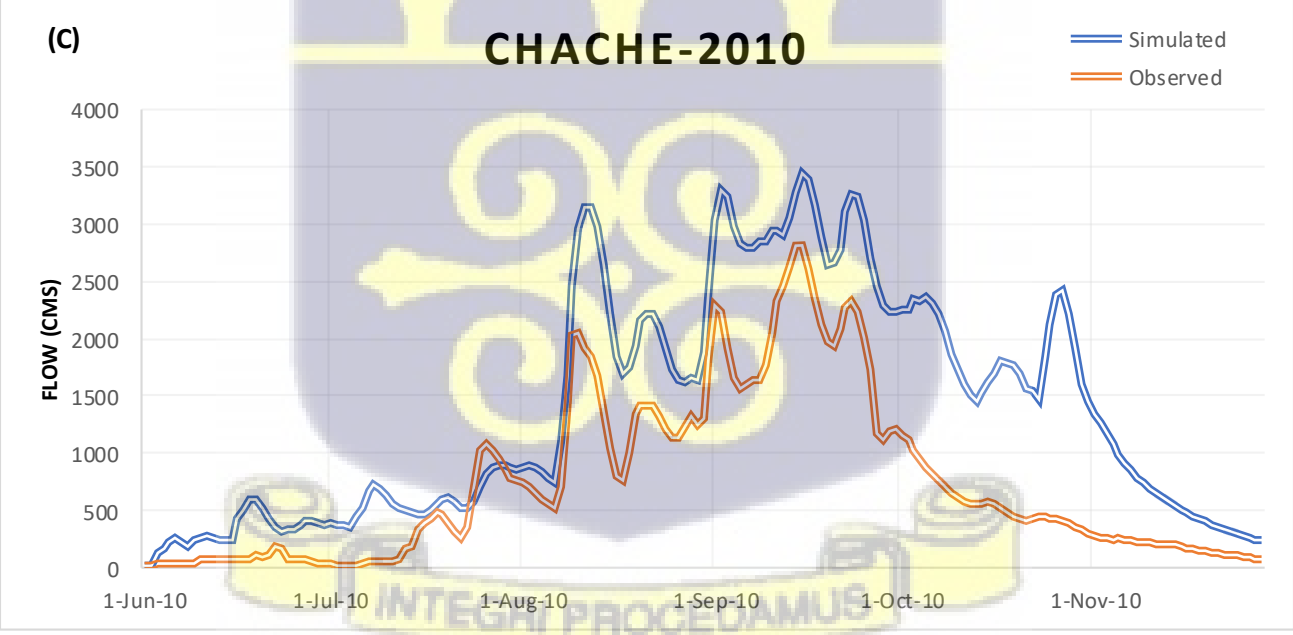

Figure 4. 20: Simulated and observed hydrographs for validation period at Chache station for 2010 event

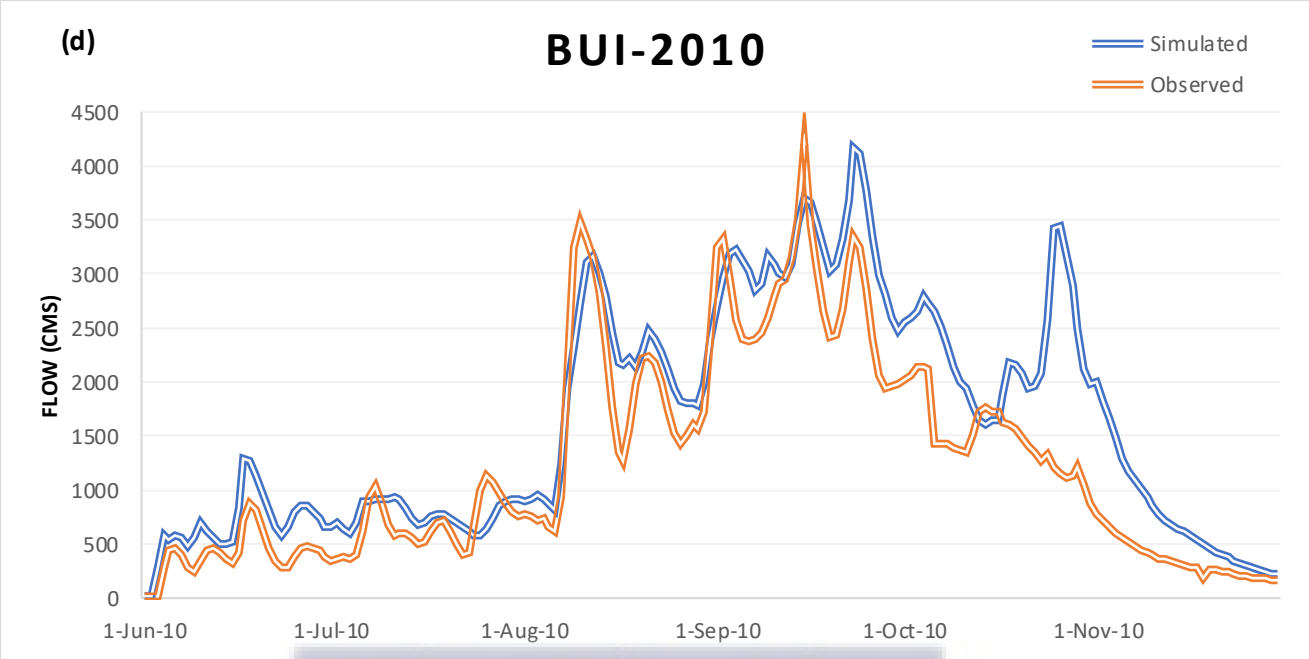

Figure 4. 21: Simulated and observed hydrographs for Validation period at Bui station for 2010 event

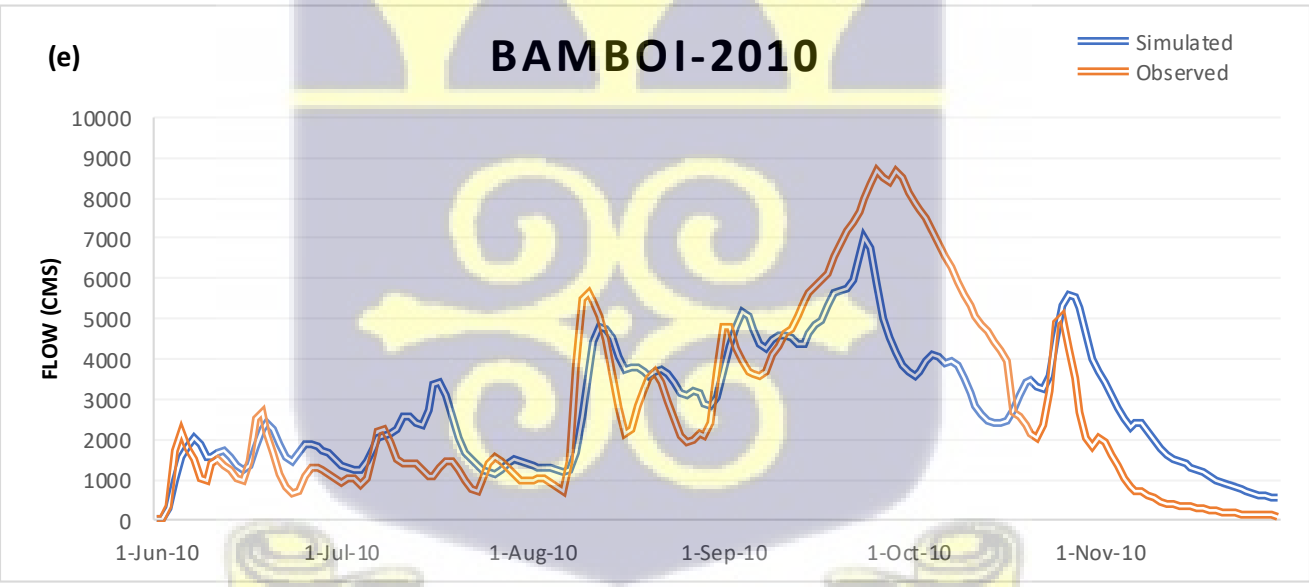

Figure 4. 22: Simulated and observed hydrographs for Validation period at Bamboi station for 2010 event

Good hydrological model calibration and validation findings show that it is possible to simulate discharge along the black Volta in Ghana even with insufficient input data, using a semi-distributed model. The HEC-HMS model has been used to model rainfall-runoff processes in various basins in various African countries such as; Ethiopia (Gebre, 2015), Morocco (Msaddek et al., 2020), Rwanda (Munyaneza et al., 2014), and Kenya (Ismael et al., 2017) among others. In each of these studies the model proved suitable for simulation of the hydrologic processes and peak flows of various events.

In the West African sub-region, not much research has been done using HEC-HMS model for rainfall-runoff modelling. However, a few studies revealed the applicability of the HEC-HMS model to simulate flood events within the region. Skhakhfa & Ouerdachi (2016) used the HEC-HMS model to simulate peak flows for wadi Ressoul in El Berda watershed, northeast of Algeria. The model calibration and validation of the aforementioned study gave good results and the study concluded that the HEC-HMS model is suitable for hydrological modelling in the West African sub-region and in a data scarce catchment. Twumasi et al (2015) employed HEC-HMS model to calculate flood volume for the Lawra District in the Upper West region of Ghana, for effective management of floodwater. According to the study, Lawra is prone to severe flash floods caused by high-intensity, short-duration rainfall. The floodwater, however, goes to waste, resulting in a shortage of water throughout the lengthy dry season. A volume of 31,313,221.5 cubic meters was obtained for August, September, and October which are the rainiest months in the district. The study proved the effectiveness of HEC-HMS model in simulating flood volume in the Lawra district of Ghana.

Results of the calibration and validation, is an indication that, peak discharges above 1000 cubic meters per second could lead to flooding in portions of the basin upstream of the Chache station. This suggestion is drawn from the peak discharges of 1026.0 cms, 1811.6 cms, 2205.6 cms and 2814.0 cms simulated for the 1996, 1999, 2007 and 2010 flooding events respectively. In addition, from peak discharge values of 1207.3 cms, 2971.8 cms, 4100 cms, and 4200 cms simulated for 1996, 1999, 2007 and 2010 flooding events, it could be suggested that, peak discharges above 1200 cms could lead to flooding at regions upstream of the Bui station. Furthermore, peak discharges of 6158.9 cms and 8680.2 cms simulated at Bamboi station for the 2007 and 2010 flooding events, is an indication that peak flows above 6000 cms could lead to severe flooding in regions upstream of Bamboi station. Hence, the established model could be used as a flood early warning and forecast tool for downstream portions of the Basin.

The established model was also used to simulate peak volumes of selected flooding events within the basin. Hence, forecasted annual rainfall values can be applied to the model to predict volume of floodwater. This could serve as a tool for assessment of water availability and effective management of water resources within the basin. Forecasted annual rainfall amounts can also be applied to the model to simulate expected peak flows. Hence, the development of serious water policy and planning strategies in accordance with the results obtained from this study could reduce the probability of floods within the basin.

The calibrated model could be used to assess the future impacts of climate and land use changes on flood risk in the basin. Using a hydraulic model like HEC-RAS, data may also be exported from the hydrologic model to create a 2-dimensional flood inundation map.

4.4 APPLICATION OF HYDROLOGIC MODEL FOR FLOOD FORECASTING

Intensity-Duration-Frequency curves of various rainfall stations within the basin is used to create frequency storms for 5-year, 10-year, 15-year, 20-year, 25-year, 50-year, 75 and 100-year return periods (recurrence intervals) of rainfall. The return period of rainfall is the probability of occurrence of particular rainfall events or an estimated time interval between rainfall of similar intensities and duration. A 100-year return period of rainfall has a 1/100 probability of occurrence or exceedance. It also means that in any given year, there is a 1% chance of occurrence of that particular rainfall intensity and duration. The Calibrated model was used to simulate expected peak runoffs using the design storms developed from the IDF curves. The simulated peak runoff obtained for Chache, Bui and Bamboi stations and their probabilities of occurrence are shown in table 4.28. Figure 4.23 shows a graph of peak flows against various return periods for the three stations within the basin.

Table 4. 28: Simulated peak discharge values for the various return periods of rainfall

RETURN PERIODS	PROBABILITY OF OCCURRENCE	PEAK DISCHARGE (M^3/S) CHACHE	PEAK DISCHARGE (M^3/S) BUI	PEAK DISCHARGE (M^3/S) BAMBOI
5	20%	1568.8	3251.7	8677.7
10	10%	1731.0	3802.9	10126.6
15	6.67%	1833.7	4149.8	10962.3
20	5%	1911.5	4375.7	11497.5
25	4%	1976.7	4561.8	12035.3
50	2%	2161.7	5123.0	13430.3
75	1.3%	2284.2	5456.7	14288.8
100	1%	2375.4	5655.0	14941.4

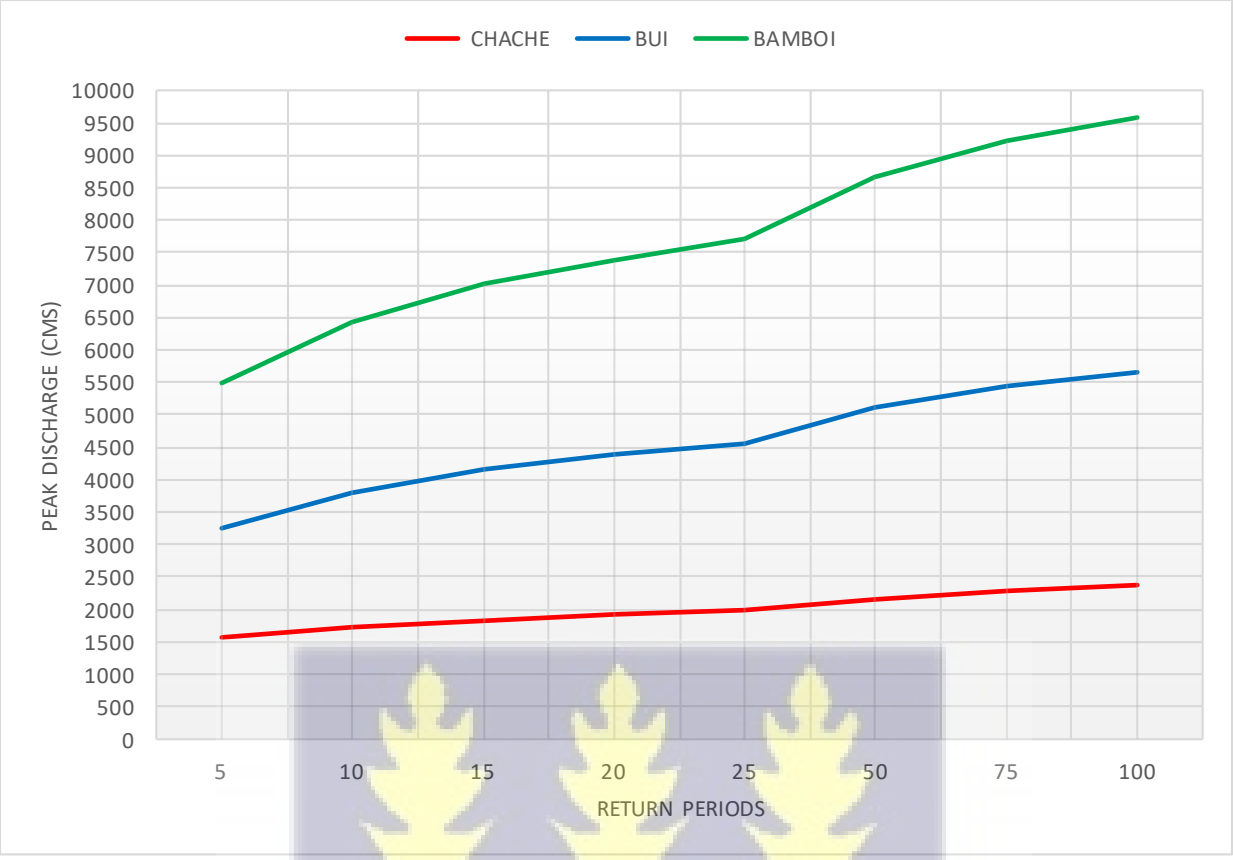

Figure 4. 23: Simulated peak discharges for selected return periods in the basin

Zhao et al (2019) used IDF curves to create design storms in Zhudong river basin in China to simulate peak flows for various reoccurrence intervals and concluded HEC-HMS is applicable for forecasting peak flows in the region. Hamidon et al (2021) also developed a hydrological model using HEC-HMS for Bukit Merah basin in Malaysia and used predicted future rainfall data to forecast peak flows of forecasted floods in the region. The study shows the applicability of HEC-HMS model in forecasting future floods.

However, despite the topic's acknowledged relevance, flood forecasting in Africa has received little attention in the scholarly literature, and previous flood predicting research has virtually exclusively focused on the Nile River Basin. (Thiemig et al., 2011). Hence this study used IDF curves to forecast peak flows in the Black Volta basin in Ghana. These results give fundamental

information on the peak flows that could be generated in the basin as a result of the various rainfall events. The results show a general increasing peak discharge values downstream of the basin. In addition, the simulated peak discharges increase with increasing return periods (Figure 4.23).

A 5-year return period of rainfall in the basin, gave expected peak discharges of 1568.8 m^3/s, 3251.7 m^3/s and 5488.9 m^3/s at Chache, Bui and Bamboi discharge stations respectively. Because of the size of the watershed, it is unlikely for a 5-year return period to cause flooding. Since

The 15-year return period simulation gave a peak discharge of 1833.7 m^3/s. When this discharge value is compared to the observed peak discharge of 1811.0 m^3/s at Chache station during the September 1999 flood event, it is reasonable to infer that the rainfall event that caused the flood was a 15-year return period rainfall.

The simulation of 15-year return period of rainfall gave a peak discharge of 4149.8 m^3/s at Bui station, this value is similar to the observed peak discharge of 4100.0 m^3/s recorded at the station during the September 2007 flood event. Hence, it is reasonable to suggest that the rainfall event, which caused the flooding event, was a 15-year return period rainfall. We can therefore infer that there is a 6.67% chance of recording that magnitude of peak discharge in any year in 15 years.

The simulation for a 10-year return period of rainfall at Bamboi station produced a peak flow of 6436.2 m^3/s, which is close to the reported peak discharge of 6158.9 m^3/s during the September 2007 flood event. We could infer that a 10-year return period of rainfall led to the September 2007 flood at Bamboi.

In addition, the 50-year return period of rainfall gave a peak discharge of 8652.2 m^3/s. This value is close to the observe peak discharge of 8680.2 m^3/s recorded at the station for the September 2010 flooding event. Hence, it is reasonable to suggest that the September 2010 flooding at Bamboi

Station event was caused by a 50-year return period of rainfall. Therefore, there is a 2% probability of recording peak discharges of this magnitude in any given year at Bamboi Station in 50 years.

The findings of this study provide fundamental information on the peak volume and peak flow generated in the watershed as a result of the various rainfall events, which may then be used to plan, design, and manage various water resource activities in the Black Volta basin in Ghana. The model's capacity to reproduce the magnitude and timing of peaks in extreme floods in the Black Volta River basin in Ghana, underlines the model's importance as a flood prediction tool, to mitigate the impacts of flooding in the area. More so, the model has been used to predict peak flows for various return periods of rainfall using IDF curves within the basin. This information can be beneficial in the identification of suitable sites for proper design and construction of flood control structures within the basin. Therefore, the study provides an established hydrological model that can be used to simulate rainfall-runoff relationships, simulate peak flows and peak volumes of various rainfall events for flood forecasting and understand the hydrological processes occurring in the Black Volta basin in Ghana.

CHAPTER FIVE

CONCLUSION, LIMITATIONS AND RECOMMENDATION

5.1 CONCLUSION

Spatio-temporal trend of rainfall in the Black Volta watershed in Ghana has been shown to be beneficial since rainfall is the most significant process for the production of a hydrological model at a basin scale, and changes in rainfall can have a big impact on surface water flows. The results of spatio-temporal trend analysis revealed a general decreasing trend of annual rainfall amount and an increasing trend of rainfall intensity for the period of 1980-2018, which is associated with impacts of climate change on rainfall patterns. This suggests that flooding in the study area is as a result of increasing rainfall intensity. The upstream parts of the basin show increasing trend of rainfall amount, while the downstream portions show decreasing trend. This suggest increasing annual rainfall within the Sahel in Ghana. The basin shows significant variability in decadal distribution of annual rainfall amount and rainfall intensity. However, the recent decade revealed decreasing trend of rainfall amount and intensity within the basin. This trend is associated to the impacts of climate change within the West African sub-region.

The hydrology of a basin is largely influenced by the land use. Land use land cover of the Black Volta basin was studied for the year 2011 to determine the various land uses types in the catchment. The results revealed that the study area was predominantly occupied by vegetation, with agricultural land being the most dominant vegetation type, which is said to produce high runoff coefficients. Suggesting that the study area is likely to generate high runoff during a rainfall event.

HEC-HMS model was capable of simulating peak flows and runoff volumes of flood events of 1996 and 2007 with an average NSE ranging from 0.789 to 0.919, suggesting a very good fit

between observed and simulated discharges. It was inferred from the sensitivity analysis that, infiltration and soil storage are the key factors that influence runoff in the basin since curve number was found to be the most sensitive parameter during calibration. The results of the validation showed the models ability to simulate peak flows of periods outside the calibration period. With NSE values ranging from 0.505 to 0.965 for the validation period, it is reasonable to conclude that the calibrated model has a good performance and is suitable for predicting peak flow and peak volumes in the Black Volta basin in Ghana.

The calibrated model was used to simulate expected peak runoffs using the design storms developed from the IDF curves for 5, 10, 15, 20, 25, 5, 75 and 100 years return periods of rainfall. Peak flows for simulated return periods range from 1,568.8 m^3/s at the upstream to 14,941.4 m^3/s at the downstream parts of the basin. This could serve as a tool for assessment of water availability and effective management of water resources within the basin and serve as a basis for the development of serious water policy and planning strategies to mitigate the impacts of floods within the basin. The present study concludes that due to increasing trend of rainfall intensity in the study area, extreme rainfall events are expected to occur within the basin. HEC-HMS model can be used as a tool to simulate runoff in the Black Volta basin in Ghana, for flood forecasting and early warning to mitigate the impacts of flooding within the basin. In addition, the model can be applied to other river basins which have similar climatic, hydrological and land use characteristics.

5.2 LIMITATIONS TO THE STUDY

The following are the key limitations that were encountered in this study:

1. Meteorological inputs are often the largest limitation in any hydrologic model. The quality and consistency of the data obtained for this study was sufficient in general; nevertheless, there was a significant amount of rainfall data unavailability for some stations, and the density of station coverage varied greatly across the basin.
2. Sub-basin delineation accuracy and resolution is another major limitation for hydrologic modeling studies. The low resolution of the SRTM DEM data affected the accuracy of basin features and in turn, the performance of the model.
3. Model calibration could not be done for recent flood events beyond the construction and operation of the Bui dam. This is due to the unavailability of data related to the operations of the dam, the Bui dam was not modelled within the catchment.

5.3 RECOMMENDATIONS

Based on the limitations stated in the previous section, following recommendations are made for future improvements;

1. Use of alternative sources of rainfall data (e.g. satellite / remotely sensed rainfall) to conduct further research into the hydrological modelling of the basin.
2. Use of high resolution SRTM DEM data to improve the accuracy of basin features.
3. Incorporation of data related to the dams and hydropower plants as well as the development of a true reservoir regulation model capable of adequately capturing the operations of these structures to adequately represent the actual conditions in the basin

REFERENCE

Abdollahi, K., Bashir, I., Verbeiren, B., Harouna, M. R., Van Griensven, A., Huysmans, M., & Batelaan, O. (2017). A Distributed Monthly Water Balance Model: Formulation and Application on Black Volta Basin. *Environmental Earth Sciences*, *76*(5). https://doi.org/10.1007/s12665-017-6512-1

Abubakari, S., Kusi, K. A., & Xiaohua, D. (2017). Revision of the Rainfall Intensity Duration Frequency Curves for the City of Kumasi-Ghana Journal of Engineering and Science. *The International Journal of Engineering and Science*, *06*(01), 51–56. https://doi.org/10.9790/1813-0601035156

Abungba, J. A., Khare, D., Pingale, S. M., Adjei, K. A., Gyamfi, C., & Odai, S. N. (2020). Assessment of Hydro-climatic Trends and Variability over the Black Volta Basin in Ghana. *Earth Systems and Environment*. https://doi.org/10.1007/s41748-020-00171-9

Ackom, E. K., Adjei, K. A., & Odai, S. N. (2020). Spatio-temporal rainfall trend and homogeneity analysis in flood prone area: case study of Odaw river basin-Ghana. *SN Applied Sciences*, *2*(12). https://doi.org/10.1007/s42452-020-03924-3

Adjei-Gyapong, T., & Asiamah, R. D. (2002). The interim Ghana soil classification system and its relation with the World Reference Base for Soil Resources. *Quatorzième Réunion Du Sous-Comité Ouest et Centre Africain de Corrélation Des Sols*, *98*, 9–13.

Adjei, K. A., Ren, L., Appiah-Adjei, E. K., & Odai, S. N. (2015). Application of Satellite-derived Rainfall for Hydrological Modelling in the Data-scarce Black Volta Trans-boundary Basin. *Hydrology Research*, *46*(5), 777–791. https://doi.org/10.2166/nh.2014.111

Afriyie, K., Ganle, J. K., & Santos, E. (2018). 'The floods came and we lost everything': weather extremes and households' asset vulnerability and adaptation in rural Ghana. *Climate and Development*, *10*(3), 259–274. https://doi.org/10.1080/17565529.2017.1291403

Agyekum, J., Annor, T., Lamptey, B., Quansah, E., & Agyeman, R. Y. K. (2018). Evaluation of CMIP5 Global Climate Models over the Volta Basin: Precipitation. *Advances in Meteorology*, *2018*(Figure 1). https://doi.org/10.1155/2018/4853681

Ahadzie, D. K., & Proverbs, D. G. (2011). Emerging issues in the management of floods in ghana. *International Journal of Safety and Security Engineering*, *1*(2), 182–192. https://doi.org/10.2495/SAFE-V1-N2-182-192

Ahern, M., Kovats, R. S., Wilkinson, P., Few, R., & Matthies, F. (2005). Global health impacts of floods: Epidemiologic evidence. *Epidemiologic Reviews*, *27*, 36–46. https://doi.org/10.1093/epirev/mxi004

Ahmad, I., Tang, D., Wang, T., Wang, M., & Wagan, B. (2015). Precipitation trends over time using Mann-Kendall and spearman's Rho tests in swat river basin, Pakistan. *Advances in Meteorology*, *2015*. https://doi.org/10.1155/2015/431860

Akpoti, K., Antwi, E. O., & Kabo-bah, A. T. (2016a). Impacts of rainfall variability, land use and land cover change on stream flow of the Black Volta basin, West Africa. *Hydrology*, *3*(3), 1–24. https://doi.org/10.3390/hydrology3030026

Akpoti, K., Antwi, E. O., & Kabo-bah, A. T. (2016b). Impacts of Rainfall Variability, Land Use and Land Cover Change on Stream Flow of the Black Volta basin, West Africa. *Hydrology*, *3*(3). https://doi.org/10.3390/hydrology3030026

Alfieri, L., Berenguer, M., Knechtl, V., Liechti, K., Sempere-torres, D., & Zappa, M. (2020). Handbook of Hydrometeorological Ensemble Forecasting. In *Handbook of Hydrometeorological Ensemble Forecasting* (Issue January). https://doi.org/10.1007/978-3-642-40457-3

Ali, A. bin M. (2018). *Flood Inundation Modeling and Hazard Mapping under Uncertainty in the Sungai Johor Basin , Malaysia*. Universiti Putra Malaysia, Serdang, Malaysia.

Almoradie, A., de Brito, M. M., Evers, M., Bossa, A., Lumor, M., Norman, C., Yacouba, Y., & Hounkpe, J. (2020). Current flood risk management practices in Ghana: gaps and opportunities for improving resilience. *Journal of Flood Risk Management*, *July*. https://doi.org/10.1111/jfr3.12664

Ampofo, S., Gyekye, E., Ampadu, B., & Sackey, I. (2021). Modelling Soil and Water Dynamics in the Black Volta Basin Using the Soil and Water Assessment Tool (SWAT) Model. *Ghana Journal of Science, Technology and Development*, *7*(2). https://doi.org/https://doi.org/10.47881/259.967x

Amproche, A., Antwi, M., & Kabo-Bah, A. (2020). Geospatial Assessment of Land Use and Land Cover Patterns in the Black Volta Basin, Ghana. *Journal of Remote Sensing & GIS*, *09*(01), 1–9. https://doi.org/10.35248/2469-4134.20.9.269

Andah, W. E. I., Giesen, N. Van De, & Biney, C. A. (2014). Water , Climate , Food , and Environment in the Volta Basin Adaptation Strategies to Changing Environments. *Journal of Environment and Earth Science*, *Vol.4*(No.16), 27–38.

Andreini, M., Van de Giesen, N., Van Edig, A., Fosu, M., & Andah, W. (2000). Volta Basin Water Balance. *ZEF Discussion Papers on Development Policy*, *21*(ISSN: 1436-9931),

pp29.

Ansah, S. O., Ahiataku, M. A., Yorke, C. K., Otu-Larbi, F., Yahaya, B., Lamptey, P. N. L., & Tanu, M. (2020). Meteorological Analysis of Floods in Ghana. *Advances in Meteorology*, *2020*. https://doi.org/10.1155/2020/4230627

Asante, F. A., & Amuakwa-Mensah, F. (2015). Climate change and variability in Ghana: Stocktaking. *Climate*, *3*(1), 78–99. https://doi.org/10.3390/cli3010078

Atanga, R. A., & Tankpa, V. (2021). Climate Change, Flood Disaster Risk and Food Security Nexus in Northern Ghana. *Frontiers in Sustainable Food Systems*, *5*(August). https://doi.org/10.3389/fsufs.2021.706721

Atulley, J. (2013). *Impact of Small Reservoirs and Dugouts in Ghana on Hydrology and Water Allocation in the Black Volta Basin*. 5. https://cgspace.cgiar.org/handle/10568/42166%5Cnhttp://ir.knust.edu.gh/handle/123456789/5380

Aziz, F., & Obuobie, E. (2017). Trend analysis in observed and projected precipitation and mean temperature over the Black Volta Basin, West Africa. *1400| International Journal of Current Engineering and Technology*, *7*(4), 2. http://inpressco.com/category/ijcet

Aziz, F., Obuobie, E., Sylla, M. B., Jeong, J., & Daggupati, P. (2019). Trends and Projections of Climate Extremes in the Black Volta River Basin in West Africa. *Theoretical and Applied Climatology*, *137*(1–2), 513–532. https://doi.org/10.1007/s00704-018-2609-z

Baddoo, T. D., Li, Z., Guan, Y., Boni, K. R. C., & Nooni, I. K. (2020). Data-driven modeling and the influence of objective function selection on model performance in limited data

regions. *International Journal of Environmental Research and Public Health*, *17*(11), 1–26. https://doi.org/10.3390/ijerph17114132

Bai, Y., Zhang, Z., & Zhao, W. (2019). Assessing the Impact of Climate Change on Flood Events Using HEC-HMS and CMIP5. *Water, Air, and Soil Pollution*, *230*(6). https://doi.org/10.1007/s11270-019-4159-0

Baldassarre, G. D., Montanari, A., Lins, H., Koutsoyiannis, D., Brandimarte, L., & Blöschl, G. (2010). Flood fatalities in Africa: From diagnosis to mitigation. *Geophysical Research Letters*, *37*(22), n/a-n/a. https://doi.org/10.1029/2010GL045467

Barry, B., Obuobie, E., Andreini, M., Andah, W., and P. M. (2005). *Comprehensive Assessment of Water Management in Agriculture; Comparative Study of River Basin Management. International Water Management Institute*. 26–49.

Basarudin, Z., Adnan, N. A., Latif, A. R. A., Tahir, W., & Syafiqah, N. (2014). Event-based rainfall-runoff modelling of the Kelantan River Basin. *IOP Conference Series: Earth and Environmental Science*, *18*(1). https://doi.org/10.1088/1755-1315/18/1/012084

Baumbach, Tyler; Burckhard, Suzette R.; and Kant, J. M. (2015). *Watershed Modeling Using Arc Hydro Tools . Geo*. *2*.

Bergstrom, S. (1991). Principles and confidence in hydrological modelling. *Nordic Hydrology*, *22*(2), 123–136. https://doi.org/10.2166/nh.1991.0009

Beven, K. (2012). Rainfall-Runoff Modelling. In *Rainfall-Runoff Modelling*. https://doi.org/10.1002/9781119951001

Bhuiyan, H. A. K. M., McNairn, H., Powers, J., & Merzouki, A. (2017). Application of HEC-

HMS in a cold region watershed and use of RADARSAT-2 soil moisture in initializing the model. *Hydrology*, *4*(1), 1–19. https://doi.org/10.3390/hydrology4010009

Braimah, M. M., Abdul-Rahaman, I., Oppong-Sekyere, D., Momori, P. H., Abdul-Mohammed, A., & Dordah, G. A. (2014). A Study into the Causes of Floods and its Socio-economic Effects on the People of Sawaba in the Bolgatanga Municipality, Upper East, Ghana. *International Journal of Pure and Applied Bioscience*, *2*(1), 189–195. www.ijpab.com

Brocca, L., Melone, F., & Moramarco, T. (2011). Distributed rainfall-runoff modelling for flood frequency estimation and flood forecasting. *Hydrological Processes*, *25*(18), 2801–2813. https://doi.org/10.1002/hyp.8042

Chow, Ven Te; Maidment, D. R., & Mays, L. W. (1988). *[Ven_Chow,_David_Maidment,_Larry_Mays]_Applied_Hyd(BookFi.org).pdf*.

Chow, V. (1953). *Frequency analysis of hydrologic data with special application to rainfall intensities*. http://www.ideals.illinois.edu/bitstream/handle/2142/4107/engineeringexperv00000i00414.pdf?sequence=3

CRED. (2015). Annual Disaster Statistical Review 2015: The numbers and trends. In *Centre for Research on the Epidemiology of Disasters (CRED) Institute of Health and Society (IRSS) Université catholique de Louvain – Brussels, Belgium.*

CRED. (2019). Natural disasters 2019: Now is the time to not give up. *Centre for Research on the Epidemiology of Disasters - CRED*. https://cred.be/sites/default/files/adsr_2019.pdf

Cunderlik, J. (2003). Hydrologic Model Selection for the CFCAS Project: Assessment of Water

Resources Risk and Vulnerability to Changing Climatic Conditions. *Water Resources Research Report*. https://ir.lib.uwo.ca/wrrr/9

Dawson, C. W., & Wilby, R. L. (2001). Hydrological modelling using artificial neural networks. *Progress in Physical Geography*, *25*(1), 80–108. https://doi.org/10.1177/030913330102500104

De Roo, A., Odijk, M., Schmuck, G., Koster, E., & Lucieer, A. (2001). Assessing the effects of land use changes on floods in the meuse and oder catchment. *Physics and Chemistry of the Earth, Part B: Hydrology, Oceans and Atmosphere*, *26*(7–8), 593–599. https://doi.org/10.1016/S1464-1909(01)00054-5

De Silva, M. M. G. T., Weerakoon, S. B., & Herath, S. (2014). Modeling of Event and Continuous Flow Hydrographs with HEC–HMS: Case Study in the Kelani River Basin, Sri Lanka. *Journal of Hydrologic Engineering*, *19*(4), 800–806. https://doi.org/10.1061/(asce)he.1943-5584.0000846

Demirkesen, A. C., Evrendilek, F., Berberoglu, S., & Kilic, S. (2007). Coastal flood risk analysis using landsat-7 ETM+ imagery and SRTM DEM: A case study of Izmir, Turkey. *Environmental Monitoring and Assessment*, *131*(1–3), 293–300. https://doi.org/10.1007/s10661-006-9476-2

Diakakis, M., Deligiannakis, G., Antoniadis, Z., Melaki, M., Katsetsiadou, N. K., Andreadakis, E., Spyrou, N. I., & Gogou, M. (2020). Proposal of a flash flood impact severity scale for the classification and mapping of flash flood impacts. *Journal of Hydrology*, *590*(September), 125452. https://doi.org/10.1016/j.jhydrol.2020.125452

Dramani, B. F. (2013). *Baseline Study into Groundwater Resources in the River Tain basin of*

the Black Volta. 83.

Duhan, S., & Kumar, M. (2017). Event and Continuous Hydrological Modeling with HEC-HMS: A Review Study. *International Journal of Engineering Technology Science and Research IJETSR*, *4*(4), 2394–3386. http://www.ijetsr.com/images/short_pdf/1491383424_nitttr1081_ijetsr.pdf

Emerson, C. H., Welty, C., & Traver, R. G. (2005). Watershed-Scale Evaluation of a System of Storm Water Detention Basins. *Journal of Hydrologic Engineering*, *10*(3), 237–242. https://doi.org/10.1061/(asce)1084-0699(2005)10:3(237)

Ersahin, B. (2020). *Simulation of Streamflow Using Hydrologic Modeling System HEC-HMS*. *2017*(1), 1–9.

Ewea, H. A., Elfeki, A. M., Bahrawi, J. A., & Al-Amri, N. S. (2018). Modeling of IDF curves for stormwater design in Makkah Al Mukarramah region, the Kingdom of Saudi Arabia. *Open Geosciences*, *10*(1), 954–969. https://doi.org/10.1515/geo-2018-0076

Ferreira, P. M. de L., Paz, A. R. da, & Bravo, J. M. (2020). Objective functions used as performance metrics for hydrological models: state-of-the-art and critical analysis. *Rbrh*, *25*. https://doi.org/10.1590/2318-0331.252020190155

Fleming, M. J., & Doan, Ja. H. (2013). *HEC-GeoHMS Geospatial Hydrologic Modeling Extension User ' s Manual: Vol. 10.1* (Issue February).

Fleming, M., & Neary, V. (2004). Continuous Hydrologic Modeling Study with the Hydrologic Modeling System. *Journal of Hydrologic Engineering*, *9*(3), 175–183. https://doi.org/10.1061/(asce)1084-0699(2004)9:3(175)

Ganyaglo, S. Y., Osae, S., Dampare, S. B., Fianko, J. R., Bhuiyan, M. A. H., Gibrilla, A., Bam, E., Ahialey, E., & Osei, J. (2012). Preliminary groundwater quality assessment in the central region of Ghana. *Environmental Earth Sciences*, *66*(2), 573–587. https://doi.org/10.1007/s12665-011-1266-7

Garcia, F., Folton, N., & Oudin, L. (2017). Which objective function to calibrate rainfall–runoff models for low-flow index simulations? *Hydrological Sciences Journal*, *62*(7), 1149–1166. https://doi.org/10.1080/02626667.2017.1308511

Gbangou, T., Ludwig, F., van Slobbe, E., Greuell, W., & Kranjac-Berisavljevic, G. (2020). Rainfall and dry spell occurrence in Ghana: trends and seasonal predictions with a dynamical and a statistical model. *Theoretical and Applied Climatology*, *141*(1–2), 371–387. https://doi.org/10.1007/s00704-020-03212-5

Gebre, S. L. (2015). Application of the HEC-HMS Model for Runoff Simulation of Upper Blue Nile River Basin. *Journal of Waste Water Treatment & Analysis*, *06*(02). https://doi.org/10.4172/2157-7587.1000199

Ghavasieh, A. R., & Norouzi, A. (2009). *Flood-level Forecasting Using Intensity-Duration-Frequency Curves*. *3*(4), 4384–4391.

Ghazavi, R., Rabori, A. M., & Reveshty, M. A. (2017). The effects of rainfall intensity-duration-frequency curves reformation on urban flood characteristics in semi-arid environment. *Ecopersia*, *5*(2), 1799–1813. https://doi.org/10.18869/modares.Ecopersia.5.2.1799

Global Water Partnership (GWP). (2012). *Volta basin*. http://www.gwp.org/en/WACDEP/IMPLEMENTATION/Where/Volta/

Gruntfest, E., & Handmer, J. (2001). Dealing with Flash Floods: Contemporary Issues and Future Possibilities. *Coping With Flash Floods*, 3–10. https://doi.org/10.1007/978-94-010-0918-8_1

GSS. (2012). *2010 Population and Housing Census Final Results Ghana Statistical Service.*

Guzha, A. C. (2018). *Journal of Hydrology : Regional Studies Impacts of land use and land cover change on surface runoff , discharge and low fl ows : Evidence from East Africa . 15*(December 2017), 49–67. https://doi.org/10.1016/j.ejrh.2017.11.005

Hagen, J. S., Cutler, A., Trambauer, P., Weerts, A., Suarez, P., & Solomatine, D. (2020). Development and evaluation of flood forecasting models for forecast-based financing using a novel model suitability matrix. *Progress in Disaster Science*, *6*, 100076. https://doi.org/10.1016/j.pdisas.2020.100076

Hall, J., Arheimer, B., Borga, M., Brázdil, R., Claps, P., Kiss, A., Kjeldsen, T. R., Kriaučiūnienė, J., Kundzewicz, Z. W., Lang, M., Llasat, M. C., Macdonald, N., McIntyre, N., Mediero, L., Merz, B., Merz, R., Molnar, P., Montanari, A., Neuhold, C., … Blöschl, G. (2014). Understanding flood regime changes in Europe: A state-of-the-art assessment. *Hydrology and Earth System Sciences*, *18*(7), 2735–2772. https://doi.org/10.5194/hess-18-2735-2014

Hamidon, N., Hong, C. J., Awang, M., Rahman, M. A. A., Ahmad, F., Musa, K., Yusof, F. M., Adnan, S. H., & Mustafa, M. S. S. (2021). *Future Flood Forecasting in Bukit Merah Using HEC-HMS Software*. *200*(ICoST), 183–189. https://doi.org/10.2991/aer.k.201229.026

Huo, J., & Liu, L. (2020). Evaluation Method of Multiobjective Functions' Combination and Its Application in Hydrological Model Evaluation. *Computational Intelligence and Neuroscience*, *2020*. https://doi.org/10.1155/2020/8594727

Hussain, F., Wu, R.-S., & Yu, K.-C. (2021). Application of Physically Based Semi-Distributed Hec-Hms Model for Flow Simulation in Tributary Catchments of Kaohsiung Area Taiwan. *Journal of Marine Science and Technology*, *29*(1). https://doi.org/10.51400/2709-6998.1003

Ibrahim-Bathis, K., & Ahmed, S. A. (2016). Rainfall-runoff modelling of Doddahalla watershed—an application of HEC-HMS and SCN-CN in ungauged agricultural watershed. *Arabian Journal of Geosciences*, *9*(3), 1–16. https://doi.org/10.1007/s12517-015-2228-2

Iddrisu, W. A., Nokoe, K. S., Luguterah, A., & Antwi, E. O. (2017). Generalized Additive Mixed Modelling of River Discharge in the Black Volta River. *Open Journal of Statistics*, *07*(04), 621–632. https://doi.org/10.4236/ojs.2017.74043

Ilori, O. W., & Ajayi, V. O. (2020). Change Detection and Trend Analysis of Future Temperature and Rainfall over West Africa. *Earth Systems and Environment*, *4*(3), 493–512. https://doi.org/10.1007/s41748-020-00174-6

Incoom, A. B. M., Adjei, K. A., & Odai, S. N. (2020). Rainfall variabilities and droughts in the Savannah zone of Ghana from 1960-2015. *Scientific African*, *10*, e00571. https://doi.org/10.1016/j.sciaf.2020.e00571

Ismael, O., Joseph, S., & Patrick, K. H. (2017). Hec-Hms Model for Runoff Simulation in Ruiru Reservoir Watershed. *American Journal of Engineering Research (AJER)*, *6*(4), 1–7.

Itiveha, K. O., & Bigg, G. R. (2008). The Variation of Discharge Entering the Niger Delta system, 1951–2000, and Estimates of Change Under Global Warming. *International Journal of Climatology*, *2029*(March 2008), 2011–2029. https://doi.org/10.1002/joc

Jajarmizadeh, M., Harun, S., Environmental, M. S.-J. of, & 2012, U. (2012). A review on

theoretical consideration and types of models in hydrology. *Academia.Edu*. https://www.academia.edu/download/34472999/A_Review_on_Theoretical_Consideration_and_Types_of_Models_in_Hydrology.pdf

Jeyaseelan, A. T. (2003). Droughts & floods assessment and monitoring using remote sensing and GIS. *Satellite Remote Sensing and GIS Applications in Agricultural Meteorology*, 291–313. http://www.wamis.org/agm/pubs/agm8/Paper-14.pdf

Jonkman, S. N. (2005). Global perspectives on loss of human life caused by floods. *Natural Hazards*, *34*(2), 151–175. https://doi.org/10.1007/s11069-004-8891-3

Judith, A. K. (2015). *Community Based Initiatives and Strategies for Adapting to Annual Floods along The Black and White and Volta Rivers in the Central Gonja District of Northern Region , Ghana*. *5*(8), 33–43.

Jung, G., Wagner, S., & Kunstmann, H. (2012). Joint Climate-hydrology Modeling: An Impact Study for the Data-sparse Environment of the Volta Basin in West Africa. *Hydrology Research*, *43*(3), 231–248. https://doi.org/10.2166/nh.2012.044

Jutla, A. S. (2006). *Hydrologic Modeling of Reconstructed Watersheds Using a System Dynamics Approach*. *January*, 199.

Kabo-Bah, A. T., Diji, C. J., Nokoe, K., Mulugetta, Y., Obeng-Ofori, D., & Akpoti, K. (2016). Multiyear rainfall and temperature trends in the Volta River basin and their potential impact on hydropower generation in Ghana. *Climate*, *4*(4). https://doi.org/10.3390/cli4040049

Kantakumar, L. N., & Neelamsetti, P. (2015). Multi-temporal land use classification using hybrid approach. *Egyptian Journal of Remote Sensing and Space Science*, *18*(2), 289–295.

https://doi.org/10.1016/j.ejrs.2015.09.003

Karamage, F., Liu, Y., Fan, X., Francis Justine, M., Wu, G., Liu, Y., Zhou, H., & Wang, R. (2018). Spatial Relationship between Precipitation and Runoff in Africa. *Hydrology and Earth System Sciences*, *October*, 1–27. https://doi.org/10.5194/hess-2018-424

Kenabatho, K. P. (2010). *Hydrological and water resources modelling under uncertainty and climate change: An application to the Limpopo basin, Botswana. September*.

Khaleghi, M. R. (2017). *The influence of deforestation and anthropogenic activities on runoff generation*. *2017*(6), 245–253. https://doi.org/10.17221/130/2016-JFS

Kim, C. (2016). Land use classification and land use change analysis using satellite images in Lombok Island, Indonesia. *Forest Science and Technology*, *12*(4), 183–191. https://doi.org/10.1080/21580103.2016.1147498

Klutse, N. A. B., Owusu, K., Nkrumah, F., & Anang, O. A. (2021). Projected rainfall changes and their implications for rainfed agriculture in northern Ghana. *Weather*, 1–9. https://doi.org/10.1002/wea.4015

Komi, K., Amisigo, B. A., Diekkrüger, B., & Hountondji, F. C. C. (2016). Regional flood frequency analysis in the Volta River Basin, West Africa. *Hydrology*, *3*(1). https://doi.org/10.3390/hydrology3010005

Komi, K., Neal, J., Trigg, M. A., & Diekkrüger, B. (2017). Modelling of flood hazard extent in data sparse areas: a case study of the Oti River basin, West Africa. *Journal of Hydrology: Regional Studies*, *10*, 122–132. https://doi.org/10.1016/j.ejrh.2017.03.001

Kpanou, M., Laux, P., Brou, T., Vissin, E., Camberlin, P., & Roucou, P. (2021). Spatial patterns

and trends of extreme rainfall over the southern coastal belt of West Africa. *Theoretical and Applied Climatology*, *143*(1–2), 473–487. https://doi.org/10.1007/s00704-020-03441-8

Kwakye, S. O., & Bárdossy, A. (2020). Hydrological Modelling in Data-Scarce Catchments: Black Volta basin in West Africa. *SN Applied Sciences*, *2*(4). https://doi.org/10.1007/s42452-020-2454-4

Lee, H., Mcintyre, N., Wheater, H., & Young, A. (2004). *Assessment of rainfall-runoff model structures for regionalisation purposes*. *I*(2002), 302–308.

Lincoln, W. S. (2009). *A modeling approach for operational flash flood forecasting for small-scale watersheds in central Iowa*. 100 pages. http://lib.dr.iastate.edu/cgi/viewcontent.cgi?article=1714&context=etd

Liu, Y. B., Gebremeskel, S., Smedt, F. De, Hoffmann, L., & Pfister, L. (2006). *Predicting storm runoff from different land-use classes using a geographical information system-based distributed model*. *548*(January 2005), 533–548. https://doi.org/10.1002/hyp.5920

Mahdi, E. S., & Mohamedmeki, M. Z. (2020). Analysis of rainfall intensity-duration-frequency (IDF) curves of Baghdad city. *IOP Conference Series: Materials Science and Engineering*, *888*(1). https://doi.org/10.1088/1757-899X/888/1/012066

Manzanas, R., Amekudzi, L. K., Preko, K., Herrera, S., & Gutiérrez, J. M. (2014). Precipitation variability and trends in Ghana: An intercomparison of observational and reanalysis products. *Climatic Change*, *124*(4), 805–819. https://doi.org/10.1007/s10584-014-1100-9

Marchi, L., Borga, M., Preciso, E., & Gaume, E. (2010). Characterisation of selected extreme flash floods in Europe and implications for flood risk management. *Journal of Hydrology*,

394(1–2), 118–133. https://doi.org/10.1016/j.jhydrol.2010.07.017

Meena, R. A. Y. S. (2012). Simulation of Runoff and Flood Inundation in Kosi River Basin Using Hydrological Models , ANN , Remote Sensing and GIS. *National Institute of Technology Rourkela Rourkela*, 91.

Mensah, H., & Ahadzie, D. K. (2020). Causes, impacts and coping strategies of floods in Ghana: a systematic review. *SN Applied Sciences*, *2*(5). https://doi.org/10.1007/s42452-020-2548-z

Mioc, D., Nickerson, B., MacGillivray, E., Morton, A., Anton, F., Fraser, D., Tang, P., & Liang, G. (2008). Early Warning and Mapping for Flood Disasters. *The Internatioanl Archives of the Photogrammetry, Remote Sensing and Spatail Information Sciences*, *37*(B4), 1507–1512.

Mouhamed, L., Traore, S. B., Alhassane, A., & Sarr, B. (2013). Evolution of some observed climate extremes in the West African Sahel. *Weather and Climate Extremes*, *1*, 19–25. https://doi.org/10.1016/j.wace.2013.07.005

Msaddek, M., Kimbowa, G., & Garouani, A. El. (2020). Hydrological Modeling of Upper OumErRabia Basin (Morocco), Comparative Study of the Event-Based and Continuous-Process HEC-HMS Model Methods. *Computational Water, Energy, and Environmental Engineering*, *09*(04), 159–184. https://doi.org/10.4236/cweee.2020.94011

Mujumdar, P. P., & Kumar, D. N. (2012). *Floods in a changing climate: hydrologic modeling*. Cambridge University Press.

Mul, M., Obuobie, E., Appoh, R., Kankam-Yeboah, K., Bekoe-Obeng, E., Amisigo, B., Logah, F. Y., Ghansah, B., & McCartney, M. (2015). Water resources assessment of the Volta

River Basin. In *IWMI Working Papers* (Vol. 166). https://doi.org/10.5337/2015.220

Munyaneza, O., Mukubwa, A., Maskey, S., Uhlenbrook, S., & Wenninger, J. (2014). Assessment of surface water resources availability using catchment modelling and the results of tracer studies in the mesoscale Migina Catchment, Rwanda. *Hydrology and Earth System Sciences*, *18*(12), 5289–5301. https://doi.org/10.5194/hess-18-5289-2014

Najibi, N., & Devineni, N. (2018). Recent trends in the frequency and duration of global floods. *Earth System Dynamics*, *9*(2), 757–783. https://doi.org/10.5194/esd-9-757-2018

Nandalal, H. K., & Ratmayake, U. R. (2010). Event Based Modeling of a Watershed Using HEC-HMS. *Engineer: Journal of the Institution of Engineers, Sri Lanka*, *43*(2), 28. https://doi.org/10.4038/engineer.v43i2.6979

Nash, J. E., & Sutcliffe, J. V. (1970). River flow forecasting through conceptual models part I - A discussion of principles. *Journal of Hydrology*, *10*(3), 282–290. https://doi.org/10.1016/0022-1694(70)90255-6

Nicholls, R., Zanuttigh, B., Vanderlinden, J. P., Weisse, R., Silva, R., Hanson, S., Narayan, S., Hoggart, S., Thompson, R. C., Vries, W. de, & Koundouri, P. (2014). Developing a Holistic Approach to Assessing and Managing Coastal Flood Risk. In *Coastal Risk Management in a Changing Climate*. Elsevier Inc. https://doi.org/10.1016/B978-0-12-397310-8.00002-6

Nouaceur, Z., & Murarescu, O. (2020). Rainfall Variability and Trend Analysis of Rainfall in West Africa (Senegal, Mauritania, Burkina Faso). *Water*, *17*. https://doi.org/doi:10.3390/w12061754

Nunes, A. N., Almeida, A. C. De, & Coelho, C. O. A. (2011). Impacts of land use and cover type

on runoff and soil erosion in a marginal area of Portugal. *Applied Geography*, *31*(2), 687–699. https://doi.org/10.1016/j.apgeog.2010.12.006

Obahoundje, S., Diedhiou, A., Ofosu, E. A., Anquetin, S., François, B., Adounkpe, J., Amoussou, E., Kouame, Y. M., Kouassi, K. L., Bi, V. H. N., & Ta, M. Y. (2018). Assessment of spatio-temporal changes of land use and land cover over South-Western African basins and their relations with variations of discharges. *Hydrology*, *5*(4). https://doi.org/10.3390/hydrology5040056

Obeng, E. B. (2005). *Application of a hydrological model in a data-poor tropical West African catchment : a case study of the Densu Basin of Ghana*. 1–228.

Odoulami, R. C., & Akinsanola, A. A. (2018). Recent assessment of West African summer monsoon daily rainfall trends. *Weather*, *73*(9), 283–287. https://doi.org/10.1002/wea.2965

Ojo, O. I., & Ilunga, M. F. (2018). Application of Nonparametric Trend Technique for Estimation of Onset and Cessation of Rainfall. *Air, Soil and Water Research*, *11*, 0–3. https://doi.org/10.1177/1178622118790264

Okyere, C. Y., Yacouba, Y., & Gilgenbach, D. (2013). The Problem of Annual Occurrences of Floods in Accra: An Integration of Hydrological, Economic and Political Perspectives. *Theoretical and Empirical Researches in Urban Management*, *8.2*, 1–50.

Ouédraogo, W. A. A., Raude, J. M., & Gathenya, J. M. (2018). Continuous modeling of the Mkurumudzi River catchment in Kenya using the HEC-HMS conceptual model: Calibration, validation, model performance evaluation and sensitivity analysis. *Hydrology*, *5*(3). https://doi.org/10.3390/hydrology5030044

Owusu, K., Waylen, P., & Qiu, Y. (2008). Changing Rainfall Inputs in the Volta basin: Implications for Water Sharing in Ghana. *GeoJournal*, *71*(4), 201–210. https://doi.org/10.1007/s10708-008-9156-6

Owusu, K., & Waylen, P. R. (2013). The changing rainy season climatology of mid-Ghana. *Theoretical and Applied Climatology*, *112*(3–4), 419–430. https://doi.org/10.1007/s00704-012-0736-5

Paeth, H., Fink, A. H., Pohle, S., Keis, F., Mächel, H., & Samimi, C. (2011). Meteorological characteristics and potential causes of the 2007 flood in sub-Saharan Africa. *International Journal of Climatology*, *31*(13), 1908–1926. https://doi.org/10.1002/joc.2199

Pechlivanidis, I. G., Jackson, B. M., Mcintyre, N. R., & Wheater, H. S. (2011). Catchment scale hydrological modelling: A review of model types, calibration approaches and uncertainty analysis methods in the context of recent developments in technology and applications. *Global Nest Journal*, *13*(3), 193–214. https://doi.org/10.30955/gnj.000778

Peel, M. C., & Blöschl, G. (2011). Hydrological modelling in a changing world. *Progress in Physical Geography*, *35*(2), 249–261. https://doi.org/10.1177/0309133311402550

Pirnia, A., Golshan, M., Darabi, H., Adamowski, J., & Rozbeh, S. (2019). Using the mann–kendall test and double mass curve method to explore stream flow changes in response to climate and human activities. *Journal of Water and Climate Change*, *10*(4), 725–742. https://doi.org/10.2166/wcc.2018.162

Qin, Y. (2020). Urban flooding mitigation techniques: A systematic review and future studies. *Water (Switzerland)*, *12*(12). https://doi.org/10.3390/w12123579

Quaye-Ballard, J. A., Okrah, T. M., Andam-Akorful, S. A., Awotwi, A., Antwi, T., Osei-Wusu, W., Tang, X., & Quaye-Ballard, N. L. (2020). Spatiotemporal dynamics of rainfall in Upper East Region of Ghana, West Africa, 1981–2016. *SN Applied Sciences*, *2*(10), 1–12. https://doi.org/10.1007/s42452-020-03463-x

Ramly, S., & Tahir, W. (2016). Application of HEC-GeoHMS and HEC-HMS as Rainfall–Runoff Model for Flood Simulation. *Isfram 2015*. https://doi.org/10.1007/978-981-10-0500-8

Rimfors, O., & Velichkin, V. (2015). *Hydrological Modelling of Al Auja Earth Dam in the Lower Jordan Valley*. https://www.diva-portal.org/smash/record.jsf?pid=diva2:844472

Rogger, M., Agnoletti, M., Alaoui, A., Bathurst, J. C., Bodner, G., Borga, M., Chaplot, V., Gallart, F., Glatzel, G., Hall, J., Holden, J., Holko, L., Horn, R., Kiss, A., Quinton, J. N., Leitinger, G., Lennartz, B., Parajka, J., Peth, S., … Viglione, A. (2016). *Water Resources Research*. *June 2013*, 5209–5219. https://doi.org/10.1002/2017WR020723.Received

Sakeyo, E. K. (2008). *Modelling the impact of deforestation on stream flow - a case of chalimbana river catchment in chongwe, zambia*. *January*.

Sampath, D. S., Weerakoon, S. B., & Herath, S. (2015). HEC-HMS model for runoff simulation in a tropical catchment with intra-basin diversions – case study of the Deduru Oya river basin, Sri Lanka. *Engineer: Journal of the Institution of Engineers, Sri Lanka*, *48*(1), 1. https://doi.org/10.4038/engineer.v48i1.6843

Sanogo, S., Fink, A. H., Omotosho, J. A., Ba, A., Redl, R., & Ermert, V. (2015). Spatio-temporal characteristics of the recent rainfall recovery in West Africa. *International Journal of Climatology*, *35*(15), 4589–4605. https://doi.org/10.1002/joc.4309

SDA Conservation Engineering Division, U. (1986). Urban Hydrology for Small Watersheds. *Soil Conservation, Technical Release 55 (TR-55)*, 164. http://scholar.google.com/scholar?hl=en&btnG=Search&q=intitle:Urban+Hydrology+for+Small+watersheds#1

Setegn, S. G., Srinivasan, R., & Dargahi, B. (2008). Hydrological Modelling in the Lake Tana Basin, Ethiopia Using SWAT Model. *The Open Hydrology Journal*, *2*(1), 49–62. https://doi.org/10.2174/1874378100802010049

Shaibu, S., Odai, S. N., Adjei, K. A., Jnr, E. M. O., & Annor, F. O. (2012). Simulation of runoff for the Black Volta Basin using satellite observation data. *International Journal of River Basin Management*, *10*(3), 245–254. https://doi.org/10.1080/15715124.2012.679735

Shen, S., & Chen, P. (2010). A real-time flood monitoring system based on GIS and hydrological model. *2010 2nd Conference on Environmental Science and Information Application Technology, ESIAT 2010*, *1*, 605–608. https://doi.org/10.1109/ESIAT.2010.5568857

Shukur, H. K. (2017). *Estimation Curve Numbers using GIS and Hec-GeoHMS Model GIS*. *23*(5), 1–11.

Skhakhfa, I. D., & Ouerdachi, L. (2016). Hydrological modelling of Wadi ressoul watershed, Algeria, by HEC-HMS model. *Journal of Water and Land Development*, *31*(1), 139–147. https://doi.org/10.1515/jwld-2016-0045

Smith, W., Davies-colley, C., Mackay, A., & Bankoff, G. (2011). *Social impact of the 2004 Manawatu floods and the ' hollowing out ' of rural New Zealand*. *35*(3), 540–553.

Stein, L., Pianosi, F., & Woods, R. (2020). Event-based classification for global study of river

flood generating processes. *Hydrological Processes*, *34*(7), 1514–1529. https://doi.org/10.1002/hyp.13678

Subaar, C., Apori, N., Fletcher, J. J., Galyuon, R., Edusei, G., & Adayira, V. W. (2018). Time Series Analysis for Prediction of Meteorological Data from Wa, Upper West Region of Ghana. *Journal of Climatology & Weather Forecasting*, *06*(03). https://doi.org/10.4172/2332-2594.1000237

Szwagrzyk, M., Kaim, D., Price, B., Wypych, A., Grabska, E., & Kozak, J. (2018). Impact of forecasted land use changes on flood risk in the Polish Carpathians. *Natural Hazards*, *94*(1), 227–240. https://doi.org/10.1007/s11069-018-3384-y

Tabari, H. (2020). Climate change impact on flood and extreme precipitation increases with water availability. *Scientific Reports*, *10*(1), 1–10. https://doi.org/10.1038/s41598-020-70816-2

Taherkhani, M., Vitousek, S., Barnard, P. L., Frazer, N., Anderson, T. R., & Fletcher, C. H. (2020). Sea-level rise exponentially increases coastal flood frequency. *Scientific Reports*, *10*(1), 1–17. https://doi.org/10.1038/s41598-020-62188-4

Tali, P. A., & Kanth, T. A. (2013). Impact of Land use/Land cover change on Runoff Regime of the Upper Jhelum Catchment. *Revista de Geomorfologie*, *15*, 29–37. http://ezlibproxy.unisa.edu.au/login?url=http://search.ebscohost.com/login.aspx?direct=true&db=aph&AN=93365677&site=ehost-live

Tassew, B. G., Belete, M. A., & Miegel, K. (2019). Application of HEC-HMS Model for Flow Simulation in the Lake Tana Basin: The Case of Gilgel Abay Catchment, Upper Blue Nile Basin, Ethiopia. *Hydrology*, *6*(21). https://doi.org/10.3390/hydrology6010021

Thapa, B., Danegulu, A., Suwal, N., Upadhyay, S., Manandhar, B., & Prajapati, R. (2020). Rainfall-Runoff Modelling of the West Rapti Basin, Nepal. *Technical Journal*, *2*(1), 99–107. https://doi.org/10.3126/tj.v2i1.32846

Thiemig, V., de Roo, A., & Gadain, H. (2011). Current status on flood forecasting and early warning in Africa. *International Journal of River Basin Management*, *9*(1), 63–78. https://doi.org/10.1080/15715124.2011.555082

Trautmann, T. (2016). *Master Thesis Macroscopic diagnostic modeling of the hydrological cycle: Understanding the dynamics of water pools in snow affected regions*.

Turkington, T., Breinl, K., Ettema, J., Alkema, D., & Jetten, V. (2016). A new flood type classification method for use in climate change impact studies. *Weather and Climate Extremes*, *14*(September), 1–16. https://doi.org/10.1016/j.wace.2016.10.001

Twumasi, Y. D., Osei Jnr, M. E., & Ayer, J. (2015). Flood prediction of the Black Volta in a climate change scenario. *International Journal of Geomatic and Geosciences*, *5*(3), 362–374.

Twumasi, Yaw Danquah, Ayer, R. J., Mathew, E., & Jnr, O. (2015). Computing Flood Volume of Dikpe Catchment using HEC-HMS. *Global Journal of Human-Social Science: B Geography, Geo-Sciences, Environmental Science & Disaster Management*, *15*(2).

Twumasiwaah, K.-A. (2016). *Urban Flood Risk Management: A Case Study of Aboabo, Kumasi*. Kwame Nkrumah University of Science and Technology.

US Army Corps of Engineers. (2021). HEC-HMS User's Manual. *US Army Corps of Engineers Hydrologic Engineering Center*, *December*, 623.

https://www.hec.usace.army.mil/confluence/hmsdocs/hmsum/4.7/release-notes/v-4-7-0-release-notes

US Army Corps of Engineers, I. for W. R. H. E. (2010). *HEC-GeoHMS Extension*. *October*.

VBA-WMO-GWP Initiative Volta IFM. (2016). *Country Needs Assessment REPORT - Ghana Project Preparation for the Implementation of Integrated Flood Management with a focus on Benin, Burkina Faso, Cote d'Ivoire, Ghana, Mali, Togo and the Volta River Basin* (Issue August).

Viessman, W, Lewis, G., Knapp, J., & Harbaugh, T. (1989). *Introduction to hydrology*. https://www.cec.uchile.cl/~biblidic/LibrosIngresados/LibrosIngresadosEnero2016.pdf

Viessman, Warren, Lewis, G. L., & Knapp, J. (1989). *introduction to hydrology*.

Viviroli, D., Zappa, M., Gurtz, J., & Weingartner, R. (2009). An introduction to the hydrological modelling system PREVAH and its pre- and post-processing-tools. *Environmental Modelling and Software*, *24*(10), 1209–1222. https://doi.org/10.1016/j.envsoft.2009.04.001

Wagener, T., Gupta, H. V, & Sorooshian, S. (2004). Stochastic formulation of a conceptual hydrological model. *Hydrology: Science & Practice for the 21st Century*, *I*(December), 398–405.

Wagener, T., Wheater, H. S., & Gupta, H. V. (2004). *Rainfall-Runoff Modelling in Gauged and Ungauged Catchments*. Imperial College Press 57 Shelton Street Covent Garden London WC2H 9HE.

Williams, T. O. (2016). The Volta River Basin. *The Volta River Basin*, 1–198. https://doi.org/10.4324/9781315707334

Wu, H., Adler, R. F., Hong, Y., Tian, Y., & Policelli, F. (2012). Evaluation of global flood detection using satellite-based rainfall and a hydrologic model. *Journal of Hydrometeorology*, *13*(4), 1268–1284. https://doi.org/10.1175/JHM-D-11-087.1

Zhang, Q., Berntell, E., Li, Q., & Ljungqvist, F. C. (2021). Understanding the variability of the rainfall dipole in West Africa using the EC-Earth last millennium simulation. *Climate Dynamics*, *57*(1–2), 93–107. https://doi.org/10.1007/s00382-021-05696-x

Zhao, R., Zhao, H., Wang, X., Zhao, Y., & Zhang, L. (2019). Application of the HEC-HMS Model for Flood Simulation in Ungauged Mountainous Area. *DEStech Transactions on Environment, Energy and Earth Sciences*, *gmee*, 6–11. https://doi.org/10.12783/dteees/gmee2018/27464

Zhou, K., Duan, J. G., Rosenberg, ; Abigail, & Shim, J. (2018). *World Environmental and Water Resources Congress*. *1*(i), 489.

Appendix A: Statistics of Decadal Monthly Rainfall amount (mm) for period (1980–2018) for Wa station in Black Volta basin in Ghana

WA										
	1980-1989					1990-1999				
	Min (mm)	Max (mm)	Mean (mm)	Std. dev	CV	Min (mm)	Max (mm)	Mean (mm)	Std. dev	CV
Jan	0.00	18.10	2.01	6.03	3.00	0.00	5.80	0.58	1.83	3.16
Feb	0.00	19.40	3.77	6.34	1.68	0.00	68.90	8.51	21.51	2.53
Mar	1.10	90.80	32.97	29.43	0.89	0.00	39.20	18.14	14.79	0.82
Apr	29.50	142.70	69.74	38.57	0.55	28.20	152.80	78.88	38.83	0.49
May	30.40	160.20	94.16	39.27	0.42	55.10	188.60	135.94	44.96	0.33
Jun	59.30	155.60	110.40	35.53	0.32	80.40	250.20	142.56	57.06	0.40
Jul	96.60	230.10	148.51	49.56	0.33	117.50	237.00	157.04	38.29	0.24
Aug	52.00	294.40	173.34	79.23	0.46	99.20	319.60	211.06	81.77	0.39
Sep	98.30	227.10	161.59	46.83	0.29	63.20	353.30	192.51	87.56	0.45
Oct	0.00	162.30	70.23	47.58	0.68	15.90	191.20	89.52	51.14	0.57
Nov	0.00	25.90	6.97	9.34	1.34	0.00	18.40	5.08	6.78	1.34
Dec	0.00	37.00	7.24	14.54	2.01	0.00	8.30	1.61	3.40	2.11
	2000-2009					2010-2018				
	Min (mm)	Max (mm)	Mean (mm)	Std. dev	CV	Min (mm)	Max (mm)	Mean (mm)	Std. dev	CV
Jan	0.00	67.50	13.00	23.24	1.79	0.00	0.00	0.00	0.00	
Feb	0.00	13.80	5.13	6.64	1.29	0.00	93.70	22.46	35.86	1.60
Mar	0.00	43.80	18.49	14.06	0.76	0.00	72.60	25.75	24.49	0.95
Apr	50.30	186.00	98.93	41.08	0.42	11.60	186.90	82.00	56.01	0.68
May	41.00	210.90	131.46	53.60	0.41	71.20	145.40	112.99	30.57	0.27
Jun	72.40	243.80	159.96	57.30	0.36	48.40	181.50	109.31	53.23	0.49
Jul	84.60	220.10	144.50	48.88	0.34	71.20	138.90	108.79	24.79	0.23
Aug	157.70	315.30	234.91	55.29	0.24	130.30	361.00	233.09	81.70	0.35
Sep	103.30	277.80	198.88	58.20	0.29	156.60	319.90	208.50	54.92	0.26
Oct	26.00	117.50	71.42	34.50	0.48	51.80	145.60	97.44	36.12	0.37
Nov	0.00	26.90	5.67	9.10	1.61	0.00	36.60	7.47	13.31	1.78
Dec	0.00	0.00	0.00	0.00		0.00	0.00	0.00	0.00	

Appendix B: Statistics of Decadal Monthly Rainfall amount (mm) for period (1980–2018) for Bui station in Black Volta basin in Ghana

BUI										
	1980-1989					1990-1999				
	Min (mm)	Max (mm)	Mean (mm)	Std. dev	CV	Min (mm)	Max (mm)	Mean (mm)	Std. dev	CV
Jan	0.00	42.70	7.12	17.43	2.45	0.00	15.30	5.07	6.07	1.20
Feb	0.00	63.00	25.59	24.81	0.97	0.00	79.40	25.50	29.21	1.15
Mar	47.40	239.90	105.36	71.03	0.67	0.80	228.90	73.65	72.32	0.98
Apr	32.50	154.50	89.34	42.51	0.48	50.20	204.70	100.09	47.51	0.47
May	91.10	287.60	150.04	77.91	0.52	66.10	407.50	166.34	96.90	0.58
Jun	78.60	305.80	152.40	84.61	0.56	110.90	225.50	161.20	37.09	0.23
Jul	60.50	268.80	152.45	73.73	0.48	20.00	219.00	90.36	51.94	0.57
Aug	41.00	264.60	138.28	62.46	0.45	42.80	201.10	101.87	44.39	0.44
Sep	106.40	308.30	230.19	67.21	0.29	80.50	308.70	169.76	70.90	0.42
Oct	47.90	210.00	132.03	51.75	0.39	48.90	291.80	167.04	72.86	0.44
Nov	0.00	33.10	10.69	11.26	1.05	0.00	57.20	15.44	20.76	1.34
Dec	0.00	0.00	0.00	0.00		0.00	48.40	8.27	15.43	1.87
	2000-2009					2010-2018				
	Min (mm)	Max (mm)	Mean (mm)	Std. dev	CV	Min (mm)	Max (mm)	Mean (mm)	Std. dev	CV
Jan	0.00	93.30	21.57	34.19	1.58	0.00	48.40	10.20	16.87	1.65
Feb	0.00	40.50	12.27	17.02	1.39	0.00	88.30	22.40	30.12	1.34
Mar	8.60	139.40	53.87	41.44	0.77	21.60	77.20	50.44	19.58	0.39
Apr	69.20	223.10	144.75	55.01	0.38	50.00	164.70	114.85	41.02	0.36
May	78.00	165.70	141.33	25.19	0.18	107.60	283.70	181.79	60.69	0.33
Jun	69.80	315.10	164.42	76.45	0.46	66.20	247.00	144.13	69.66	0.48
Jul	43.90	293.20	148.74	93.66	0.63	37.20	225.70	108.14	71.25	0.66
Aug	46.50	216.50	114.39	61.97	0.54	39.50	298.80	113.16	90.36	0.80
Sep	134.00	258.50	184.98	40.69	0.22	147.30	271.20	195.24	45.21	0.23
Oct	42.20	238.40	121.30	67.95	0.56	47.00	179.90	113.99	54.59	0.48
Nov	0.00	32.80	13.98	12.34	0.88	0.00	551.20	94.94	186.35	1.96
Dec	0.00	40.20	9.21	14.17	1.54	0.00	439.40	64.73	165.24	2.55

Appendix C: Statistics of Decadal Monthly Rainfall amount (mm) for period (1980–2018) for Damongo station in Black Volta basin in Ghana

DAMONGO										
1980-1989						**1990-1999**				
	Min (mm)	**Max (mm)**	**Mean (mm)**	**Std. dev**	**CV**	**Min (mm)**	**Max (mm)**	**Mean (mm)**	**Std. dev**	**CV**
Jan	0.00	0.00	0.00	0.00		0.00	63.50	7.06	21.17	3.00
Feb	0.00	12.00	3.24	4.86	1.50	0.00	45.70	8.10	14.35	1.77
Mar	33.70	83.50	53.84	18.79	0.35	0.00	57.70	22.84	22.06	0.97
Apr	29.20	195.60	99.29	51.66	0.52	59.60	235.90	121.22	59.33	0.49
May	67.60	191.40	135.91	39.60	0.29	57.30	223.30	136.07	50.72	0.37
Jun	61.50	259.60	141.84	58.56	0.41	72.90	219.90	131.42	50.02	0.38
Jul	75.50	304.30	173.85	75.79	0.44	39.00	261.00	143.25	72.06	0.50
Aug	78.40	280.50	197.00	60.25	0.31	63.90	333.20	180.90	67.78	0.37
Sep	76.70	303.50	211.38	61.81	0.29	134.50	363.30	215.12	76.05	0.35
Oct	6.30	218.10	92.28	63.98	0.69	40.30	195.00	115.50	52.35	0.45
Nov	0.00	27.00	9.77	10.99	1.12	0.00	22.50	5.65	8.08	1.43
Dec	0.00	1.40	0.18	0.45	2.48	0.00	29.80	4.63	9.87	2.13
	2000-2009					**2010-2018**				
	Min (mm)	**Max (mm)**	**Mean (mm)**	**Std. dev**	**CV**	**Min (mm)**	**Max (mm)**	**Mean (mm)**	**Std. dev**	**CV**
Jan	0.00	8.10	1.75	3.07	1.76	0.00	13.10	1.53	4.34	2.83
Feb	0.00	23.00	6.82	8.43	1.24	0.00	41.40	17.00	14.94	0.88
Mar	11.70	118.20	40.46	33.95	0.84	1.60	58.60	33.68	20.97	0.62
Apr	48.20	201.50	107.74	45.25	0.42	24.70	165.50	90.10	44.58	0.49
May	70.10	169.70	117.70	39.24	0.33	59.90	169.80	125.44	40.61	0.32
Jun	80.90	281.30	145.55	55.50	0.38	75.60	270.50	163.58	62.06	0.38
Jul	30.50	326.20	161.46	87.81	0.54	64.50	171.30	121.99	32.89	0.27
Aug	89.00	285.90	208.55	60.24	0.29	27.20	247.80	161.88	75.30	0.47
Sep	109.40	222.70	177.35	39.84	0.22	116.40	299.90	201.49	71.93	0.36
Oct	15.20	146.50	84.74	40.75	0.48	40.40	215.50	98.56	51.98	0.53
Nov	0.00	42.80	12.29	14.22	1.16	0.00	77.80	11.61	25.23	2.17
Dec	0.00	9.80	1.20	3.08	2.57	0.00	10.90	1.92	3.62	1.88

Appendix D: Statistics of Decadal Monthly Rainfall amount (mm) for period (1980–2018) for Bole station in Black Volta basin in Ghana

BOLE										
1980-1989						**1990-1999**				
	Min	**Max**	**Mean**	**Std. dev**	**CV**	**Min**	**Max**	**Mean**	**Std. dev**	**CV**
Jan	0.00	6.10	0.61	1.93	3.16	0.00	12.50	1.78	4.05	2.28
Feb	0.00	20.40	6.79	8.52	1.25	0.00	59.70	13.46	21.11	1.57
Mar	15.80	155.60	60.69	39.04	0.64	0.00	79.30	34.03	29.50	0.87
Apr	33.10	134.00	71.41	27.28	0.38	17.00	189.10	116.68	55.48	0.48
May	81.10	183.70	138.33	30.68	0.22	38.70	390.40	134.87	99.10	0.73
Jun	90.10	304.70	163.05	77.13	0.47	48.00	211.30	127.95	47.26	0.37
Jul	68.30	240.80	155.49	56.14	0.36	103.90	234.40	148.86	49.71	0.33
Aug	95.70	219.90	155.64	37.57	0.24	78.00	268.60	149.69	67.36	0.45
Sep	96.00	348.00	213.62	74.68	0.35	123.60	294.60	214.37	55.88	0.26
Oct	31.90	209.30	98.00	58.64	0.60	44.10	260.50	108.98	66.90	0.61
Nov	0.00	30.00	9.65	9.36	0.97	0.00	74.00	24.37	28.64	1.18
Dec	0.00	48.80	5.24	15.33	2.92	0.00	23.90	4.52	8.21	1.82
	2000-2009					**2010-2018**				
	Min	**Max**	**Mean**	**Std. dev**	**CV**	**Min**	**Max**	**Mean**	**Std. dev**	**CV**
Jan	0.00	50.80	5.61	15.93	2.84	0.00	21.70	2.41	7.23	3.00
Feb	0.00	84.90	14.39	26.69	1.85	0.00	38.70	15.17	16.41	1.08
Mar	3.30	134.20	49.97	44.27	0.89	21.10	138.70	48.96	37.23	0.76
Apr	64.60	171.20	116.61	40.83	0.35	56.30	136.30	90.66	25.31	0.28
May	69.80	190.40	137.26	45.75	0.33	72.00	182.30	115.63	40.76	0.35
Jun	65.40	235.10	142.91	51.74	0.36	85.40	268.20	156.81	56.74	0.36
Jul	49.60	259.80	147.59	74.15	0.50	60.30	200.20	126.78	52.57	0.41
Aug	94.20	268.40	181.71	59.25	0.33	64.70	239.50	151.56	67.92	0.45
Sep	118.60	304.10	204.79	64.45	0.31	60.80	275.00	188.11	68.30	0.36
Oct	47.90	152.70	101.49	34.81	0.34	39.70	347.50	113.08	93.35	0.83
Nov	0.00	56.00	20.78	21.87	1.05	0.00	34.20	12.81	12.55	0.98
Dec	0.00	55.00	8.54	17.67	2.07	0.00	0.50	0.06	0.17	3.00

Appendix E: Statistics of Decadal Monthly Rainfall amount (mm) for period (1980–2018) for Sunyani station in Black Volta basin in Ghana

SUNYANI										
	1980-1989					1990-1999				
	Min	Max	Mean	Std. dev	CV	Min	Max	Mean	Std. dev	CV
Jan	0.00	19.90	6.43	8.82	1.37	0.00	24.50	8.51	10.23	1.20
Feb	0.20	141.00	46.59	49.73	1.07	0.00	159.80	49.86	48.60	0.97
Mar	55.90	236.40	151.78	60.17	0.40	17.70	152.40	76.76	46.96	0.61
Apr	67.30	166.50	110.01	35.52	0.32	59.20	268.70	147.05	57.06	0.39
May	66.80	252.80	146.84	58.94	0.40	58.60	245.70	143.84	58.12	0.40
Jun	85.00	364.80	179.12	84.44	0.47	124.80	222.50	165.64	35.22	0.21
Jul	11.50	248.20	134.42	66.17	0.49	16.20	126.80	69.00	39.04	0.57
Aug	7.40	186.40	95.15	61.97	0.65	1.50	125.60	54.96	40.96	0.75
Sep	65.10	296.20	171.84	65.58	0.38	62.10	203.60	149.82	55.36	0.37
Oct	42.70	319.60	154.82	86.74	0.56	126.20	243.20	165.56	40.04	0.24
Nov	6.40	67.40	23.34	22.37	0.96	6.50	86.50	39.85	26.79	0.67
Dec	0.00	45.10	9.18	15.00	1.63	0.00	207.40	33.70	62.49	1.85
	2000-2009					2010-2018				
	Min	Max	Mean	Std. dev	CV	Min	Max	Mean	Std. dev	CV
Jan	0.00	47.60	14.39	16.91	1.17	0.00	24.50	3.94	8.41	2.14
Feb	0.00	63.90	31.91	24.17	0.76	17.50	130.60	64.68	38.33	0.59
Mar	48.20	161.30	94.64	38.85	0.41	36.60	133.50	94.33	29.46	0.31
Apr	65.50	398.60	195.62	92.14	0.47	32.00	220.60	124.97	61.07	0.49
May	76.30	183.30	140.13	34.90	0.25	73.40	320.70	177.41	92.55	0.52
Jun	59.50	311.30	184.31	73.32	0.40	78.40	325.50	204.03	99.92	0.49
Jul	32.00	172.10	94.17	40.64	0.43	14.50	209.50	105.77	57.65	0.55
Aug	8.50	154.40	70.25	52.83	0.75	7.50	160.80	51.97	50.39	0.97
Sep	67.70	330.40	165.08	93.27	0.57	55.40	232.80	148.03	63.77	0.43
Oct	59.30	267.60	169.08	73.92	0.44	22.80	232.80	153.68	68.95	0.45
Nov	15.00	203.00	73.87	52.98	0.72	12.40	111.60	49.80	28.73	0.58
Dec	0.00	39.30	10.80	13.58	1.26	0.00	20.00	5.62	8.35	1.48

Appendix F: Statistics of Decadal Monthly Rainfall amount (mm) for period (1980–2018) for Wenchi station in Black Volta basin in Ghana

WENCHI										
	1980-1989					1990-1999				
	Min	Max	Mean	Std. dev	CV	Min	Max	Mean	Std. dev	CV
Jan	0.00	27.80	5.23	8.96	1.71	0.00	3.20	1.10	1.39	1.26
Feb	0.00	54.50	15.53	17.72	1.14	0.00	94.40	25.85	28.37	1.10
Mar	12.60	229.70	134.49	69.52	0.52	0.00	283.00	100.01	87.39	0.87
Apr	34.10	213.40	145.21	53.28	0.37	80.90	232.30	160.00	56.09	0.35
May	78.10	264.40	139.92	53.27	0.38	101.50	344.10	186.12	69.42	0.37
Jun	60.90	347.00	138.32	79.78	0.58	92.30	205.80	148.79	34.38	0.23
Jul	19.00	237.00	153.47	62.01	0.40	19.70	170.70	82.13	46.98	0.57
Aug	4.30	214.00	116.38	67.10	0.58	13.50	158.00	87.83	45.61	0.52
Sep	103.20	297.80	199.66	59.94	0.30	82.50	290.60	175.59	87.72	0.50
Oct	63.20	274.40	175.43	65.29	0.37	16.00	274.10	142.11	81.87	0.58
Nov	0.30	97.20	33.43	32.17	0.96	1.80	142.80	51.89	42.35	0.82
Dec	0.00	21.30	4.43	8.66	1.95	0.00	96.50	20.63	29.39	1.42
	2000-2009					2010-2018				
	Min	Max	Mean	Std. dev	CV	Min	Max	Mean	Std. dev	CV
Jan	0.00	61.10	18.05	21.72	1.20	0.00	14.00	3.03	5.38	1.77
Feb	0.00	101.10	25.06	30.74	1.23	18.70	77.40	38.88	18.90	0.49
Mar	15.50	172.30	80.62	46.34	0.57	17.50	143.10	78.51	40.12	0.51
Apr	121.20	304.80	164.20	54.48	0.33	85.50	217.60	132.79	52.60	0.40
May	85.30	231.50	154.11	45.56	0.30	81.40	255.50	167.12	54.59	0.33
Jun	63.40	294.00	150.41	67.54	0.45	79.00	228.60	154.91	50.83	0.33
Jul	45.50	298.20	134.60	70.41	0.52	52.40	263.10	122.39	61.95	0.51
Aug	46.40	192.30	90.95	55.79	0.61	3.10	237.00	82.46	69.60	0.84
Sep	90.40	245.90	170.34	60.52	0.36	89.10	368.40	185.09	85.79	0.46
Oct	138.60	299.10	205.57	58.80	0.29	64.30	244.80	181.14	58.03	0.32
Nov	20.40	128.70	64.47	33.36	0.52	6.90	103.80	48.08	32.38	0.67
Dec	0.00	51.50	13.49	16.90	1.25	0.00	31.00	6.54	11.12	1.70

Appendix G: Statistics of Decadal Monthly Rainfall amount (mm) for period (1980–2018) for Kintampo station in Black Volta basin in Ghana

KINTAMPO										
	1980-1989					1990-1999				
	Min	Max	Mean	Std. dev	CV	Min	Max	Mean	Std. dev	CV
Jan	0.00	39.50	4.08	12.45	3.05	0.00	11.10	1.92	4.11	2.14
Feb	0.00	62.70	17.42	19.93	1.14	0.00	41.90	16.19	15.57	0.96
Mar	38.10	180.60	100.91	45.21	0.45	0.00	108.30	52.95	38.35	0.72
Apr	29.10	211.10	138.29	50.52	0.37	55.60	259.70	148.88	70.55	0.47
May	59.60	292.50	121.89	67.92	0.56	91.60	334.20	165.60	71.56	0.43
Jun	89.00	319.50	183.84	70.85	0.39	92.40	274.50	183.56	53.62	0.29
Jul	47.60	360.00	194.88	99.42	0.51	32.00	302.30	113.88	90.86	0.80
Aug	53.70	300.30	168.62	101.42	0.60	9.20	160.30	114.25	45.31	0.40
Sep	166.60	415.70	265.63	79.40	0.30	106.70	373.40	196.79	80.14	0.41
Oct	53.70	229.40	131.48	53.34	0.41	115.00	271.90	173.30	54.34	0.31
Nov	0.00	73.20	27.52	22.47	0.82	0.00	89.70	41.64	33.07	0.79
Dec	0.00	11.20	2.58	4.32	1.68	0.00	117.40	20.10	36.48	1.81
	2000-2009					2010-2018				
	Min	Max	Mean	Std. dev	CV	Min	Max	Mean	Std. dev	CV
Jan	0.00	70.80	12.85	24.10	1.88	0.00	26.60	6.74	10.29	1.53
Feb	0.00	107.70	29.56	35.80	1.21	12.40	54.80	28.51	16.14	0.57
Mar	7.30	113.60	63.22	34.12	0.54	5.80	148.80	84.97	50.63	0.60
Apr	66.60	229.70	131.01	48.56	0.37	65.60	229.60	125.16	61.49	0.49
May	56.90	212.60	150.47	53.14	0.35	131.70	419.20	231.29	111.06	0.48
Jun	45.00	255.90	174.59	69.03	0.40	62.90	340.00	169.37	87.36	0.52
Jul	31.30	291.70	133.29	73.15	0.55	68.40	366.40	137.17	93.58	0.68
Aug	22.00	280.90	117.33	81.67	0.70	12.70	157.50	83.21	43.86	0.53
Sep	141.40	270.80	213.85	45.46	0.21	143.10	364.40	255.32	79.11	0.31
Oct	93.00	283.30	195.43	61.83	0.32	111.00	447.40	223.66	115.19	0.52
Nov	0.00	92.40	32.52	24.80	0.76	2.00	85.80	43.25	31.74	0.73
Dec	0.00	59.20	13.03	19.49	1.50	0.00	4.80	1.16	2.02	1.75